Doctoral theses at NTNU, 2013:287

Bronislav Novák

On the chemical and electrochemical formation of aluminium carbide in aluminium electrolysis

Doctoral Thesis

Bronislav Novák

ISBN 978-82-471-4704-7 (printed version)
ISBN 978-82-471-4706-1 (electronic version)
ISSN 1503-8181

NTNU – Trondheim
Norwegian University of
Science and Technology

NTNU
Norwegian University of Science and Technology
Thesis for the degree of Philosophiae Doctor
Faculty of Natural Sciences and Technology
Department of Materials Science and Engineering

Doctoral theses at NTNU, 2013:287

NTNU – Trondheim
Norwegian University of
Science and Technology

NTNU

Bronislav Novák

On the chemical and electrochemical formation of aluminium carbide in aluminium electrolysis

Thesis for the degree of Philosophiae Doctor

Trondheim, August 2013

Norwegian University of Science and Technology
Faculty of Natural Sciences and Technology
Department of Materials Science and Engineering

NTNU – Trondheim
Norwegian University of
Science and Technology

NTNU
Norwegian University of Science and Technology

Thesis for the degree of Philosophiae Doctor

Faculty of Natural Sciences and Technology
Department of Materials Science and Engineering

ISBN 978-82-471-4704-7 (printed version)
ISBN 978-82-471-4706-1 (electronic version)
ISSN 1503-8181

IMT-Report 2013:184

Doctoral theses at NTNU, 2013:287

Printed by Skipnes Kommunikasjon as

This thesis has been submitted to

Department of Materials Science and Engineering
Norwegian University of Science and Technology

In partial fulfilment of the requirements for
the academic degree

Philosophiae Doctor

August 2013

Acknowledgment

I am approaching to the end of my PhD life and during this period I have learned a lot from the field of aluminium electrolysis and also developed myself as a researcher. This thesis could not have been done without the help from a lot of people and I would like to take this opportunity to thank everyone who was supporting me during this period.

Most of all, I would like to thank my supervisor, Prof. Tor Grande for his helpful advices and guidance during all 3 years of my work. His broad scientific knowledge was very valuable source for the research. I would like to thank him especially for his patience during some difficult periods, when I was struggling with my experimental work. He was always giving me advices how to solve the problem and encouraged me to move forward.

I would like to thank also to my co-supervisor Arne Petter Ratvik for helpful advices and reading all the manuscripts. It was him who opened me the door to PhD study at NTNU.

I have to thank project leader Egil Skybakmoen and also to other people working on the DuraMat project, Kati Tschöpe, Asbjørn Solheim, Anne Støre for fruitful discussions on our regular weekly meetings. Their experiences and knowledge in the field were very helpful.

I would like to thank to technical stuff for their help, to Julian Tolchard for helping me with EDS analysis of my samples, to Eli Beate Larsen, Elin Albertsen and Pei Na Kui for helping me with the construction of a new furnace, to Gunn Torill Wikdahl for helping me when I was missing something in the polishing lab, to Ove Paulsen and Ove Darell for helping me with designing of the new experimental setups.

At last, but not least, I would like to give special thank to my parents, they were always giving me support during my PhD life. They are researchers themselves and their experience and advices were also helpful for my work as a scientist.

Preface

The thesis is submitted to the Norwegian University of Science and Technology (NTNU) in partial fulfilment of the requirements for the degree of Philosophiae doctor. The dissertation is based on work carried out at the Department of Materials Science and Engineering, the Norwegian University of Science and Technology (NTNU), under the supervision of Prof. Tor Grande. The work was done during the period August 16th 2010 to August 29th, 2013.

The work is a part of the project Durable Materials in Primary Aluminium Production (DuraMat). The project is financed by the Research Council of Norway, Hydro Aluminium, Elkem Carbon and Sør-Norge Aluminium.

All the experiments have been conducted by the author. Initial thermodynamic calculations in the Al-O system were performed by Kati Tschöpe.

Parts of this dissertation have been published in the following two publications:

B. Novak, K. Tschöpe, A.P. Ratvik and T. Grande, "Fundamentals of Aluminum Carbide Formation", *Light Metals,* 2012, pp. 1343-48.

B. Novak, K. Tschöpe, A.P. Ratvik and T. Grande, "The effect of Cryolite on the Formation of Aluminum Carbide at the Carbon Aluminum Interface", *Light Metals,* 2013, pp. 1245-50.

Summary

Cathode wear is considered as one of the key factors for limiting the lifetime of aluminium electrolysis cells. This phenomenon has become more important as aluminium smelters have steadily increased the amperage of the cells and shifted towards graphitized cathode materials with higher electrical conductivity. The present work has focused on the fundamentals of the formation of aluminium carbide at the carbon-aluminium interface. The objective was to investigate the mechanism(s) of the formation of Al_4C_3 and the influence of reaction parameters such as temperature, presence of cryolite and electrical current. The reaction between aluminium and carbon was first examined by diffusion couples experiments. Formation of aluminium carbide was observed at the interface after annealing at 1100 °C or higher temperatures. Two distinct layers of aluminium carbide could be observed at the interface by optical and electron microscopy. The composition of the two layers was confirmed by EDS element mapping, and the analysis revealed a relative high oxygen content in the layer towards Al and a lower oxygen content in the layer towards C. Based on a thermodynamic analysis it was suggested that the reaction may proceed by transport through the gas phase due to volatile species, which is also important for the removal of the oxide scale on the surface of molten aluminium. The influence of cryolite on the reaction of Al and C was examined also by introduction of a thin film at the Al/C interface. The presence of a catalytic amount of cryolite changed dramatically the reaction, and an aluminium carbide layer was found at the carbon surface already after 3 hours at 1030 °C. Needle-like crystals of aluminium carbide were found towards aluminium, while cryolite was not found due to the significant vapour pressure of $NaAlF_4(g)$. When a higher volume of molten cryolite was present in the crucible, the formation of Al_4C_3 was slowed down. The influence of applying an electric current through the diffusion couple was also investigated, and the carbon material was cathodically polarized. Formation of aluminium carbide could not be confirmed in these experiments without cryolite present at the interface. The cell voltage was however oscillating during the experiment, which could be explained by a periodically formation and fracture of aluminium carbide at the interface contact points. When catalytic amount of cryolite was introduced at the Al/C interface, the observations were similar to experiments without polarization, but the amount of aluminium carbide formed was higher, which suggests that the current passing through the diffusion couple enhances the formation of aluminium carbide. Finally, electrolysis experiments were performed in electrochemical cells with various setups of the electrodes. First a conventional cell analogue to industrial cells was used. Second, an inverted cell with opposite polarization was applied, where the cathode was exposed directly to the bath. Finally, an inverted cell was applied without Al metal present initially. These electrolysis experiments demonstrated quite similar results, where an aluminium carbide layer was found along the entire cathode surface already after 30 minutes of electrolysis. In case of the inverted cell without aluminium, the carbide layer was thinner compared to

other cells, which was explained by higher amount of bath in the vicinity of the cathode leading to faster dissolution of the carbide layer. Analysis of the interior of the cathodically polarized carbon materials revealed that the molten bath infiltrated the cathode and that aluminium carbide was formed on the walls of the pores, while no Al metal was found. Aluminium carbide was suggested to be deposited electrochemically directly from the bath without involvement of the aluminium pad. The present work has demonstrated that the formation of aluminium carbide by an electrochemical reaction is significantly faster than a purely chemical reaction between the two elements. The role of cryolite for the carbide formation is twofold. Cryolite is involved as a reactant in the electrochemical formation of aluminium carbide and it also works as a solvent of the carbide. Finally, it is proposed that the exchange rate of the molten bath between the carbon cathode and the aluminium pad is the rate determining step for the cathode wear rate.

Contents

Chapter 1

1 Introduction

1.1 Hall-Héroult process

Aluminium is produced by electrochemical reduction of aluminium oxide desolved in a molten salt [1]. The technology is called the Hall-Héroult process, and an illustration of an electrolysis cell is shown in Figure 1. The overall reaction in the cell is:

$$2Al_2O_3(dissolved) + 3C(s) \rightarrow 4Al(l) + 3CO_2(g) \qquad (1.1)$$

The electrolyte is a melt based on cryolite (Na_3AlF_6) with excess AlF_3 in addition to some other additives (CaF_2, LiF), which are modifying the important properties of the bath such as the melting point, the electrical conductivity and the alumina solubility [1]. The temperature in the cell is about 960 °C and it is adjusted with respect to the melting point of the bath, and 5-10 °C superheat is usually used.

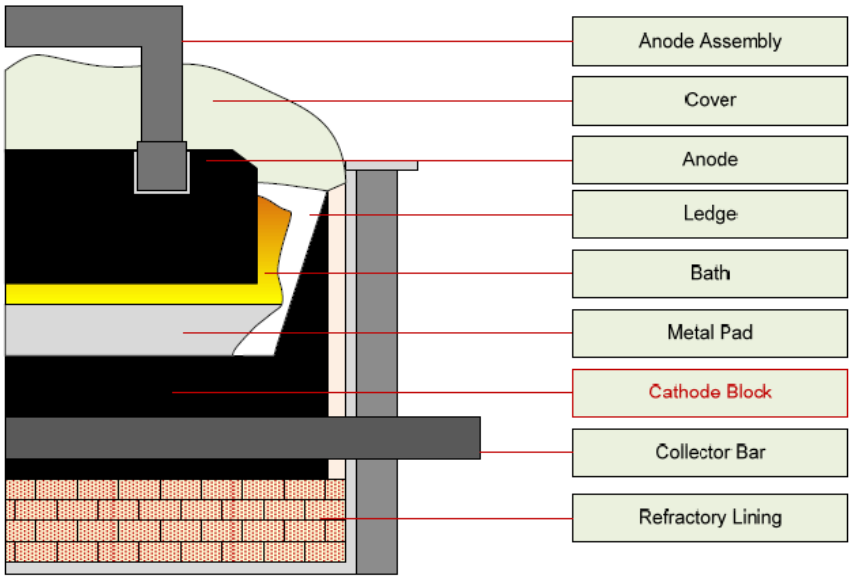

Figure 1.1: An illustration of the aluminium electrolysis cell [2].

Alumina is fed to the cell regularly during the operation of the cell and aluminium is deposited continuously on the cathode [1]. The current efficiency of the electrolysis process is typically 92-96 %. CO_2 formation takes place at the carbon anodes surfaces, which are consumed and need to be changed regularly during the

operation. The aluminium pad is the real electrochemical cathode where the cathodic reaction takes place, but the carbon bottom of the cell is also considered in the aluminium industry as the cathode. The carbon cathode does not take part in the reaction but serves only as a container and electrical connection to the metal pad. However, there is an unwanted wear of the carbon block [3]. Only a complete relining of the cathode is feasible and the cathode wear will therefore limit the lifetime of the cell. The cathode wear phenomenon, which is the motivation for the present thesis work, is described further below.

1.2 The cathode wear phenomenon

The main reason for the shut down of electrochemical cells in the aluminium industry is the cathode wear [4]. The carbon block is worn continuously during operation until the steel collector bars become exposed to the aluminium pad. Then the cell must shut down because of higher iron content in the produced aluminium [5]. The lifetime of electrochemical cell is usually determined by the lifetime of the cathode lining.

Figure 1.2: Industrial cathode shut down after 2184 days operation [13].

The cathode wear mechanism is rather complex and mechanical, chemical and electrochemical mechanisms have been suggested [3]. The carbon cathode might be worn mechanically by abrasion due to the metal pad movement caused by the strong magnetic field [6]. The carbon block can also react with the aluminium pad resulting in formation of aluminium carbide. Aluminium carbide is further

dissolved in the bath, transported through the bath and become oxidised at the anode. Electrochemical formation of aluminium carbide is also likely because the bath contain aluminium species, which can be transported to the cathode due to the charge transport through the bath. There are many species in the bath which can take part in the electrochemical reactions. Considerable research has been performed to investigate cathode wear [3], but the mechanisms are still poorly understood. Nowadays, aluminium smelters are increasing the amperage in the cells and graphitized cathode blocks with higher electrical conductivity have become the most common cathode materials to reduce the ohmic losses in the lining. However, graphitized cathodes have been reported to have higher wear rates [7], and cathode wear have during the last decade become one of the main challenges in the aluminium industry. The present thesis is motivated by the need for a more fundamental understanding of the mechanism(s) causing cathode wear.

1.3 Objective of the work

This PhD work is a part of the project "Durable Materials in Primary Aluminium Production" (DuraMat). One of the main objectives of the DuraMat project is fundamental studies of the cathode wear mechanism. The present PhD thesis was focused on the chemical interaction between aluminium and carbon and on the fundamentals of the formation of aluminium carbide. The main purpose was to understand the reaction mechanism, which is poorly understood. This was approached by studying both the thermodynamics and kinetics of the reaction, and conditions that could enhance the reaction rate or the mass transport related to the reaction. The influence of the presence of cryolite at the carbon-aluminium interface and the influence of current density was examined. Traditional experimental electrolysis methods were also considered, but a simple diffusion couple were first introduced where the different parameters could be studied in detail separately or combined. It is also important to use idealized and well defined materials for more fundamental work and a highly graphitized material was used. The objectives of the thesis can be divided into two separate parts:

Aluminium-carbon diffusion couples: The aim was to study aluminium carbide formation at the Al/C interface. These investigations were conducted at relatively higher temperature relative to the conventional temperature of the Hall-Héroult process since Al_4C_3 is not known to form easily without the presence of cryolite at the operation temperature of the industrial cells [8]. The morphology and the thickness of the carbide layer were examined and the reaction mechanism was suggested. Thermodynamic calculations were performed in order to support the proposed reaction mechanism(s). The pure Al/C diffusion couples without the presence of cryolite were not directly applicable for the industrial case, but they served as a reference for the experiments conducted with cryolite present at the interface. The catalytic effect of cryolite on the reaction was studied by

introduction of a thin cryolite film at the Al/C interface. The role of cryolite for the reaction mechanism was proposed based on the experimental observations.

Aluminium carbide formed in electrochemical cells: The aim was to study electrochemical formation of aluminium carbide. An electrochemical cell with a setup similar to the Al/C diffusion couples was used, but the carbon was cathodically polarized. Electrochemical formation of aluminium carbide was also studied in several different electrochemical cell setups where larger amount of cryolite was present and carbon cathode was or was not initially in direct contact with aluminium. Electrochemical deposition from the bath and direct reaction with aluminium could then be distinguished. The conditions for electrochemical formation of aluminium carbide were identified based on the experimental findings.

Chapter 2

2 The Hall-Héroult process

Aluminium metal is produced by the Hall-Héroult process, which correspond to electrochemical reduction of alumina in a molten salt [1]. Charles M. Hall and Paul L.T. Héroult invented and patented the technology independently of each other in 1886. The overall reaction is given in equation (1.1). The electrode reactions in the cell are:

Cathode: $$Al^{3+} + 3\bar{e} \rightarrow Al \quad (2.1)$$

Anode: $$2O^{2-} + C \rightarrow CO_2 + 4\bar{e} \quad (2.2)$$

The decomposition voltage of alumina (Reaction 1.1) is 1.2 V. Molten aluminium is deposited on the cathode, while CO_2 is produced on the anode [1]. The main electrolyte constituent is cryolite (Na_3AlF_6), which satisfies well the physical requirements for the bath. It has a very good solubility of alumina and at the same time a low solubility of aluminium. Excess of AlF_3 is added and the cryolite ratio ($NaF:AlF_3$) is about 2.3, but some other additives are also used to modify the properties of the bath. The desired physical properties for the electrolyte are high solubility of alumina, low melting point, high electrical conductivity, low density (lower miscibility with liquid aluminium), low metal solubility and low vapour pressure. Around 5-8 % CaF_2 is added to decrease the melting point and the vapour pressure, while LiF is sometimes added to increase the electrical conductivity. The exact composition of the electrolyte is always a compromise; each component improves one parameter, but also harms another. The operation temperature of the cell is about 960 ºC (melting point of pure cryolite is 1012 ºC) and about 5-10 ºC overheating is used [1]. There are some losses of bath due to evaporation, hydrolysis forming HF and infiltration of the electrolyte into the cathode. The main component of the vapour above the bath is $NaAlF_4$(g). HF is formed by the reaction with moisture, which is introduced to the cell mainly during replacement of the anodes and alumina feeding. Bath penetrates to the pores and cracks of the carbon cathode block, and also deeper to the refractory bricks. Therefore AlF_3 must be fed to the bath to compensate for these losses.

Alumina is the Al feedstock in the aluminium electrolysis process. It is consumed by reaction (1.1) and needs to be fed to the cell regularly [1]. Alumina hopper is situated above the cell and the feeding is done by special point feeders. These point feeders have a drill, so-called crust breaker, which provide a hole in the top crust above the bath and the feeding is then possible. 1-2 kg of alumina is added every minute and the alumina concentration is kept in the range of 2-3 wt%. Solubility of alumina in the bath is about 10 % [9], but a high concentration may lead to

formation of un-dissolved alumina sludge, which is accumulating under the metal pad [1]. Alumina must therefore be added in smaller amounts and more frequent. The dissolution of alumina is an endothermic process and additional heat is needed for the heating of alumina to the temperature of the bath [1]. Alumina used in the aluminium industry is a powder with agglomerated particle sizes 40-150 μm, containing several crystallographic phases. During feeding, γ-alumina undergoes a conversion to α-alumina, which is catalysed by presence of fluorides [10]. This conversion is slightly exothermic and α-alumina particles formed may sinter together. It takes longer time for these sintered agglomerates to dissolve, but the convection in the cell and small additions of alumina are important issues for efficient dispersion and dissolution into the bath. Low alumina content in the bath might lead to anode effect, which is described further below [1].

The carbon anodes are continuously consumed due to Reaction (1) [1]. The main anode reaction lead to formation of CO_2, but also some CO is formed (2-5 %) mainly due to back reaction of Al (dissolved in the bath) with CO_2 and the Boudovard reaction. Electrochemically active ionic species taking part in the anode reaction are various oxyfluorides. Overvoltage on the anode is quite high (0.3-0.4 V) and the CO_2 bubbles formed are decreasing the effective anode surface, thus the current density increases and higher anode potential is needed. Self baking Søderberg or prebaked anodes are used, which are made from a mixture of petroleum coke aggregate and coal tar pitch binder formed into blocks. The prebaked anodes are baked in a furnace at about 1100 ºC. The Søderberg anode blocks are baked in the cell during the operation. The prebaked anodes contain about 15 % of coal tar pitch, Søderberg 25-30 % [1]. The Søderberg cells have one single anode, which is continuously fed with new carbon materials from the top and is baked during the process. The prebaked cells have 16-40 smaller anodes, and they need to be replaced by new anodes since when they are consumed. The lifetime of prebaked anode in the cell is 22-30 days. Today, the Sødeberg technology is phased out in most countries [1]. Cells using prebaked anodes have better operation performance due to the lower binder content and are also "cleaner", because there is no baking and less emission during cell operation. The binder in the anode reacts more preferably than aggregates and the coke particles might detach. Detached particles form carbon dust, which is dispersed in the bath or rises to the surface of the bath. This phenomenon is called anode dusting. Impurities present in the anodes are important for the anode consumption, the current efficiency and the purity of the produced aluminium. Metals like V, Ca and Na are catalyst for carbon air burn and the reaction with CO_2 (Boudovard reaction). The theoretical consumption of anodes due to Reaction (1.1) is 333 kg per ton produced aluminium, but the real consumption is more than 400 kg due to the reactions mentioned above and anode dusting [1]. The residues of the anodes, the so-called anode butts are recycled. Bath is removed from the butts, before they are crushed into pieces and added to the coke aggregate for anode making. When there is a lack of alumina in the bath (low oxygen activity), the anode potential increases and the formation of CF_4 and C_2F_6 is becoming thermodynamically favoured. These compounds behave as current insulators, which blocks the anode surface and

the potential on the anode increases even more. The cell voltage usually varies from 15 to 40 V. This is called the anode effect. The tendency of a bath composition to provoke anode effect can be expressed by the critical current density. It is the maximum current density before the main anode reaction will be superseded, and it is determined mostly by the alumina content in the bath. When the anode effect occurs, proper amount of alumina is added and anodes are moved up and down in order to stir the electrolyte and help to dissolve the added alumina. Short circuiting of the cell is also an efficient way to stop the anode effect. The duration of the anode effect might be from 40 seconds to several minutes. Søderberg cells have in average 2 anode effects per day and modern prebaked cells with point feeders have frequency 0.1 per day [1]. Good alumina feeding control decreases the number of anode effects in the cell.

Liquid aluminium is produced at the carbon cathode in the cell [1]. The cathode consists of the carbon container and the aluminium pad. It is common for aluminium electrolysis to call the carbon container as the "cathode". The cathodes can be made from anthracitic, graphitic and graphitized carbon materials [3]. The carbon cathode is not involved in the cathode reaction, but there is an unwanted degradation due to cathode wear as discussed in chapter 1.2.

The aluminium deposition takes place at the surface of the metal pad and the cathodic reaction (2.3) is controlled by the diffusion of aluminium fluoride anions from the bulk of the electrolyte to the surface.

$$AlF_4^- + 3\bar{e} \rightarrow Al + 4F^- \qquad (2.3)$$

The mass transport and concentration gradients in the diffusion layer are illustrated in Figure 2.1 [11]. The sodium cation is transported to the cathode by migration and there is a sodium built up, which results in a higher cryolite ratio in the bath. The cathodic overvoltage is 0.1 V and it is caused by the lower concentration of aluminium fluoride anions at the cathode surface.

The current efficiency is up to 96 % for prebaked cells, while only 85 % for older Søderberg cells [1]. The major losses are caused by dissolution of aluminium into the bath. Dissolved aluminium then reacts with the anode gases and aluminium oxide is formed. Despite the high concentration of sodium in the bath, the Na content in the produced aluminium is low because sodium is less noble than aluminium. Deposition of more noble metals than aluminium also takes place, but it is only a small contribution in lowering the current efficiency, and the purity of produced aluminium is higher than 99.8 %. Iron and silicon are the main impurities in Al, which are introduced to the cell through the alumina feedstock. Other impurities come from the anodes. Elements like phosphorus and sulphur are periodically oxidized and reduced in the cell and thereby reducing the current efficiency [1].

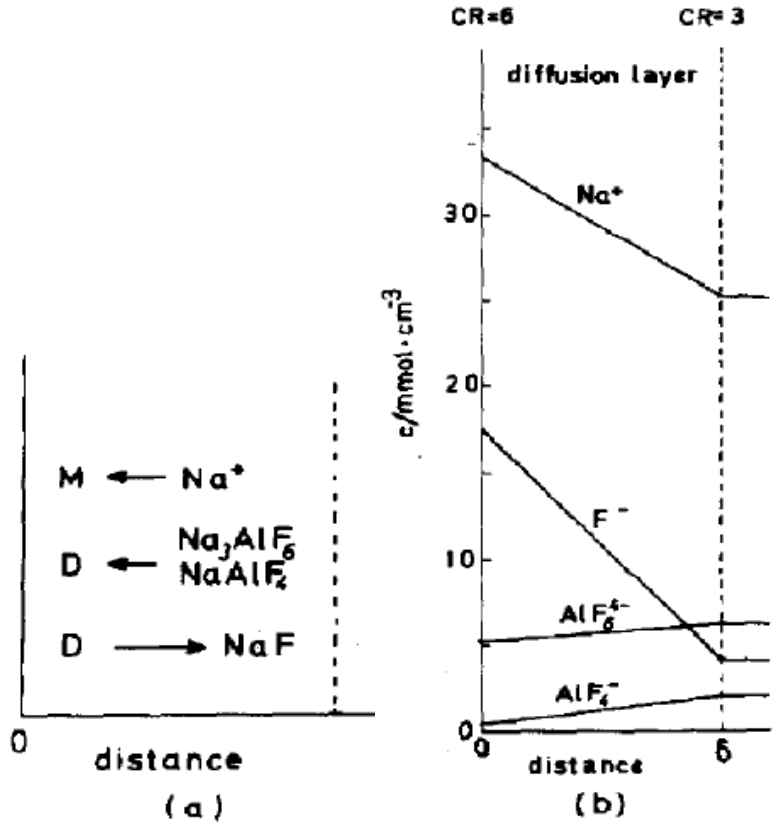

Figure 2.1: a) schematic illustration of mass transfer by migration (M) and diffusion (D), b) calculated concentration gradients of ionic species in the diffusion layer [11].

The interpolar distance in aluminium cells is about 4 cm [1], which is the safe distance to prevent short circuiting and minimize the back reaction, but a reduced interpolar distance is desired to reduce the ohmic losses. The level of the metal pad is not calm, because there are metal waves caused by the strong magnetic field. Modern aluminium cells have high amperage up to 400-500 kA, which is accompanied by strong magnetic field. The magnetic field must be compensated and this is done by a parallel set up of the cells, where the magnetic fields from each cell cancel out each other. The voltage drop in the bath is the main contribution to the overall cell voltage and the aluminium smelters are trying to reduce the ACD in order to save energy by stabilizing the metal pad. This can be done by improved magnetic field compensation and innovative cell design, especially new cathode design with modified topography [12]. Stability measurements of the newest test cells have shown that the anode –cathode distance (ACD) can be reduced down to 2 cm [13]. The interpolar distance is important also for the heat balance of the cell, the cell temperature is kept by resistance heating. It is necessary to keep the desired temperature gradient at the sidewall in order to have a frozen ledge with a certain thickness. The voltage drop in the bath is about

1.7 V and the decomposition voltage for alumina is 1.2 V. The cathode reaction is diffusion controlled and the concentration overvoltage is about 0.1 V. Relatively high overvoltage (0.3-0.4 V) is observed on the anode. Overall voltage in the cell is 4 – 4.6 V, but with latest innovations it is possible to reduce cell voltage down to 3.7 V [12]. The specific power consumption is 12-13 kWh/kg per produced aluminium.

The main emissions from Hall-Héroult cells are CO_2 from the anode reaction and fluorides from the bath [1]. The emissions can be divided into gaseous and particulates. The dominant vapour species above the electrolyte is $NaAlF_4(g)$. Fluorides then react with moisture and HF is formed, which is the major gaseous component present in emissions after CO_2 and CO. Emission of particulates consists of fluorides and carbon dust. Søderberg cells have in addition gas release from the anode baking. Modern prebaked cells are equipped with close-fitting hoods to collect the evolved gases. The gases are sucked from the cell and about 99 % of HF emissions are collected [1]. Dry alumina scrubbers are used and gaseous fluorides are captured by chemisorption on the primary alumina. The residual gases leave the scrubber through a bag filter, where the particulate emissions are captured. The reacted alumina from the scrubbers, the so called secondary alumina is fed to the cell. Thus fluorides are recycled, but also impurities are returned back to the cell. The accumulation of the impurities means that current efficiency in the cell is decreasing with the age of the cell.

The principle of Hall-Héroult process is basically the same since the technology was invented [1]. Increased amperage, modifications of the cell materials, improved process control and absorption of the emissions are the main improvements over time. The introduction of inert anodes may change the technology dramatically [1], but these are still in the stage of research. The principle of the inert anodes is that oxygen is evolved instead of CO_2 at the anode. Inert anodes are not consumed in the anode reaction, but there is reduction of oxide anion from oxygen containing species in the bath. The overall cell reaction will then be changed to:

$$1/2\, Al_2O_3 \rightarrow Al + 3/4\, O_2 \qquad \text{E=2.2 V} \qquad (2.4)$$

The potential of the decomposition of alumina is then 1 V higher compared to reaction (1.1), but the inert anode overvoltage is about 0.3-0.4 V lower. Despite the fact that inert anodes are not consumed, they will undergo slow degradation. Potential inert anode materials are metals, ceramics or cermets (ceramic metal composites). The problem of metals is oxidation at higher temperatures in the presence of oxygen, while oxide ceramics have low electric conductivity and certain solubility in cryolite [1]. Metal inert anodes should be covered by a dense oxide layer in order to protect the metal from oxidation [1]. The growth of the layer should be balanced by its dissolution into the bath. The rate of corrosion is important not only for the lifetime of the anode, but especially for the purity of the

produced aluminium. The inert anodes consist of metals, respectively oxides, which are nobler than aluminium. They are therefore preferably deposited on the cathode after their dissolution into the bath.

Another innovation, which can improve the technology, is the introduction of the inert, wettable cathodes [14]. The traditional carbon anode is not wetted by liquid aluminium and in order to maintain the pool of aluminium flat and stable, the height of the aluminium pad must be fairly thick (10-40 cm). When a wettable cathode is used, only a thin film of aluminium can be maintained and the interpolar distance can be reduced. The choice of the material is a critical issue in the environment of molten cryolite and molten aluminium. Titanium boride was suggested as a wettable cathode material by Ransley [14]. A high phase pure TiB_2 cathode is required in order to avoid intergranular corrosion. The solubility of TiB_2 in Al is in order of 10^{-5} wt% [15]. Thus the theoretical wear rate should correspond to 0.2 mm per year. One of the challenges is the high price of the material. The company Moltech tested the application of TiB_2 coating on a conventional carbon cathode [16]. This "TINOR" coating is made from slurry of a TiB_2 powder and a colloidal aluminium hydrate, acting as a binder. The lifetime of this coating was proposed to be 2-4 years, and penetration of the bath into the cathode was suggested to be slowed down.

One of the novel cell designs with wettable cathode is drained cathode cells [17]. The principle of these cells is sloping cathodes with a channel between them, where the produced aluminium is collected. The surface of the cathodes is covered by a thin flowing film of aluminium. Thus a very low anode-cathode distance is possible, which means that the cell voltage can be reduced leading to lower energy consumption of the process.

Chapter 3

3 Cathodes in the aluminium industry

3.1 Carbon materials

Carbon has atomic number six and a molar weight of 12.011 g/mol. Carbon consists of the isotopes ^{12}C, ^{13}C and ^{14}C and has the electron configuration $1s^2$, $2s^2$, $2p^2$, thus 4 valence electrons are available for formation of chemical bonds. The C-C bond is very stable and this is the reason why carbon is able to form a large variety of allotropic modifications and organic compounds [18].

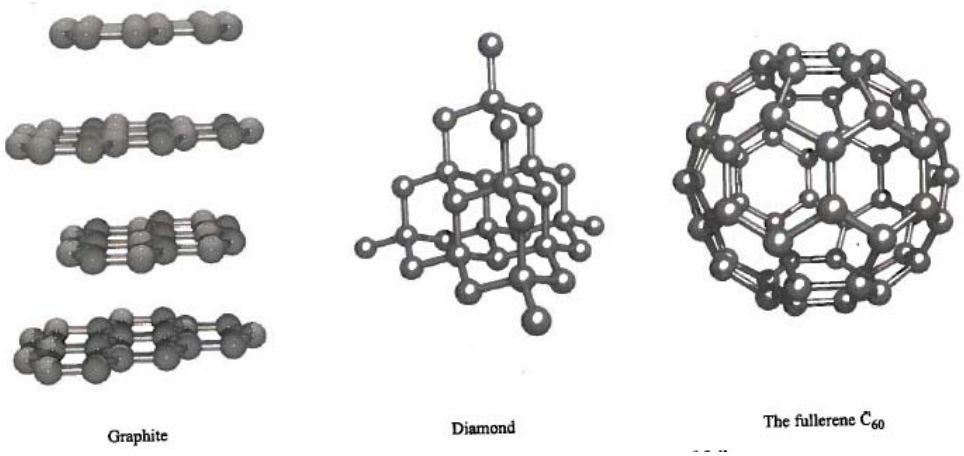

Figure 3.1: The structures of three allotropic modifications of carbon a) graphite, b) diamond, c) fullerene C_{60} [19].

Diamond consists of tetragonal bonding via sp^3 hybridization. It is the hardest known material so it is used for cutting and grinding. The thermal conductivity of diamond is very high, and the electrical conductivity is very low. Natural diamond is formed deep in earth mantle at high temperature and pressure. Synthetic diamond is synthesized at high temperatures and pressures, which is used mainly for cutting and brushing tools. Fullerene is a spherical molecule made of pentagonal and hexagonal C rings. Typical molecular forms of carbon have the compositions C_{20}, C_{60} and C_{70}. Graphite is the most common modification of carbon. It consists of layers of graphene with a hexagonal pattern of sp^2 hybridized C. Within the layer, each atom is bonded with three other atoms via the sp^2 hybridization, thus hexagonal rings are formed. Layers are connected by weak interplanar van der Waals bonds. Graphite is an anisotropic material, and the thermal and the electrical conductivity is high along the layers, because of free π-electrons, and poor perpendicular to the layers along the long c-axis [18].

3.2 Making of carbon cathodes

3.2.1 Raw materials

Cathode blocks are generally made of dry aggregate (coke, graphite or anthracite) and the binder (coal tar pitch) [3]. Petroleum coke is a product of crude oil processing. Residues of the distillation and cracking of the oil are the feeds for the coking process, where the heat treatment at temperatures about 500 °C takes place. The volatiles are evolved and planar aromatic molecules grow by polymerization and condensation reactions. The properties of the feedstock and coking parameters like heat up rate, temperature and dwell time are determining the properties of the coke. Sponge coke or regular coke is used for making anodes for the Al industry. Shot coke is made of asphaltenes containing feedstock and consists of small isotropic particles (2-3 mm) with a smooth surface and a high hardness (Figure 3.2). Shot coke is used for making of graphitized cathodes because of its good graphitizability, hardness and abrasion resistance.

Figure 3.2: Shot coke- used as an aggregate for making of graphitized cathodes [3].

Needle coke is made from highly aromatic feed, which results into highly anisotropic coke [3]. It is the most expensive type of coke with the best graphitizability and is used in the steel industry for making of the graphite electrodes with high electrical conductivity. Shot coke is less graphitizable than needle coke, but the choice of shot coke for graphitized cathodes is due to the higher abrasion resistance. The largest fraction of coke production is fuel coke, which has a low coking temperature and a high content of volatiles and can be used only as an energy carrier. The product of coking, the green coke, is heat treated at 1200-1350 °C in the process of calcination [3]. The green coke undergoes thermal

dehydrogenation and shrinkage and the density and electrical conductivity are increased. Two types of calciners are used, rotary kiln calciner and rotary hearth calciner. The kiln calciner has longitudinal temperature gradient and heat up rate of the feed is slower compared to the hearth calciner.

Anthracite is geologically the oldest coal material, which is about 300 million years old [3]. It is harder and has lower volatiles content compared to "younger" coal materials. It has the highest coal rank with the carbon content around 92-98 % [3]. Natural anthracite needs to be calcined to increase the electrical conductivity. There are two types of calcined anthracite made by two different ways of calcination; gas calcined anthracite (GCA) and electro calcined anthracite (ECA). GCA is calcined in a rotary kiln heated by gas, where the temperature inside is up to 1350 °C. ECA is calcined in electro-calciner, where the heat is generated by resistive heating. The temperature in the center of the calciner reaches more than 2500 °C, but only about 1000 °C on the border. GCA is not graphitized (low temperature) and relatively hard. The properties of ECA are uneven due to the temperature gradient in the calciner. The product is a mixture of hard, not graphitized and soft, graphitized calcined anthracite. ECA has higher electrical and thermal conductivity, but lower abrasion resistance.

Coal tar pitch is a product of bituminous coal processing [3]. The coal is heat treated and the volatiles are evaporated. The solid product is metallurgical coke and the liquid by-product is coal tar, which is then distilled and the residue of the distillation is coal tar pitch. Binder pitch is a mixture of thousands of organic compounds, mainly polyaromatic hydrocarbons. The properties are close to "liquid carbon", it has no sharp melting point and the viscosity is changing continuously with temperature. The job of coal tar pitch is to be a liquid with good wetting of the aggregate particles at temperature of mixing (150-200 °C). During the baking process, the binder should release the volatiles evenly and create inter-particle bonds with the aggregates.

Ramming paste is a carbonaceous material used for sealing the joints between the cathode blocks and also between peripheral blocks and the sidewall [3]. The paste is plastic at installation temperature and undergoes baking during heating. Cushioning effect is another purpose of the ramming paste. The cathode blocks are expanding during heating, but the volatiles from the paste are released, which leads to shrinkage. Thus the ramming pastes have a so-called negative coefficient of thermal expansion. Two main types of ramming pastes are known. Hot ramming paste is a mixture of coal tar pitch and anthracite or graphite. The influence of filler selection on the final properties is the same as for cathode blocks. Hot ramming pastes are rammed at high temperatures. This operation is associated with exposure to volatiles. Room temperature or tepid pastes are dominant nowadays. Softeners can be added to decrease the softening point. The ramming operation is cleaner and safer. These are based on coal tar pitch with addition of softeners, which make the paste rammable at room temperature. The modern, high amperage cells used to day need to release more heat, thus ramming pastes with high thermal conductivity are

desired. This can be accomplished by using synthetic graphite instead of anthracite as filler [3].

3.2.2 The manufacturing process

Dry aggregate (coke, graphite, anthracite) and the coal tar pitch are mixed at temperatures 150-200 °C [3]. The particle size distribution of the aggregate is important and the coke should occupy as much space as possible because it is cheaper than the binder. Blocks can be formed either by extrusion or vibropressing. During extrusion the particles tend to order in the direction of extrusion and it results into macro anisotropy, which means that the electrical, thermal and mechanical properties are different when measured in different directions. Vibration orders the aggregate particles randomly and properties of such a block are isotropic. The shaped cathode blocks are baked in ring furnaces at temperatures around 1200 ºC. The heating up is relatively slow in order to avoid any local weaknesses, which might result in cathode failure [3]. Graphitized cathodes are prebaked at around 900 ºC and then may be impregnated with the pitch to reduce the open porosity of the block. These blocks are graphitized in Acheson furnaces at temperatures up to 3000 ºC [3]. The differences in making of the main types of cathodes are summarized in Figure 3.3.

As the temperature is rising, residual hydrogen and other volatiles are released and the binder is calcined at about 1200 ºC. At higher temperatures (1500-2000 ºC), nitrogen and sulfur are evolved from the coke and it may result into sulfur puffing [3]. Finally, the graphitization takes place and crystalline growth predominates, and the thermal and electrical conductivity reaches an optimum at 3000 ºC. The changes in graphitizable carbon material during heat treatment are illustrated in Figure 3.4.

Prebaked cathode blocks were traditionally made from anthracitic aggregates. Anthracitic cathodes are made from anthracitic aggregates (GCA and ECA). Graphitic blocks are also made from anthracitic aggregates with 30-50 % addition of graphite [3]. Most common cathode blocks used by aluminium smelters these days are graphitized blocks. The aluminium producers have increased the amperage of the cells and switched to graphitized blocks because of their higher electrical conductivity [3]. Needle coke is the type of petroleum coke with the best graphitizability, but more isotropic, shot coke is preferred. Shot coke is less graphitizable than needle coke, but the reason for this preference is much higher hardness. Mechanical abrasion resistance of the cathode is then becoming better and the lifetime of the cell can be longer [3].

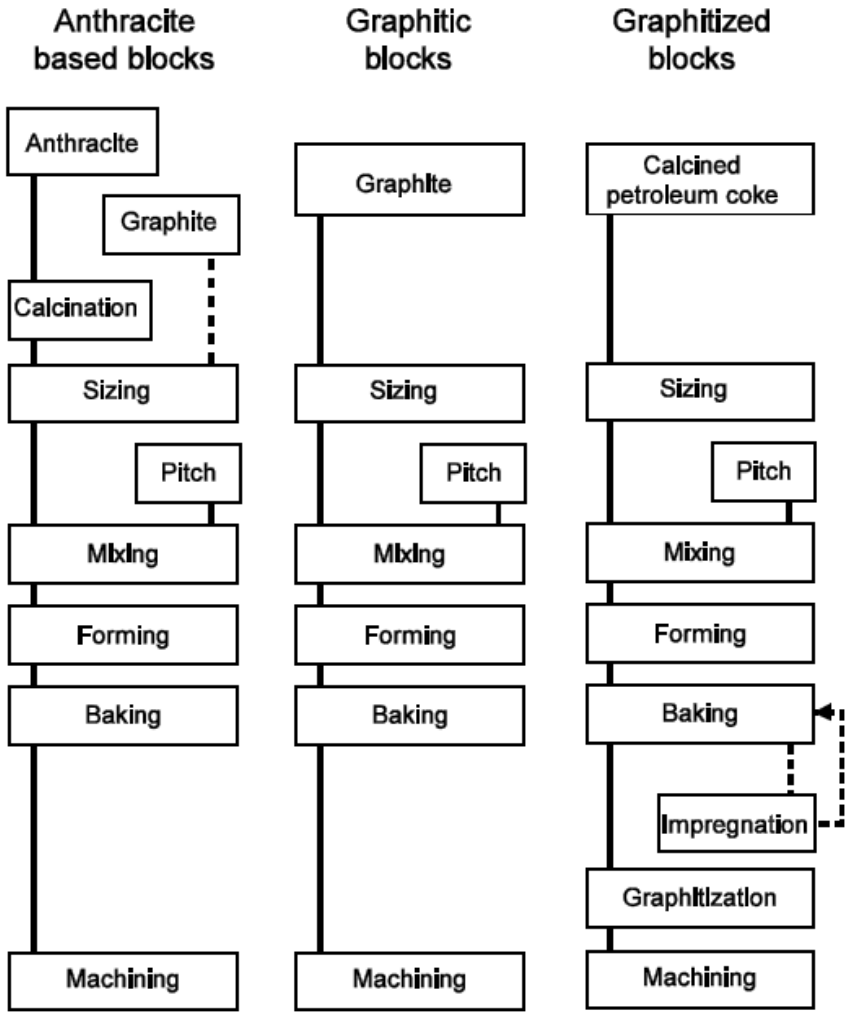

Figure 3.3: Steps in making of different types of cathode blocks [7].

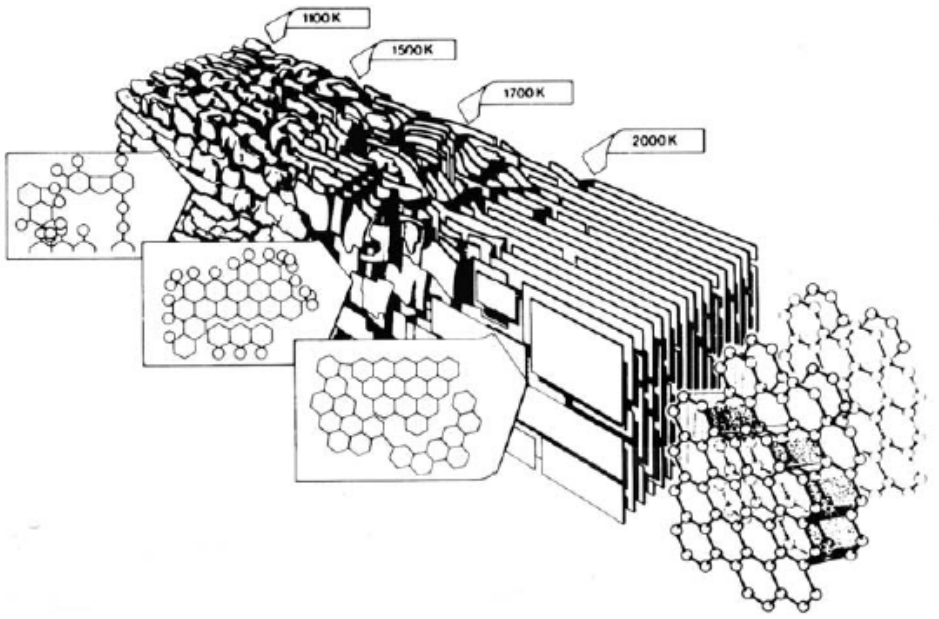

Figure 3.4: Changes in graphitizable carbon during heat treatment [20].

The cathode blocks can be classified into three groups [3]:

- **Anthracitic** or **Amorphous:** The filler is a combination of graphite and anthracite (30-50 %). The block is baked at ~1200 °C.

- **Graphitic:** The aggregate is graphitized petroleum coke or scrap electrode graphite. The block is baked at ~1200 °C.

- **Graphitized:** Both filler and binder are made of graphitizable materials. The block is graphitized at temperatures up to 3000 °C. It means all block is graphitized including the binder.

The main properties of the most common types of cathode blocks are listed in Figure 3.5. The graphitized cathodes are more expensive and have higher wear rate than anthracitic cathodes, but these costs are balanced by the lower energy consumption [7]. The graphitized blocks have 3-5 times higher electrical conductivity, which means a lower voltage drop [22]. This parameter becomes more important as the current densities of the industrial cells are rising in order to increase the productivity. Low coefficient of thermal expansion is an advantage for heating up and high thermal conductivity is important for the heat balance and the formation of the side ledge at the cathode. Graphitized cathodes are also less sensitive to sodium intercalation and expansion, because the well ordered graphite structure with delocalized π-electrons does not attract sodium so much as less ordered carbon.

COMPARATIVE PROPERTIES	AMORPHOUS BASED	GRAPHITIC	GRAPHITIZED
Price **	1	1.5 to 1.8	2 to 3
Abrasion resistance	excellent	good	poor
Thermal shock resistance	acceptable	very good	excellent
Thermal conductivity	moderate	high	very high
Electrical resistance			
- room temperature	high	low	very low
- pot temperature	medium	very low	very low
Crushing strength	high	adequate	low
Swelling/sodium	adequate	low	very low

**) Subject to variation

Figure 3.5: Comparison of the main types of cathode blocks [7].

3.2.3 Cathode design

Monolitic carbon lining, which is illustrated in Figure 3.6a, was initially used in the Hall-Héroult process. A green carbonaceous plastic body, which consisted of tar binder, anthracite, petroleum and metallurgical coke, was rammed into place and this green paste was baked during the operation. The installation costs were low, but it was hard to obtain a high quality, defect free block since volatiles were released during heating. Local weaknesses might lead to formation of pothole and cathode failure. The carbon lining was in direct contact with the steel tank, which used to serve as a cathodic connection. Monolithic blocks are no longer installed today, and typical cathode linings, shown Figure 3.6b, are built of smaller, prebaked carbon blocks. These blocks were traditionally made of gas calcined anthracite or metallurgical coke as filler. Ramming paste is used only between the prebaked blocks as a sealant and for cushioning effect. The prebaked blocks are thermally inert during preheating of the cell, only the ramming paste undergoes baking. The prebaked carbon blocks appeared the first time in 1920 in Saint-Jean-de-Maurienne, France [21]. The amperage of these cells was 20 kA. Later, in 1927, steel collector bars were inserted horizontally in the cathode bottom. The cathode voltage drop was reduced by 0.6 V and the potlife was extended by more than 2 years. Since the steel tank was no longer the current carrier, refractory and insulation materials could be installed in order to reduce the energy consumption and to serve also as a protection of the steel shell. Figure 3.6c shows an advanced cathode lining, which is also built of small carbon blocks without ramming paste between the blocks. The cathode blocks are glued together and high precision is needed for machining the blocks, they must fit together perfectly prior to gluing. The installation is very expensive and difficult to perform.

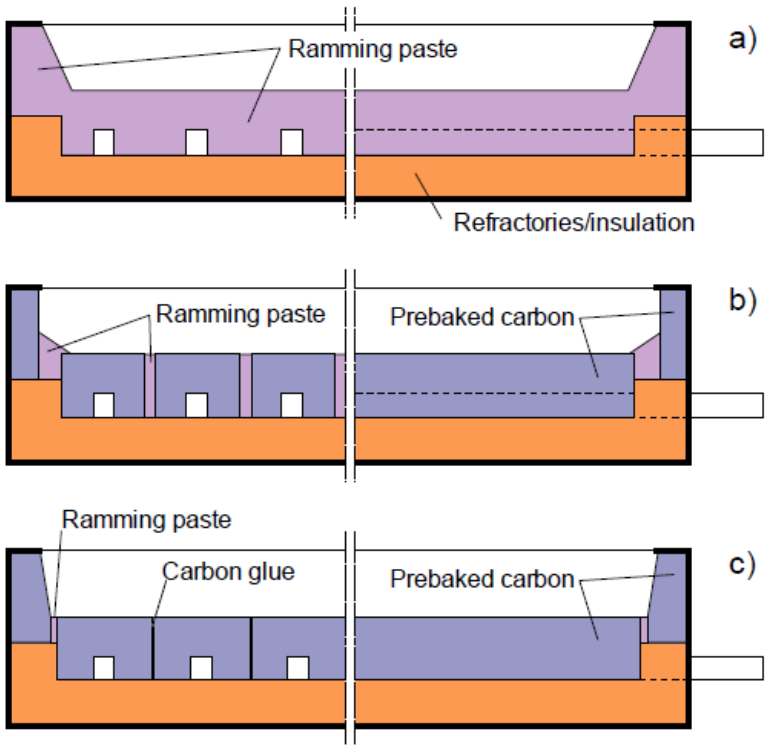

Figure 3.6: Types of cathode construction: a) monolithic cathode lining b) prebaked cathode blocks with ramming paste joints c) glued prebaked blocks, ramming paste only between the periphery blocks and the sidewall [3].

The supply of electrical current to the carbon cathode blocks is provided by iron collector bars. Good and uniform contact is important to give a low electrical contact resistance. The installation of the collector bars is the main challenge. Coefficient of thermal expansion of iron is several times higher than for carbon, which means that the collector bar might crack the carbon block during heating up. The rodding can be done at room temperature using ramming paste. This method is not expensive and the occurrence of cracks in the carbon blocks is rare, but the contact electrical resistance is relatively high. The most common method is cast iron sealing. The collector bar is preheated to 500-600 ºC and cast iron with temperature 1400 ºC is poured into the slot. The cast iron provides a high electrical conductivity, but the cracking in the corners of the slots is a constant problem. Another method is thermal expansion fit, where no sealant is used and a high precision is needed in order to get the proper contact and to avoid cracking at the same time. The contact pressure must be high enough to obtain good electrical contact, but too high pressure might result into cracks in the carbon block [3].

New trend in cathode design is the introduction of cathodes with special topography. The purpose of this innovation is to stabilize the aluminum pad by reducing its velocity. Then the anode-cathode distance can be lowered and the cell voltage can be reduced down to 3.7 V [13]. The current efficiency of such a cell

goes down by 1 %, but still 1 kWh of energy per kilogram of produced aluminium is saved [12].

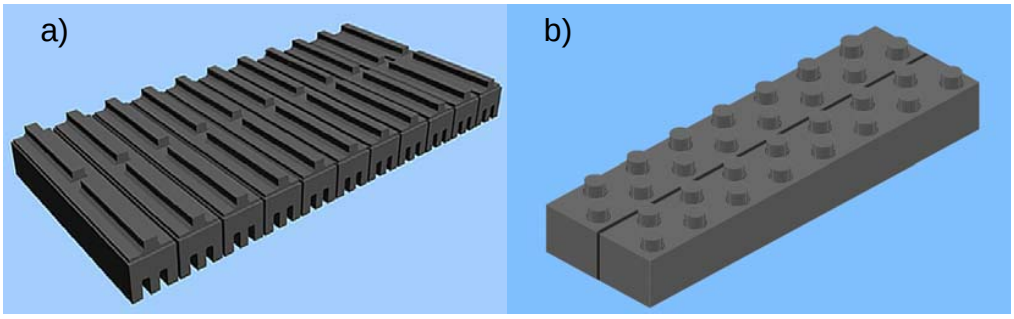

Figure 3.7: New cathode topography with a) ridges and b) cones [12]

3.3 Degradation of cathodes in industrial cells

The carbon cathodes in aluminium industry serve as a container and electrical connection to the liquid aluminium pad, which is the real electrochemical cathode [3]. The carbon block is supposed to be inert and should not take part in the cathodic reaction, but the cathode is worn during the operation of the cells. The average wear rate in industrial cells has been reported to be 2-4 cm per year [23]. When the cathode wears down to the collector bar, the aluminium becomes contaminated by iron and the cell must be shut down. The lifetime of the carbon lining usually determines the lifetime of the cell. The average lifetime can be around 3000 days for older types of cells with lower amperage, but in modern cells with graphitized cathodes and higher amperage, the lifetime has been reduced down to 2000 days [5]. The mechanisms of cathode wear are still not very well understood. There are 3 main categories of mechanisms. The first category is the mechanical wear, where aluminium metal pad is moving due to strong magnetic field caused by high electric current passing through the cell [6]. The magnetic fields are compensated by parallel setup of the cells, but the level of the aluminium pad is still moving. This movement may lead to mechanical abrasion of the carbon cathode. A typical metal pad moving pattern is shown in Figure 3.8. The movement of un-dissolved alumina might also contribute to the wear [24]. The second category of wear is chemical wear. The aluminium pad might react with the carbon cathode and aluminium carbide is formed. Aluminium carbide can be dissolved into the bath and oxidized at the anode [25]. Carbon cathode is not in direct contact with the bath, but a thin bath film may be present between the carbon and the aluminium pad. Kinetics of the dissolution of aluminium carbide into the bath is very important and the mass exchange rate of the bath film is often considered as the rate determining step [26]. Data from operating cells have shown that the wear rate decreases with the increasing height of the metal pad and improved magnetic compensation [23]. The third category of wear is electrochemical wear. Electric

current is passing through the cathode and aluminium carbide may be formed also by an electrochemical reaction at the cathode.

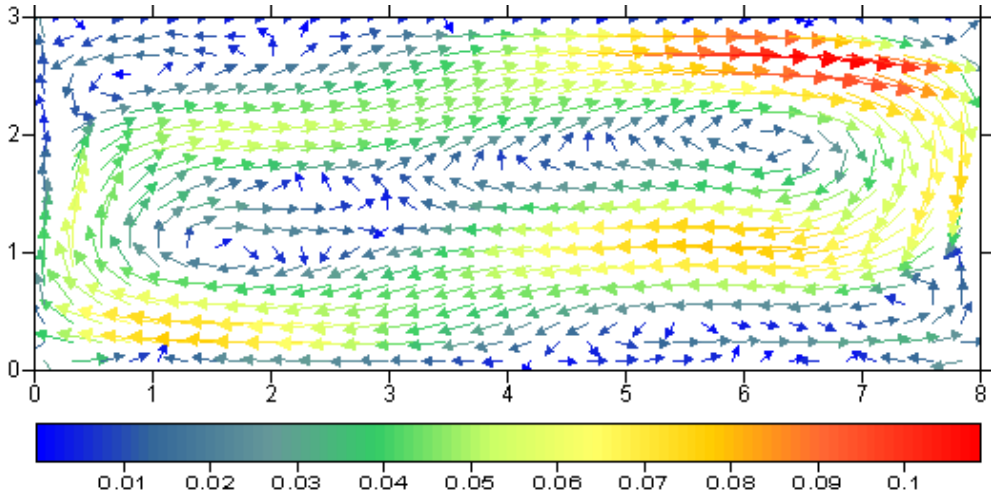

Figure 3.8: Modelling of metal pad movement, moving patterns and local velocities (m/s) [6].

The highest wear is close to the edges, because these areas have the highest local current density and the highest velocity of the metal pad. The exchange rate of the bath film from the aluminium/carbon interface is the highest at the edges, which means faster dissolution of aluminium carbide. Therefore it is difficult to say which effect is the most significant. The ramming paste is worn less preferably than the prebaked blocks and results in a local wear pattern typical for each block, which can be seen in Figure 3.9 [13]. The ramming paste is baked only at the operation temperature of the cell, and it is not graphitized and has a higher wear resistance. The current density is lower in this region, because the collector bar is located in the middle of the prebaked block. Higher wear rate is usually observed near the metal tapping area [27]. The frequent removal of aluminium results in faster movement of the metal pad in this region. Therefore it is convenient to change the tapping position to make the cathode wear more even [27]. The lowest wear is observed in the middle of the cell in the channel between the anodes, especially near the location of the alumina feeding. Un-dissolved alumina is probably protecting these places from the wear [28]. The local higher wear in the vicinity of the alumina feeders might be caused by a periodical dissolution of alumina. Carbon and aluminium carbide can diffuse into the solid alumina [28]. Special type of extreme local wear has been referred to as pothole [29]. These potholes can be initiated by a small crack or flaws in the cathode block. During the operation the potholes are filled with molten aluminium and there is a local turbulence caused by the magnetic field. This makes the wear in the pothole faster than ordinary wear at the surface of the cathode. The pothole often results into early shut down of the cell. However, it is possible to fill the potholes with α-alumina and the lifetime of a cell can be prolonged by one year [30].

The wear in industrial cell is uneven and it varies from place to place [5]. Typical w or double w-wear patterns observed by autopsy of shutdown cells are shown in Figures. 3.9 and 3.10.

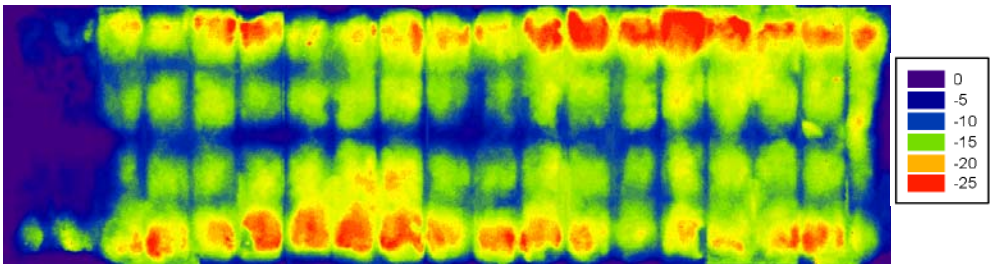

Figure 3.9: Topography of an industrial cathode after shut down [5].

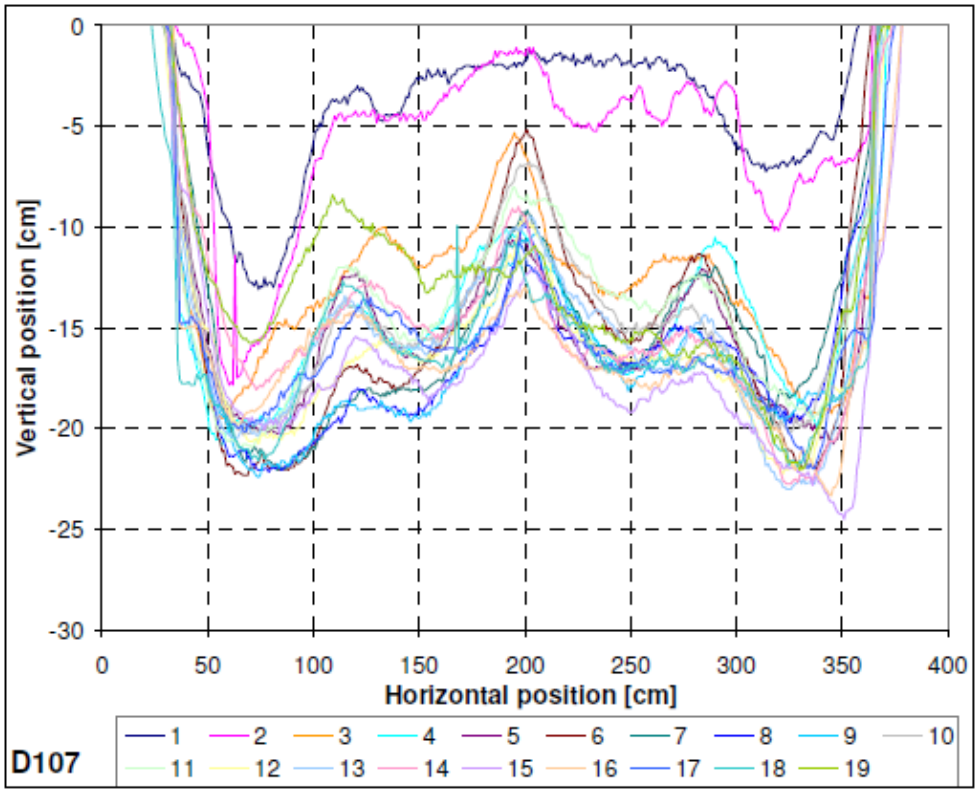

Figure 3.10: Typical double-w wear pattern of an industrial cell [5].

Chapter 4

4 Aluminium carbide formation

4.1 Interaction between aluminium and carbon

Aluminium carbide can be formed by the direct reaction between the two elements.

$$4Al + 3C \rightarrow Al_4C_3 \qquad (4.1)$$

The reaction is thermodynamically favoured (ΔG°= - 147 kJ (970° C) at the temperature corresponding to the operation of the cell [31], but the reaction is kinetically hindered. Lack of direct contact between liquid aluminium and the carbon cathode may hinder the reaction to proceed. It is not possible to form proper amount of carbide suggested by thermodynamics below 1000 ºC without the presence of the bath [8]. However, it is possible to form aluminium carbide also at lower temperatures by reaction of fine carbon and aluminium powder [32]. Aluminium carbide was formed already at temperature lower than melting point of aluminium [32]. The conditions and surface properties are different compared to a flat interface, and the reaction depends very much on the particle size. Etter et al. have reported the formation of aluminium carbide at 750 °C by pressing of liquid aluminium into a porous structure of graphite under vacuum [33].

Aluminium does not wet carbon [34,36] and the wetting angle is more than 90° as it is shown in Figure 4.4a further below. In addition, the surface of aluminium is covered by a thin protective layer of aluminium oxide. The wetting angle thereby becomes higher and corresponds to the wetting of aluminium on alumina. The oxide layer represents a barrier between aluminium and carbon. The reaction is controlled by slow diffusion of aluminium through this layer [36]. Aluminium oxide layer might be removed from the surface mechanically by the volume expansion due to the melting of aluminium as illustrated in Figure 4.1.

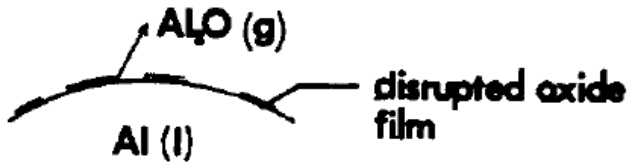

Figure 4.1: Disruption of aluminium oxide layer by expansion due to melting of aluminium [35].

The layer can also be evaporated by the following reaction at higher temperature and/or lower total pressure

$$Al_2O_3(s) + 4Al(l) \rightarrow 3Al_2O(g) \qquad (4.2)$$

The stages of the process and the contact angles of Al/C interaction are described in Figure 4.2a [34]. The initial contact angle between Al and C is characterized by a high wetting angle between Al/Al_2O_3 (θ_0). During the evaporation of the oxide layer, the wetting angle is decreasing. When the removal of the oxide layer is finalized, contact between aluminium and carbon is formed and the wetting is characterized by the wetting angle between Al/C (θ_1). Then reaction between Al and C takes place at the interface and aluminium carbide is formed. The wetting angle decreases during the reaction and the final wetting angle Al/Al_4C_3 (θ_F) is reached.

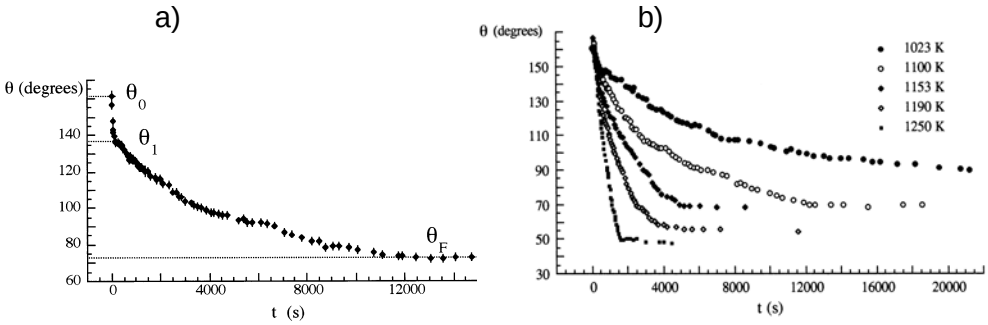

Figure 4.2: Contact angles during Al-C interaction a) definition of contact angles (1100 K) b) contact angles at various temperatures [34].

The evaporation of the oxide layer at 1100 K under vacuum takes couple of minutes, which can be interpreted from the wetting experiments shown in Figure 4.2a [34]. The formation of a carbide layer varies very much with the temperature as shown in Figure 4.2b. It takes less than an hour at 1250 K and about 8 hours at 1000 K. These wetting experiments have been performed under low pressure (10^{-3} Pa). The kinetic data are not directly applicable to the conditions in an industrial cell, but the process of the removal of the oxide layer and the initial stage of aluminium carbide formation can be understood from these experiments. The Al-C wetting properties depend also on the type of carbon material. The higher the atomic density of carbon substrate in contact with aluminium, the higher the adhesion energy and the lower the contact angle. Wetting angle of various carbon materials is decreasing in following order: vitreous carbon > pyrolytic carbon > graphite > pseudosingle crystal. The roughness of the interface is also important, and a polished surface is better wetted than a rough surface [34].

Carbon has a low solubility in aluminium just above the melting point of aluminium, as shown in the Al-C phase diagram displayed in Figure 4.3a. The solubility at the operation temperature (around 1000 ºC) is 40 ppm [37], which is 2-3 orders of magnitude lower than the solubility of Al_4C_3 in cryolite. If the mechanism of carbon cathode dissolution into the aluminium pad is considered, the calculated wear rate would be 5-15 mm per year [38]. This might contribute to the

wear rate in the industrial cells (2-4 cm/year), but cannot be the dominant mechanism [3]. Figure 4.3b shows the solubility of C in Al at temperatures over 2000 ºC, where the solubility goes over 20 at% [39]. This is one of the main challenges in the alternative carbothermic reduction technology [39].

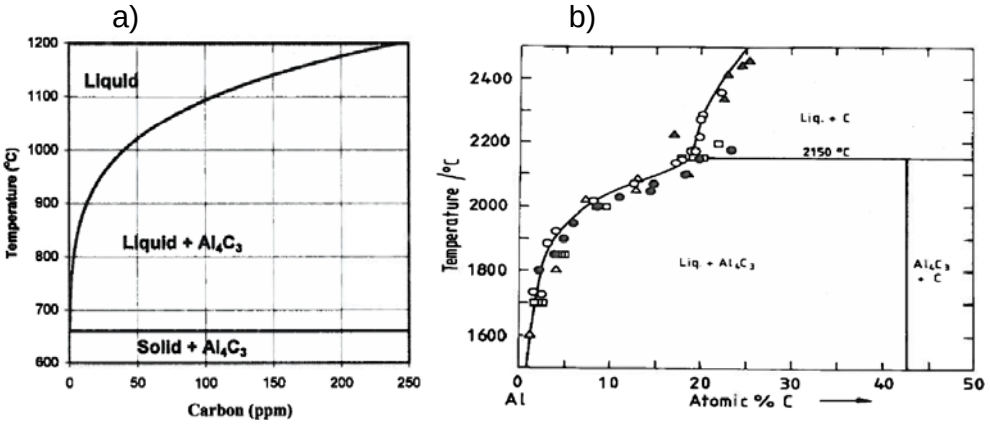

Figure 4.3: Carbon solubility in aluminium at a) temperatures relevant to electrolysis [37] b) higher temperatures relevant for carbothermic reduction [39].

4.2 The influence of cryolite

Cryolite has a catalytic effect on the reaction between aluminium and carbon. It can act as a solvent of the aluminium oxide protective layer, which represents the barrier for the direct reaction [9]. It is also a wetting agent since a film of cryolite on the aluminium-carbon interface makes perfect wetting (≈0 deg.) [36]. The results of experiments performed by Dorward are shown in Figure 4.4. Cryolite itself does not wet carbon materials, and a wetting angle of 115° was reported [36]. Addition of aluminium oxide to the cryolite changed the properties from non-wetting to wetting (65°), while addition of aluminium made the wetting almost perfect (≈0 deg.). The formation of aluminium carbide was suggested as the reason for this change. The high atomic density of aluminium carbide results in better adhesion.

When the carbon is cathodically polarized, the wetting of cryolite (containing alumina) improves with current density and it was also explained by aluminium carbide formation [40]. Initial wetting angles without polarization were about 90° and were reduced to less than 20°, depending on the carbon material.

Another role of cryolite is that it also may act as a solvent for aluminium carbide [41]. A layer of Al_4C_3 formed at the C/Al interface represents also a barrier against mass transfer. The solubility of aluminium carbide in cryolite is shown in Figure 4.5. Maximum solubility is 2.15 wt% and it is dependent on the cryolite ratio.

Additives like Al_2O_3 and CaF_2 are decreasing the solubility of aluminium carbide in cryolitic melts [41].

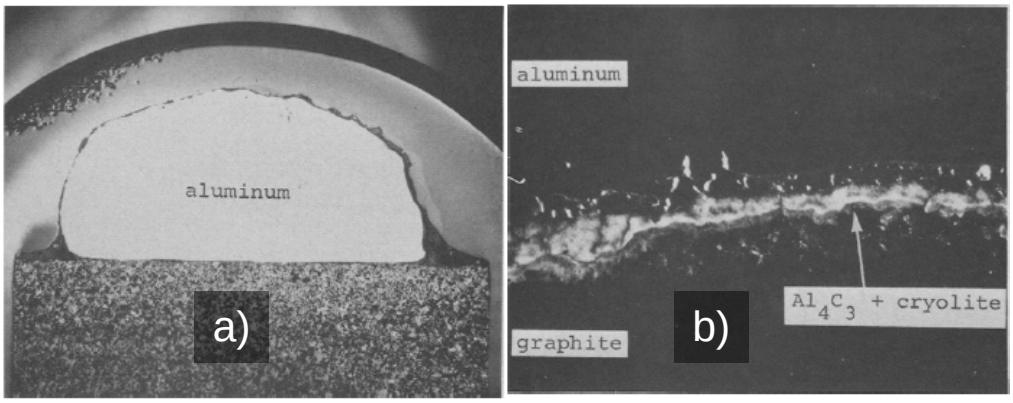

Figure 4.4: The interaction of aluminium and carbon, 5 min. experiments a) without cryolite b) with cryolite [36].

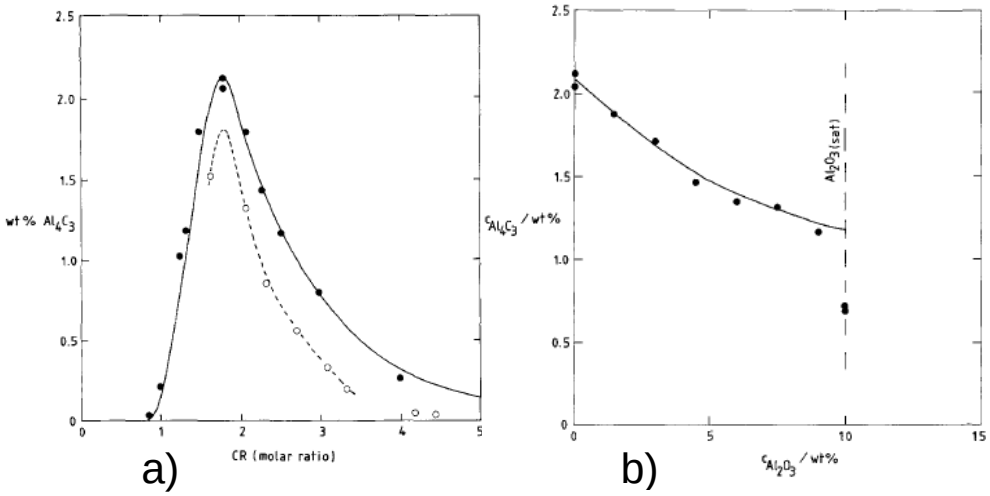

Figure 4.5: Solubility of aluminium carbide in cryolite as a function of a) cryolite ratio, b) alumina content c) content [41].

The dissolution of aluminium carbide in cryolite has been suggested by the following reaction

$$Al_4C_3 + 5AlF_3 + 9NaF \rightarrow 3Na_3Al_3CF_8 \qquad (4.3)$$

The stoichiometry of this reaction corresponds to CR=1.8, which is the value of CR where the solubility of aluminium carbide reaches a maximum [41]. The influence of cryolite ratio on the cathode wear was studied by Patel [2]. Higher excess of

AlF_3 (lower CR) increased the cathode wear and the results were discussed with respect to two factors: The solubility of aluminium carbide is higher at lower CR and the dissolution of aluminium carbide is thereby faster. Higher excess of AlF_3 also means a higher concentration of AlF_4^- and formation of another aluminium containing ion, which are proposed as the active specie for electrochemical formation of aluminium carbide. However, these experiments have been performed in inverted cathode test cell, where the bath is always in direct contact with the carbon cathode and allows faster dissolution. In industrial cells the aluminium pad, which is present on the cathode, hinders the dissolution of aluminium carbide into the bath. The influence of bath composition is not so significant and the wear rate probably depends on the exchange rate of the bath at the aluminium pad-carbon interface [23].

Formation of a dense carbide layer on the carbon surface might slow down the formation of carbide dramatically. Grjotheim et al. studied aluminium carbide formation by direct reaction of Al and C in cryolite melts without electrolysis [42]. The carbon crucible, where the experiment was performed was crushed after the experiment and reacted with an acidic solution. Aluminium carbide was then analysed quantitatively (both solid and dissolved) by barometric analysis and gas chromatography. The amount of produced carbide was increasing parabolically with the reaction time until it saturated as shown in Figure 4.6a. The reaction proceeded until saturation of cryolite melt and a formation of an aluminium carbide layer at the carbon surface was suggested. The layer developed until a certain thickness and represented a diffusion barrier. Figure 4.6b demonstrates the strong correlation between the amount of produced carbide and the porosity of the carbon material.

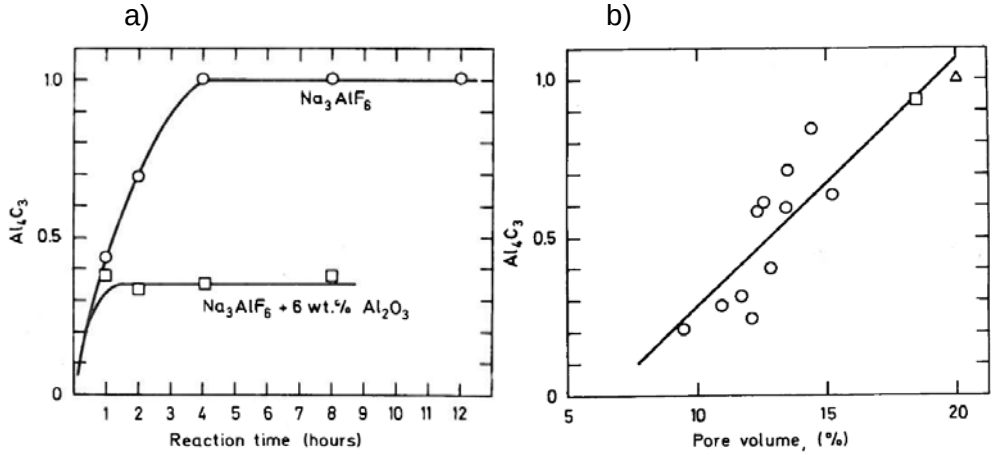

Figure 4.6: Relative amounts of produced aluminium carbide as a function of a) time b) porosity of carbon material [42].

Grjotheim et al. suggested also the formation of Al_2OC in cryolite with higher content of alumina [43]. However, this compound is stable only at temperatures

above 1700 °C and compound Al_4O_4C is the only possible oxycarbide which is stable at the operation temperature [44].

4.3 Electrochemical formation of aluminium carbide

Electric current is passing through the cathode and electrochemical formation of aluminium carbide has also been suggested by the reaction

$$3C + 4Al^{3+} + 12\bar{e} \rightarrow Al_4C_3 \qquad (4.4)$$

A strong correlation between local wear rate and local current density has been observed in industrial cells [5]. As the amperage was rising the average lifetime of the cathode and the cell went down from 3000 to 2000 days [5, 23].

In laboratory scale the cathode wear has been studied in so-called "inverted cell", where the carbon bottom with aluminium pad is anodically polarized and the cathode on the top is in direct contact with the bath. Illustrations of two inverted cells are shown in Figure 4.7. Rotation of the cathode is possible to simulate the metal pad movement in industrial cells. The reduced aluminium falls down to the anode and the cathode surface is always exposed directly to the bath. It leads to faster dissolution of aluminium carbide from the carbon surface and thereby to faster wear rate. Typical wear rate in inverted cell is around 50 cm/year (2-4 cm/year in industrial cell) and it is possible to quantify the wear precisely already after 24 hour experiments. The influence of parameters such as the current density, the bath composition, the rotation speed and the type of carbon materials is possible. Patel was using the setup shown in Figure 4.6a, but uneven current density led to uneven wear, and the measurement of the wear rate was challenging. Vasshaug introduced alumina linings to the top and the bottom of the cathode and well defined surface with even current density was accomplished [45]. However, the lining from alumina suffered in the cryolitic bath due to dissolution and further improvement by Tschöpe et al. was conducted by using inert silicon nitride lining [46].

Patel investigated the influences of various parameters on cathode in inverted cell and the current density was found to be the most significant [2]. The wear rate in inverted cell is rising parabolically with current density and reaches the asymptotic value as shown in Figure 4.7 [45,47]. A higher current density means a lower current efficiency for the carbon consumption [45]. The process is limited probably by the aluminium carbide dissolution into the bath and the mass transfer through the electrolyte.

However, aluminium carbide can be deposited on the carbon cathode from the bath, without direct involvement and contact with aluminium. The molten cryolitic bath with dissolved alumina contains various aluminium, fluorine and oxygen complexes which might be involved in electrochemical reactions. Gudbrandsen et

al. studied the influence of the current density on the cathode wear [48]. The wear rate was rising parabolically with the current density and reached an asymptotic value. A cathodic carbon consumption reaction was suggested, where the reactions of aluminium carbide formation (4.4) and dissolution (4.3) were combined in one reaction, yielding the following total reaction

$$C + 3AlF_3 + 4Na^+ + 4\bar{e} \rightarrow Na_3Al_3CF_8 + NaF \qquad (4.5)$$

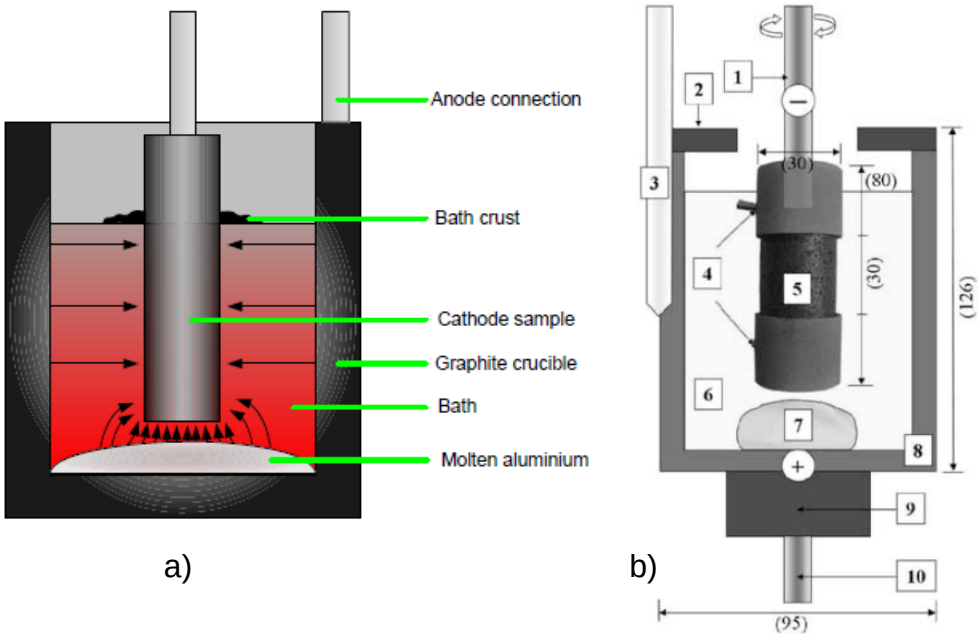

Figure 4.7: Inverted cell setups by a) Patel [2] b) Tschöpe et al. [46].

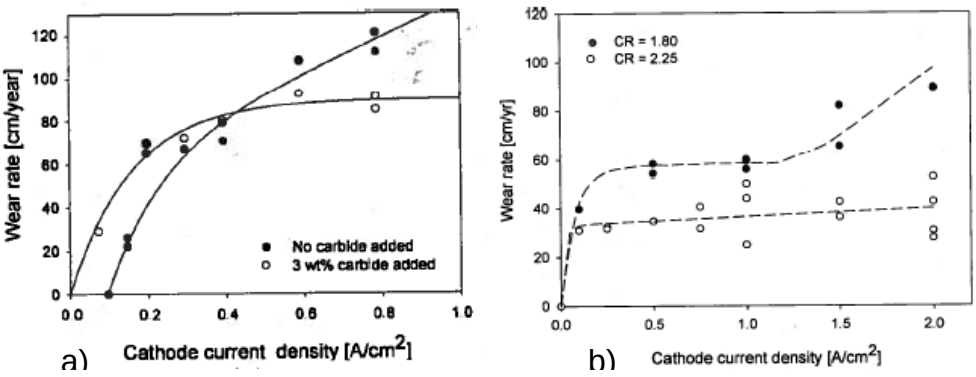

Figure 4.8: The cathode wear rate as a function of current density a) Liao and Øye [47] b) Vasshaug [45].

Aluminium carbide is known to be an electrical insulator [49], and a carbide layer formed at the cathode surface will represent a resistive barrier. Pietrzyk examined possible carbide layer in situ during electrolysis and concluded that there was a carbide layer at the carbon surface [8]. Solheim and Tschöpe have suggested that the carbide layer is discontinuous and consist of "carbide islands", which will behave as current shields [50]. A simulation of the carbide island and the current density distribution are shown in Figure 4.9. The current density and the wear rate are higher in regions not covered by carbide, especially on the edges of the carbide islands. Excessive wear on the edges of the carbide islands was suggested to lead to pitting and the formation of potholes.

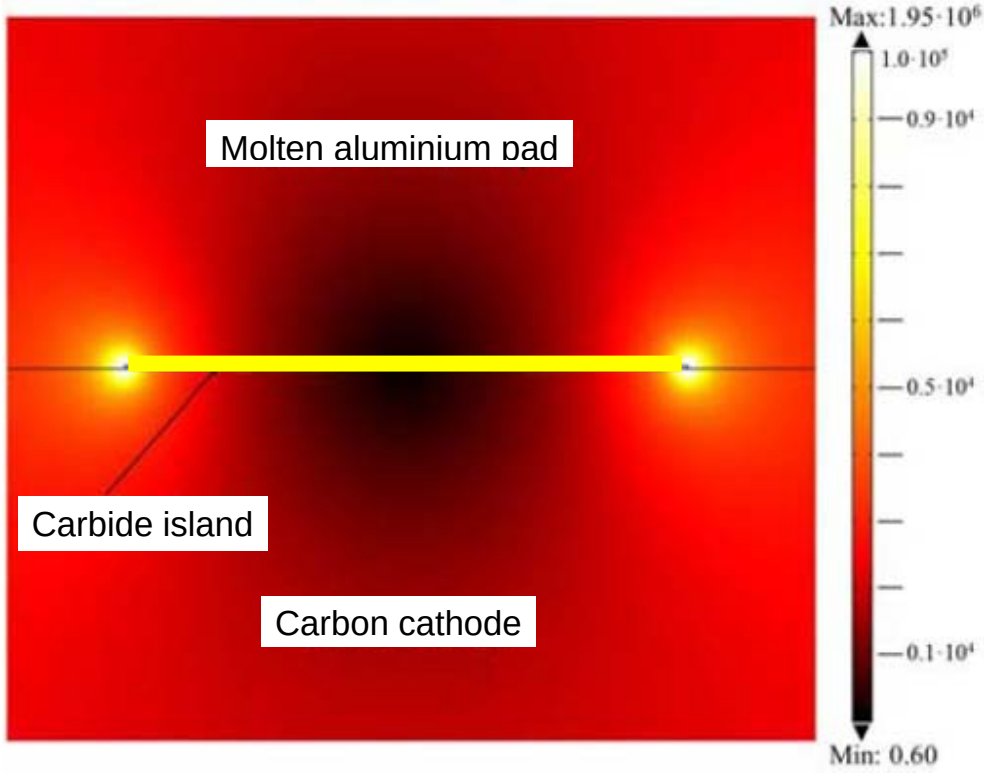

Figure 4.9: Calculated current densities around "carbide island" (2 cm diameter, 100 μm thick [50].

Electrochemical measurements of aluminium carbide deposition are challenging, because the current efficiency of aluminium carbide deposition is low and the potential is close to the potential of reaction (1.1). It is also difficult to identify the aluminium carbide peak by voltammetry. Reported cyclic voltammetry of carbon in cryolitic melt is shown in Figure 4.10. The anodic peaks of aluminium oxidation and also the oxidation of aluminium carbide present in the bath after electrolysis was detected [45]. The oxidation of penetrated sodium might be another process taking place, but it is a slow process not likely to happen at higher sweep rates. Deintercalation of sodium might also be visible as an anodic peak. In the cathodic

direction it was difficult to see the peak of aluminium carbide formation due to similar potential and very low current efficiency compared to reaction (1.1). Østrem has used Al^{3+}/Al reference electrode for electrolysis and observed aluminium carbide formation at positive potentials [51]. The potential of aluminium carbide formation was suggested to be a little bit higher than the potential of aluminium deposition.

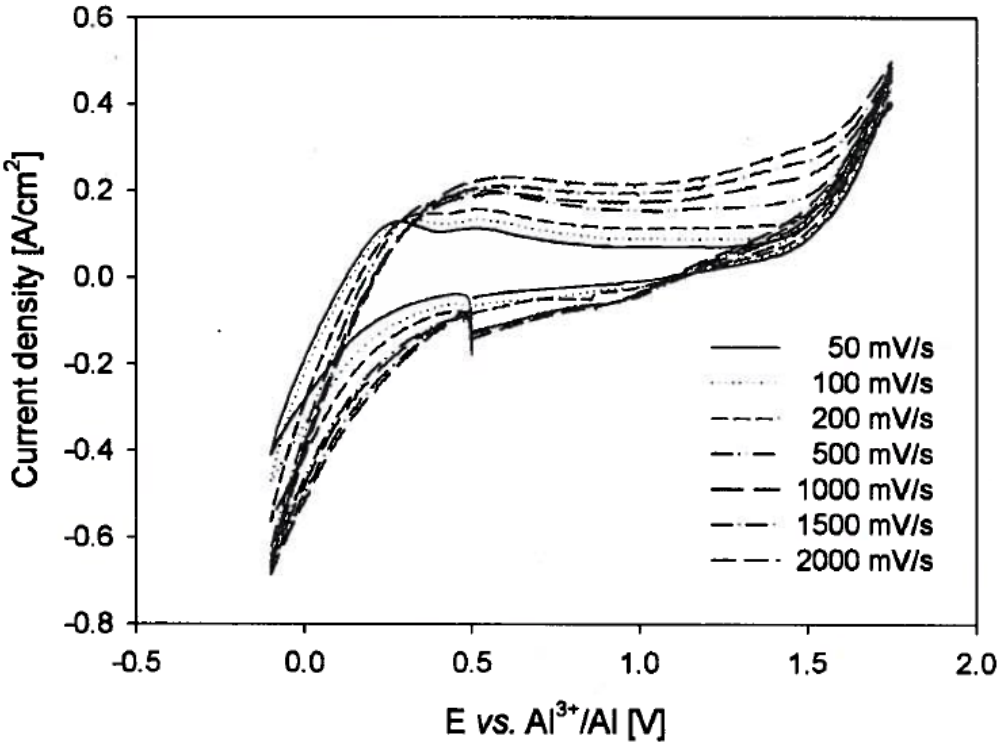

Figure 4.10: Cyclic voltammograms recorded on a carbon electrode after electrolysis (0,6 Ah/cm^2). Melt composition: CR=2,25. Temperature: 960 °C. [45].

4.4 The influence of the type of carbon materials

The comparison of industrial cathode blocks and their performances in industrial cells was treated in chapters 3.2.2., 3.3. and 3.4. The lifetime of the cells with graphitized cathode blocks is lower compared to the cells with anthracitic cathodes [3, 5, 23]. The expected difference in wear rate was not confirmed by recent studies using the laboratory test cell, where the results are shown in Figure 4.7b [46]. Industrial cells with graphitized cathodes are operated at higher current densities, and this was suggested to be the main reason for the higher wear rate. Figure 4.11 shows that higher electrical conductivity contributes to more uneven current

density distribution in the cathode and the wear rate of the areas with the highest current densities (close to the edges) is thereby enhanced [46, 51].

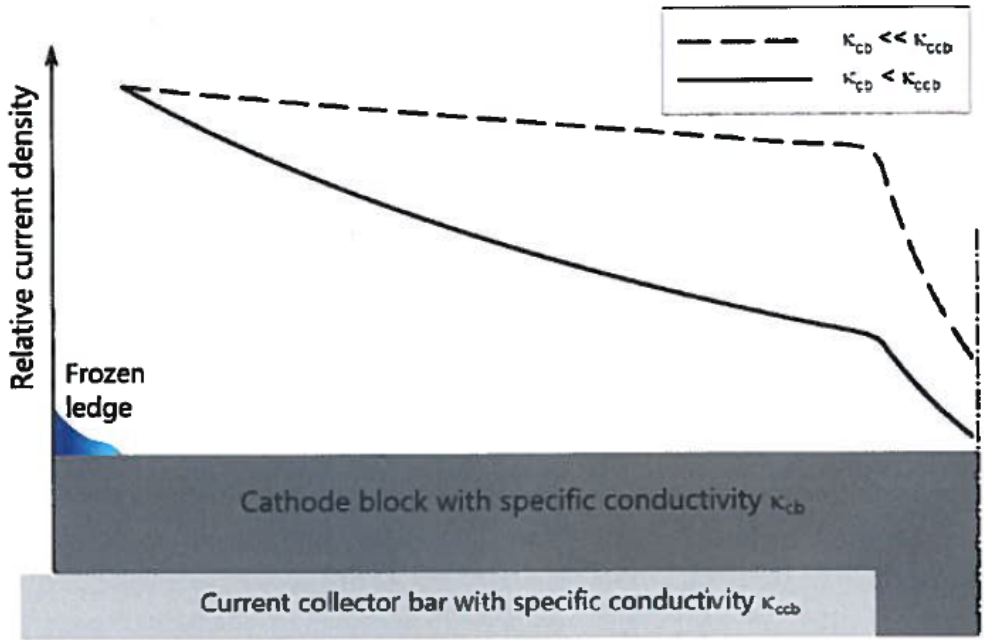

Figure 4.11: Current density distribution in cathodes with different electrical conductivities [51].

Liao and Øye have reported higher wear rate of graphitized materials compared to anthracitic, but only the mechanical abrasion of cathode materials was tested [52]. The sample from carbon material was rotating in the bath containing alumina slurry. Graphitized material is softer and more brittle thus showing higher wear rate. They also performed similar experiments with electrolysis and concluded the low significance of physical abrasion to the carbon wear phenomenon.

Porosity has significant influence on the cathode wear [2]. Bath penetrates into the pores, provides wetting and allows for aluminium carbide formation in the interior of the material. The reaction is enhanced because of the lower potential inside the cathode. This was observed if the pores were greater than 50μm [2]. Patel has seen differences in the wear rate of various carbon materials, which is contrary to observations by Tschöpe et al. [46]. The explanation might be that commercial materials tested by Tschöpe et al. did not have sufficient differences in porosity, while Patel tested carbon materials prepared in laboratory scale with significant differences in porosity. Higher porosity resulted in a larger active surface area and aluminium carbide formation in the pores might lead to tunnelling and particle detachment. Østrem observed particle detachment in the samples from industrial cells, which is shown in Figure 4.12 [51].

Chauke and Garbers-Craig performed XRD analysis of crushed cathode samples [53]. Aluminium carbide was found in one of the samples from an industrial cell after shut down, but could not be detected in any of the samples from the laboratory scale electrolysis. The inability to detect aluminium carbide in the crushed samples was explained by a low concentration below the XRD detection limit.

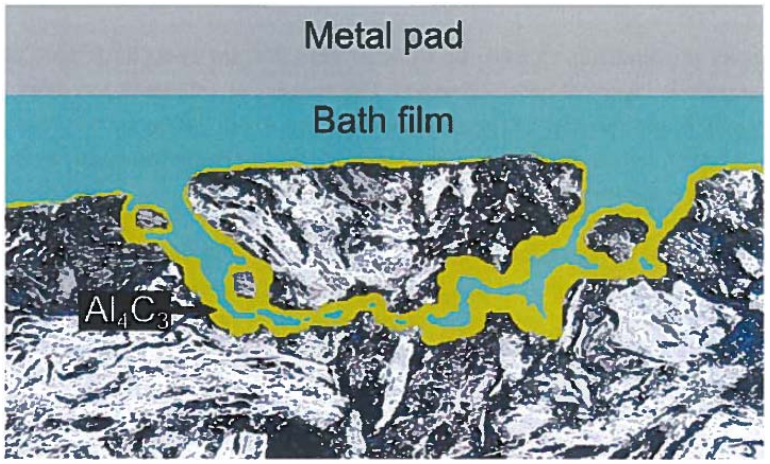

Figure 4.12: Illustration of particle detachment; bath penetration and aluminium carbide formation in the pores [51].

Tschöpe et al. have performed experiments in inverted cell where slots were introduced on the cathode surface as illustrated in Figure 4.13 [54].

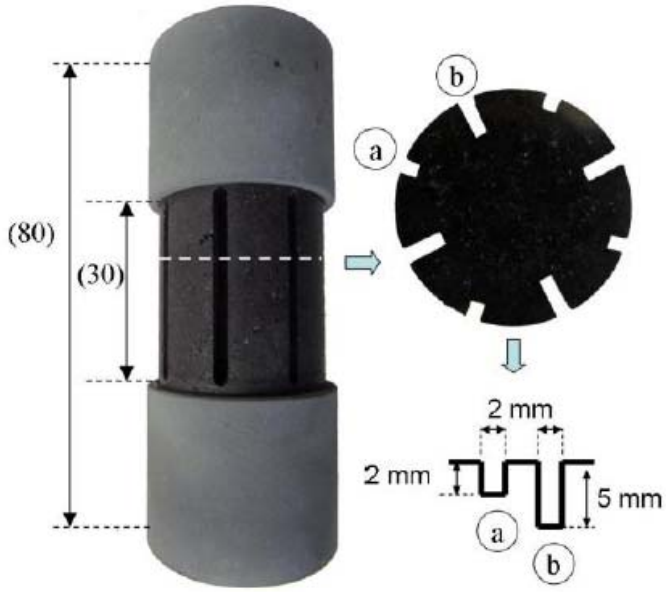

Figure 4.13: Inverted rotating cathode with slots [54]

The original purpose was to simulate porosity and to study the effect of convection, but it is also relevant for the innovative cathode design with special topography (Figure 3.7) [12]. The wear pattern of this cathode is shown in Figure 4.14a.

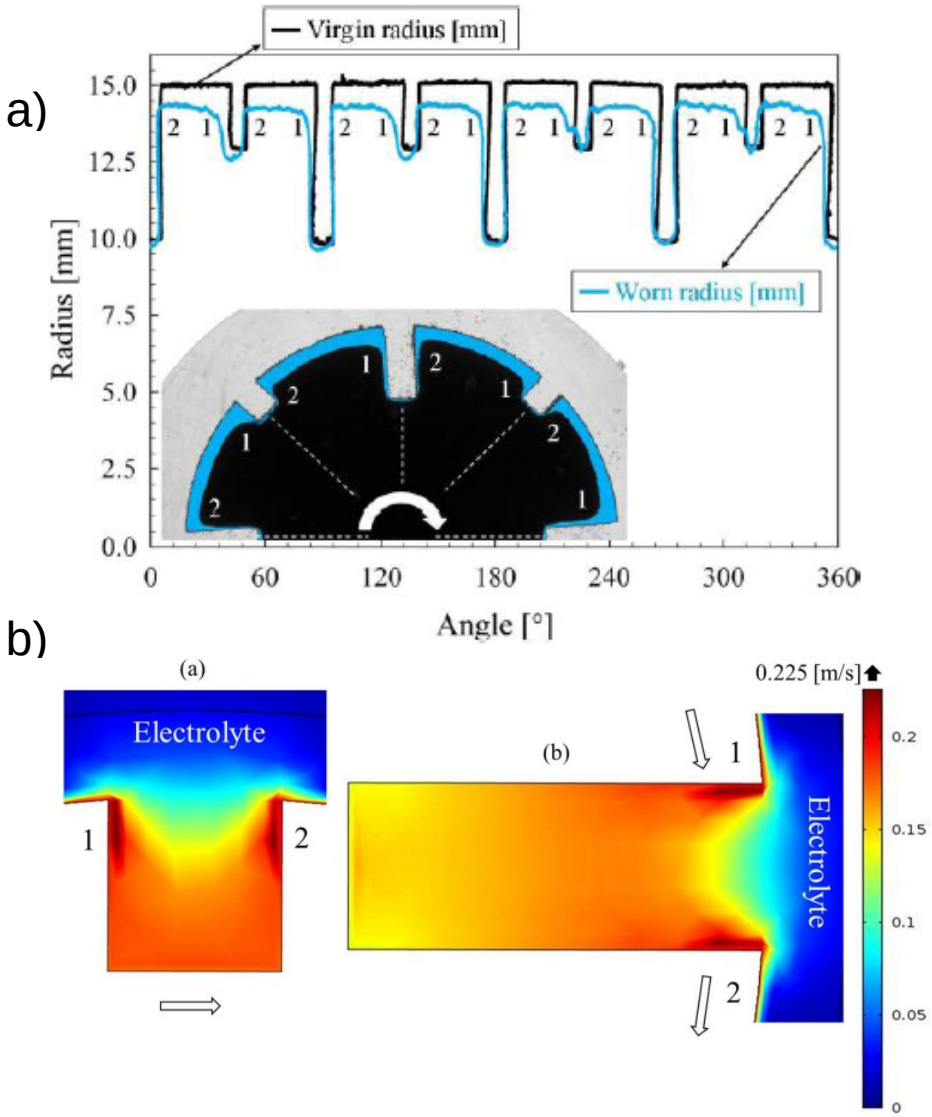

Figure 4.14: Results of the experiments with slots a) indication of the wear overlap of the sample before and after experiment [54] b) modelling of local velocities [55]

The results showed lower wear rate inside the slots and higher wear rate on the surface of the cathode. This is caused not just by higher current density, but also by hydrodynamic conditions. The edges of the slots were worn the most, especially those on the side of the rotation direction. The high velocity of the bath on the edges means higher friction and thinner diffusion layer, which means faster mass transfer of the produced aluminium carbide. The local velocities according to

modelling are shown in Figure 4.14b. The modelling supports the experimental observations, where the highest bath velocity is on the edges. These results emphasize the importance of hydrodynamics on the cathode wear and also indicate faster wear for the innovative cathodes.

Chapter 5

5 Experimental methods to study aluminium carbide formation

5.1 Reaction mechanisms of aluminium carbide formation

Aluminium carbide has strong covalent Al-C bonds, which result in a dense crystal structure [18]. The melting point of Al_4C_3 is 2200 °C, but aluminium carbide decomposes thermally above 1400 °C. Reaction with oxygen, Reaction (5.1) and water, Reaction (5.2) makes aluminium carbide unstable even at ambient conditions [3,18]. Due to this high sensitivity experiments must be performed in inert atmosphere. Sample preparation with Al_4C_3 has to be performed carefully without exposure to humidity.

$$Al_4C_3 + 6O_2 \rightarrow 2Al_2O_3 + 3CO_2 \quad (5.1)$$

$$Al_4C_3 + 12H_2O \rightarrow 4Al(OH)_3 + 3CH_4 \quad (5.2)$$

The reaction between liquid aluminium and solid carbon at the Al/C interface is illustrated in Figure 5.1. The reaction product may dissolve into the liquid and then precipitate either at the interface or other places, depending on the surface character and temperature as shown in Figure 5.1a. The solubility of carbon in molten Al is an important issue with respect to transport of carbon away from the interface. The solubility of carbon/aluminium carbide in aluminium [37] was treated in Chapter 4.1. If the reaction product is a solid compound insoluble in the liquid, it will remain at the interface where nucleation and growth of the reaction product takes place. A layer is formed and this layer will act as a diffusion barrier for further growth. Figure 5.1b demonstrates the reaction controlled by the diffusion through the reaction product, which can be the transport of Al towards C, the transport of C towards Al or a combination of both.

Diffusion is a movement of atoms/ions due to concentration in-homogeneities, where they are moving from regions with higher concentration to regions with lower concentration [56]. The diffusion in solid state is much slower compared to diffusion in liquids and gases. In solid state there are many possibilities of movements. In interstitial lattice diffusion, the diffusant diffuses through interstitial sites in the structure. In substitutional lattice diffusion, the atom can only move by jumping from ordinary lattice sites and it depends on the availability of the vacant lattice sites in the crystal lattice. Diffusing particles migrate from vacant site to vacant site by random walk diffusion. Diffusion in polycrystalline materials can

involve short circuit diffusion mechanisms. For example, along the grain boundaries and certain crystalline defects such as dislocations, where more open space are available thereby allowing for lower activation energy for diffusion. Atomic diffusion in polycrystalline materials is therefore often modelled using an effective diffusion coefficient, which is a combination of lattice and grain boundary diffusion coefficient. In general, surface diffusion occurs much faster than grain boundary diffusion, and grain boundary diffusion occurs much faster than lattice diffusion [57]. Solid state reactions are slow due to slow diffusion in solids, but they might be enhanced by increasing temperature.

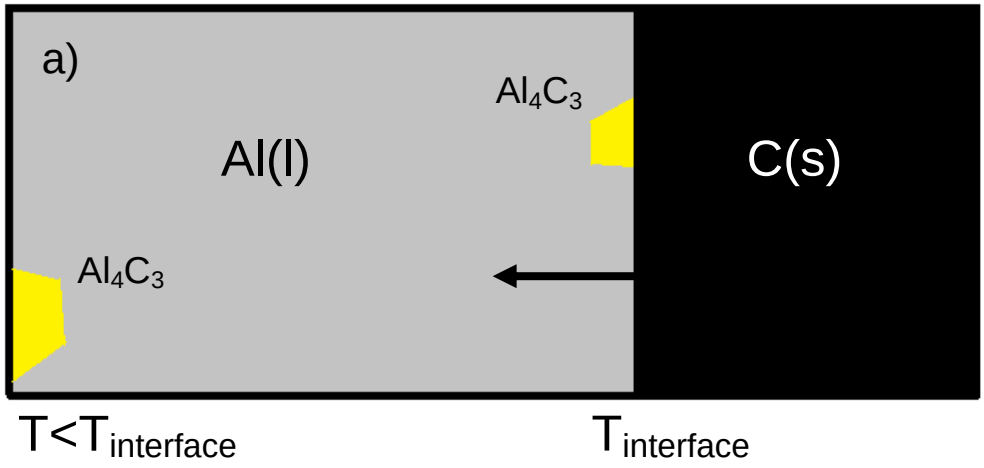

Figure 5.1: Illustrations of possible mechanisms of aluminium carbide formation a) dissolution-reprecipitation mechanism b) reaction controlled by diffusion through aluminium carbide layer.

The strong covalent bonding and low vacancy concentration in aluminium carbide structure suggests low diffusivity of Al and C. As the product layer grows, the carbide layer becomes thicker and the growth rate is decreasing with time. Thus thickness of the layer is proportional to the square root of the reaction time [56]. According to the stoichiometry of reaction (4.1) 4 atoms of aluminium must diffuse through the layer to form one molecule of aluminium carbide.

The reaction between Al(l) and C(s) may also involve the gas phase if one or both elements are volatile or form volatile molecules due to other impurity elements such as O. CO(g) is known to form from carbon in atmospheres with low concentration of oxygen. $Al_2O(g)$ is thermodynamically stable at higher temperatures, which is relevant for the carbothermal production of aluminium [44]. The diffusion in the gas phase is significantly faster, especially when we consider the dense crystal structure of aluminium carbide. The vapour pressures in the system are very important in this case and they are strongly dependent on the conditions in the system as the temperature, total pressure and the chemical composition of the atmosphere. Special mechanism of growth, where the gas phase is involved is the so-called vapour-solid-liquid mechanism [58]. The gas is entering the liquid phase and it leads into precipitation of a solid compound. The droplet is placed on the top of the growing solid phase, which means that the whiskers and needle-like crystals are formed by this mechanism, as it is illustrated in Figure 5.2.

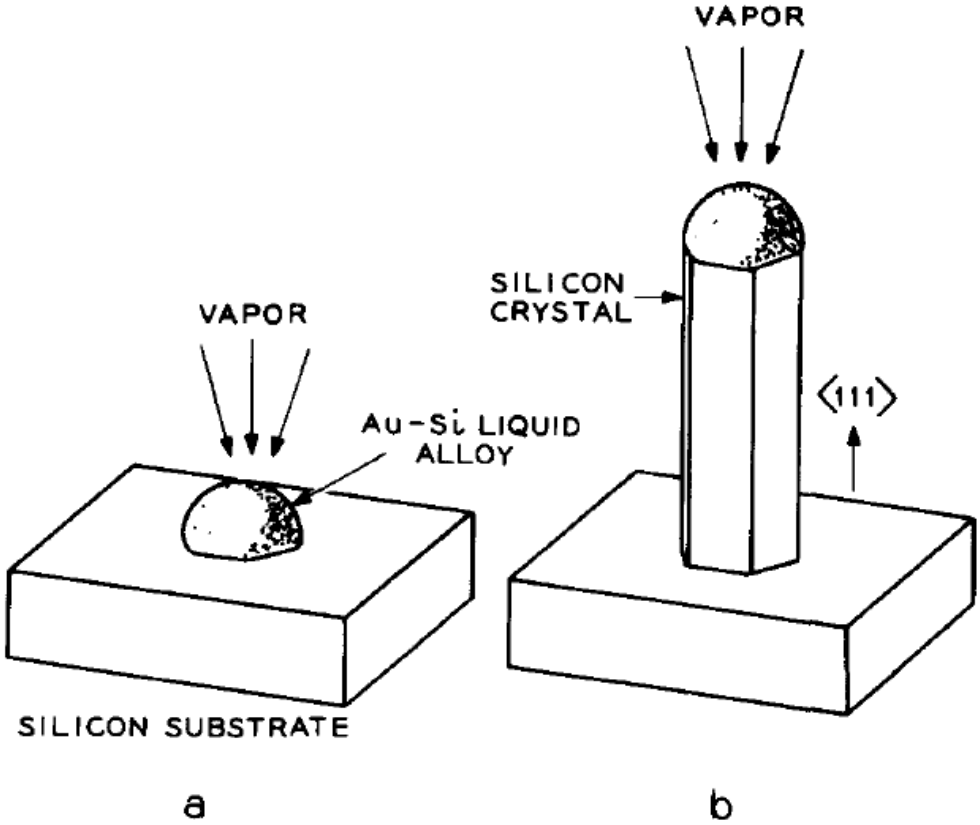

Figure 5.2: Schematic illustration of the growth of a silicon crystal by vapour-solid-liquid mechanism a) initial stage b) growing crystal with the liquid droplet on the top [58].

5.2 Wetting experiments

The interaction between Al(l) and C(s) will be influenced by the wetting of the carbon material as described previously. Wetting is a process, when liquid and solid phase become in contact. The wetting angle or wetting coefficient (Equation 5.3) characterizes the interface between liquid and solid as it is described in Figure 5.2.

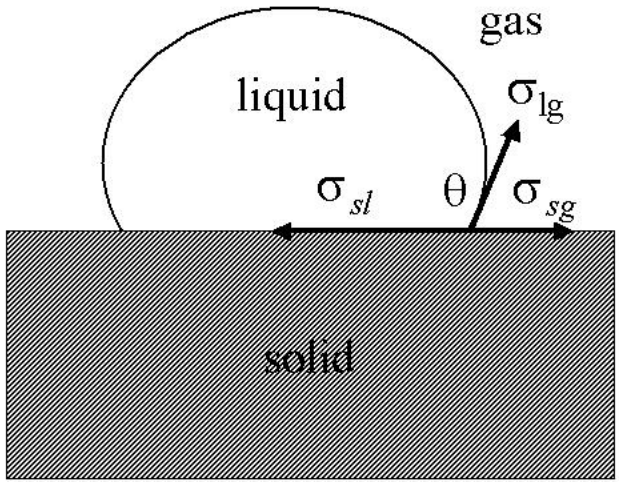

Figure 5.3: Contact of liquid, solid and gas, definition of contact angles [59].

The greater the angle is the better are the wetting properties. When the wetting angle is 180°, the wetting is ideal and the droplet spread itself on the surface. The same property can be also given by the wetting coefficient k,

$$k = \frac{\gamma^{sg} - \gamma^{sl}}{\sigma^{lg}} = \cos\theta \qquad (5.3)$$

where γ^{sg} and γ^{sl} are the surface energies between the solid-gas and the solid-liquid phases respectively and σ^{lg} is the surface tension between the liquid and the gas phase. The sessile drop wetting measurements are based on measuring the wetting angle using the configuration shown in Figure 5.3. If the surface tension of the liquid is known the differences between the interfacial energies of the solid-gas and the solid-liquid can be determined. It is difficult to obtain reproducible data experimentally because the roughness of the surface and impurities have significant influence on the surface properties.

The challenges with the investigation of wetting by aluminium are that the experiments need to be performed under vacuum and that the protective oxide layer is removed relatively fast (Reaction 4.2). Landry showed that the removal of aluminium oxide layer is the most important issue during Al-C wetting and interaction [34]. Such results are not directly applicable to the corresponding wetting process at atmospheric conditions.

Chapter 6

6 Experimental

6.1 Al-C diffusion couples

The interaction of molten aluminium and carbon was studied by diffusion couple experiments. Initial experiments were performed by pressing the pellets of Al and C together into an alumina crucible (Haldenwanger) as illustrated in Figure 6.1a. The alumina crucible was replaced with a carbon crucible because alumina made polishing of the diffusion couple more difficult and it might also influence the reaction between Al and C. A carbon crucible from the tested material was prepared as shown Figure 6.1b. The aluminium cylinder (super purity of 99.99 %) was forced into the crucible and covered by a carbon pellet as illustrated in Figure 6.1.b. Extra load (alumina cylinder) on the top was applied to improve the contact at elevated temperatures. Two different carbon materials were used in the study. The first experiments were conducted using electrode graphite (Svensk specialgrafit AB) with a density of 1.54 g/cm^3. Later, fully graphitized carbon IG-15 (Toyo Tanso, graphitization temperature of 3000 °C with a bulk density of 1.9 g/cm^3) was chosen because of its high degree of graphitization.

The crucible was placed into a fused silica-liner. The silica-liner was flushed with Ar gas as shown in Figure 6.1. Ar 5.0 (Yara Praxair) contains 2 ppm of oxygen and 3 ppm of water. In order to reduce the possible effect of the oxygen impurities, similar experiments were also performed in stagnant Ar atmosphere. In this case the silica-liner was evacuated down to 2 mbar and refilled with Ar to 0.8 bar total pressure. The silica-liner was then heat treated in a water-cooled tube furnace. The temperature was measured with a thermocouple (S-type) placed on the outside of the Pythagoras tube. The exact temperature in the middle of the tube, where the sample was placed, was measured prior to the experiments. The experiments were performed at 1000 - 1200 °C for 1 – 16 days. The heating rate was 300 °C per hour and the silica-liner with the sample was quenched in water at the end of the experiments.

The influence of presence of cryolite on the aluminium-carbon interaction was studied by diffusion couple experiments with a film of cryolite at the interface. Cryolite was introduced by submerging of an Al cylinder into a suspension of fine cryolite powder and 100 % ethanol. A small amount of cryolite (10-20 mg) was introduced in order to serve only as a wetting agent. The coated Al cylinder was placed into the carbon crucible and dried. Natural cryolite was used for the initial experiments, but was later replaced with synthetic cryolite (Sigma-Aldrich) in order to reduce the grain size of the fluoride. Al/C couples experiments with a film

of cryolite were performed at 1030 °C (the melting point of cryolite is 1012 °C) and the duration of the experiments was from 3 hours to 3 days.

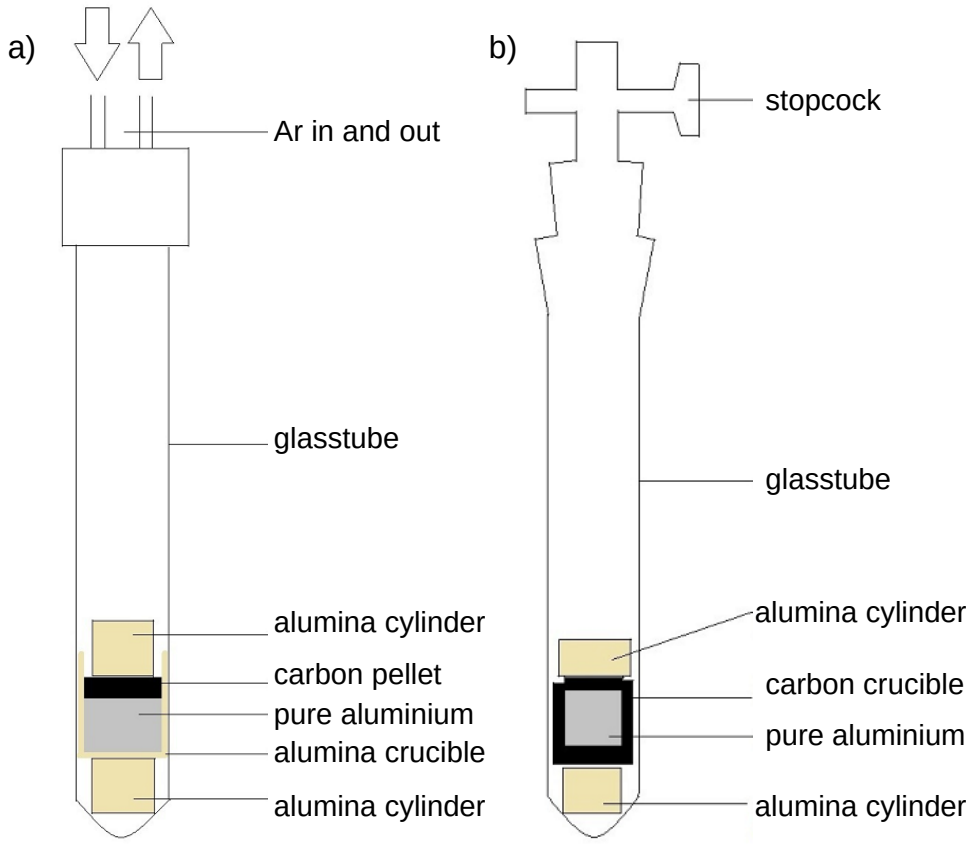

Figure 6.1: Experimental setups of diffusion couples experiments; a) setup with alumina crucible flushed with Ar b) setup with carbon crucible in stagnant Ar.

Experiments with larger amount of cryolite were also performed. The same experimental setup, shown in Figure 6.1b was used, but the size of the aluminium cylinder was reduced and the remaining part of the crucible was filled with cryolite as it is illustrated in Figure 6.2. The cryolite melt was modified by addition of 20 wt% of CaF_2 (Alfa Aesar) and the experimental temperature was reduced to 980 °C in order to reduce the vapour pressure and thereby supress evaporation and the reaction with the glass tube.

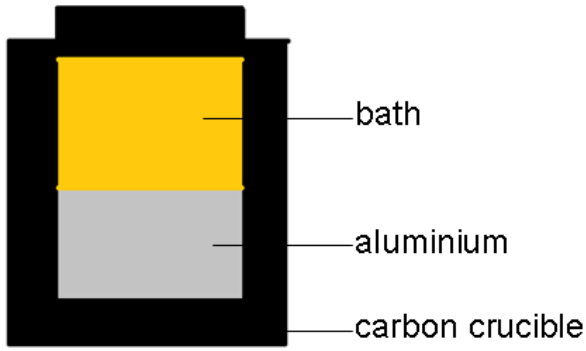

Figure 6.2: Illustration of the setup of diffusion couple with proper amount of cryolite.

6.2 Al-C couples with polarization

The influence of polarization and electric current on the aluminium–carbon interaction was studied by diffusion couple experiments with polarization of the two carbon materials on each side of aluminium. A cylinder of aluminium and two pellets carbon (one serving as a cathode while the second as an anode) were placed in a alumina crucible as illustrated in Figure 6.3b.

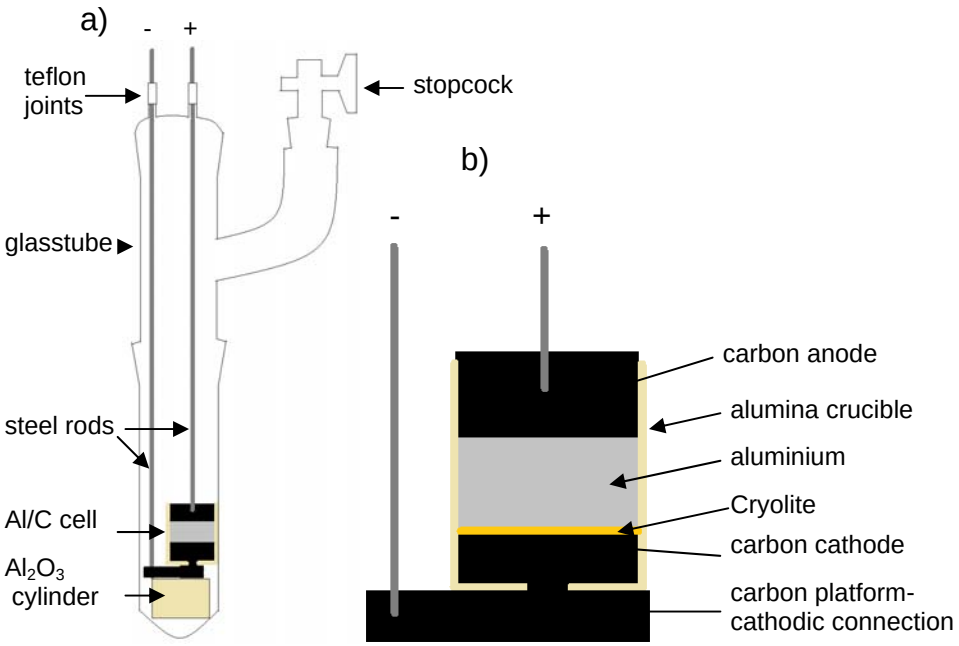

Figure 6.3: Experimental setup of diffusion couples with polarization; a) entire setup b) the detail of the cell.

A hole was drilled in the bottom of the alumina crucible in order to provide the electrical connection to a carbon platform. For some experiments cryolite was introduced on the interface by submerging of the Al cylinder into a suspension of fine cryolite powder and 100 % ethanol. The cell was placed into a silica-liner, which is illustrated in Figure 6.3a. The silica-liner was evacuated down to 2 mbar and refilled with Ar to 0.8 bar total pressure. The current is supplied to the electrodes by steel rods, which are inserted to the glass tube through teflon joints. The gaps between the rods and teflon were sealed with vacuum grease and the rods could thereby move freely to follow the expansions of the materials during heating. The experiments were performed at temperatures between 980 and 1100 °C and the heating rate was 300 °C/hour. The duration was from 3 hours to 3 days and the electrolysis were performed at constant current 0.4 A. The surface of the electrodes was 2 cm^2, thus the current density was 0.2 A/ cm^2, which is lower than in an industrial cells.

6.3 Electrochemical cells

The electrochemical formation of aluminium carbide was investigated in several electrochemical cells with different configurations of the electrodes. The same setup as for diffusion couples with polarization was used (Figure 6.3a), only the arrangements of aluminium and cryolite in the cells were modified. Illustrations of electrochemical cells are shown in Figure 6.4. Conventional cell has the same setup as industrial cell, where liquid aluminium is located at the carbon cathode. Inverted cell has the same setup as conventional cell, but the polarization is reversed.

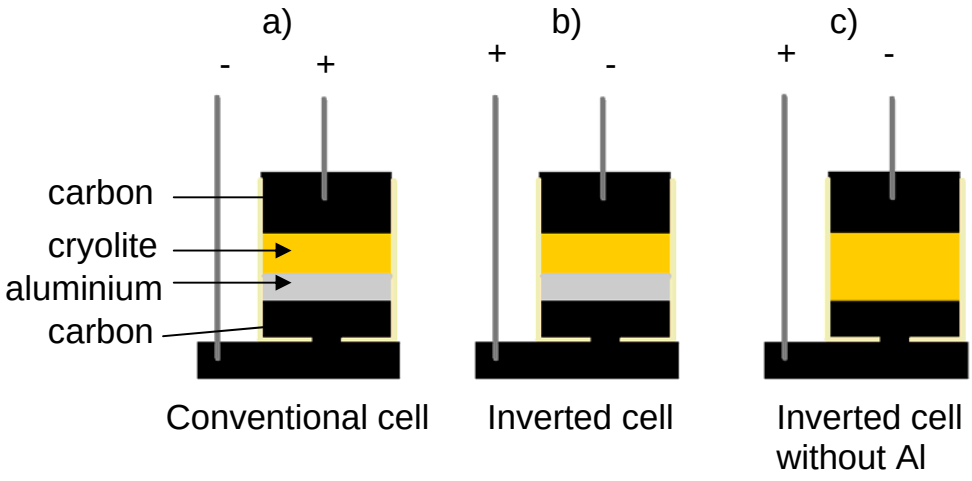

Figure 6.4: Illustration of electrochemical cells; a) real cell b) inverted cell c) inverted cell without aluminium.

Cryolite with addition of 20 wt% of CaF_2 was used and 5-7 % of alumina (Merck) was also added to the electrolyte in order to enable aluminium reduction. The duration of the experiments was from 30 minutes to 1 day.

6.4 Characterization of the diffusion couples and electrochemical cells

After the experiment the samples (Al-C couples, electrochemical cells) were quenched and embedded in epoxy resin. The sample was then cut into two parts to obtain a cross section of the diffusion couple. The cross section was then ground with SiC abrasive paper and polished using diamond sprays down to ¼ μm. The polished cross sections of the diffusion couples are shown in Figure 6.5. 100 % ethanol was used for cutting, grinding and polishing to reduce possible reaction with water. The Al-C interface was analysed by optical microscope REICHERT MeF3A using bright field (BF) and polarizing filter (POL MET). Electron microscope (LV-SEM HITACHI S-3500 N) was also used and EDS analysis (HITACHI S-3400) was performed to confirm the presence and composition of the carbide layers. Acceleration voltage 7 V was used, which is suitable for the system with such a composition. For some Al-C samples with catalytic amount of cryolite, X-ray diffraction (Siemens D5005) of aluminium and carbon surfaces of the interfacial regions was performed. The data were collected with a step size of 0.015° over the 2θ range from 20° to 70°.

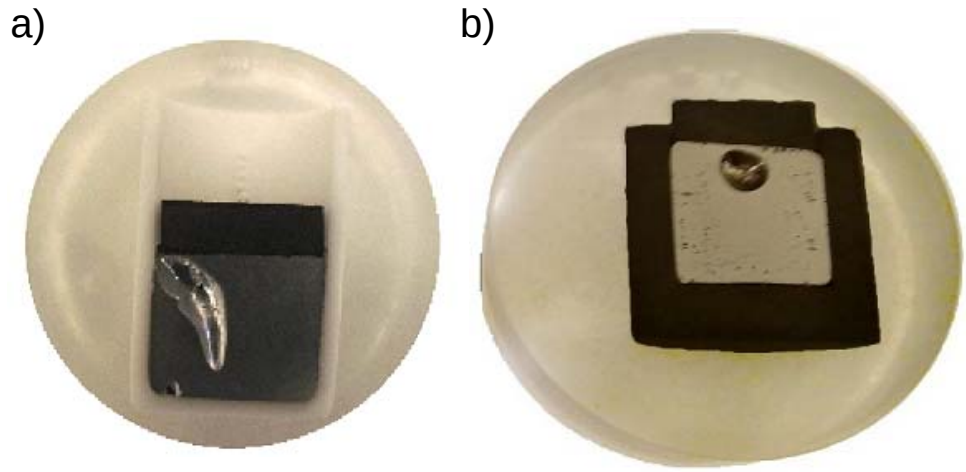

Figure 6.5: Diffusion couples embedded in epoxy; a) setup with alumina crucible b) setup with carbon crucible.

Chapter 7

7 Results and discussion

7.1 Al-C diffusion couples

The formation of aluminium carbide at the Al/C interface could be identified after annealing the diffusion couples at temperatures between 1100 and 1200 °C. A representative micrograph of the cross section of the diffusion couple after annealing at 1150 °C for 10 days is shown in Figure 7.1. Two layers with different appearance and chemical composition could be identified.

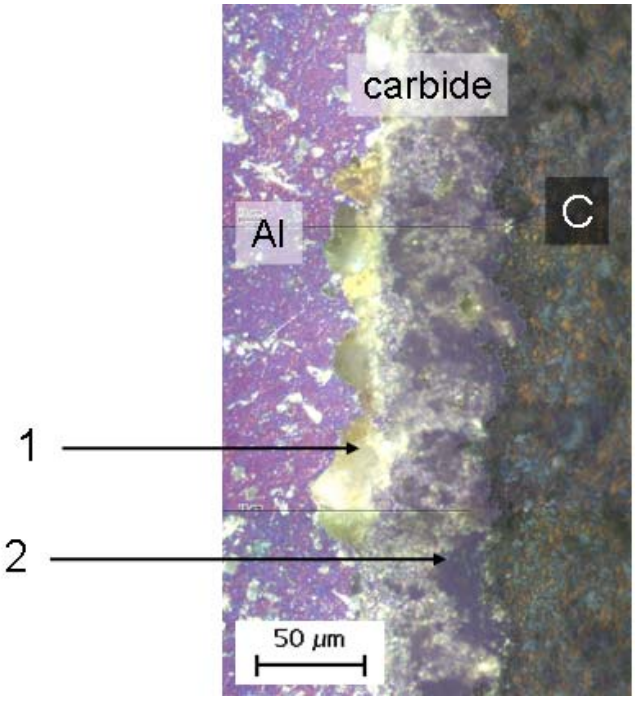

Figure 7.1: Optical micrograph of two different layers of aluminium carbide at the Al/C interface after 10 days at 1150 °C. The experiment was performed in stagnant Ar atmosphere.

The first layer towards aluminium is around 10-20 µm thick and was shown by EDS to have a relatively high oxygen content. The second layer towards carbon is around 50-60 µm thick and has a lower oxygen content. The element distribution maps of a diffusion couple after 10 days annealing at 1200 °C are shown in Figure 7.2. The two layers at the interface can be identified in the optical micrograph in Figure 7.2a, the distribution map of oxygen in Figure 7.2b and to some degree in the Al distribution map shown in Figure 7.2c. The EDS spectra of the two layers,

shown in Figures 7.2e and 7.2f, revealed that the layer towards Al has higher oxygen content than the layer towards C. The oxygen element map, Figure 7.2b, demonstrates the second carbide layer has lower oxygen content than the first layer. The purple colour of this layer in the optical image using polarizing filter (Figure 7.1) also suggests the presence of pure aluminium carbide.

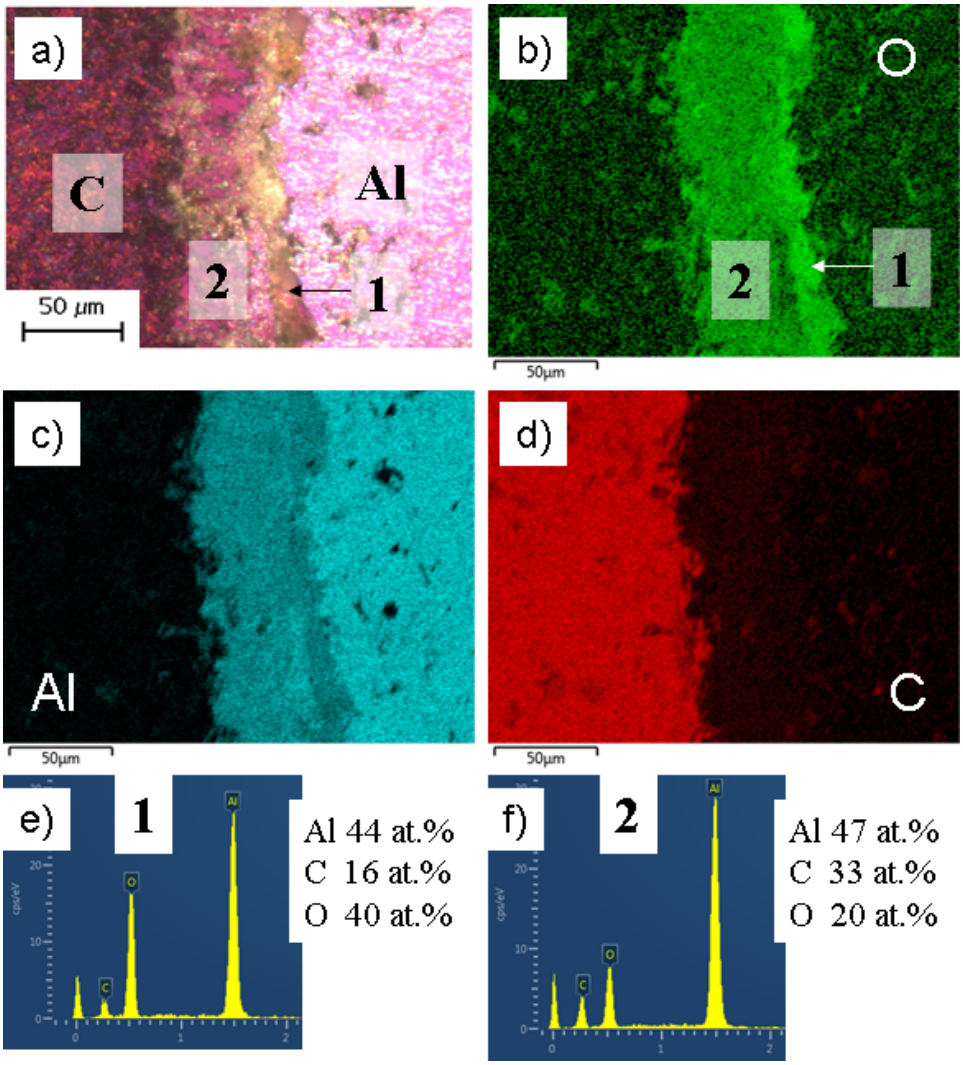

Figure 7.2: Micrograph and element maps of two layers formed at the Al/C interface after 10 days annealing at 1200 °C in stagnant Ar atmosphere a) optical image, b) oxygen element map, c) aluminium element map, d) carbon element map, e) EDS spectra obtained at point 1, f) EDS spectra obtained at point 2.

The first carbide layer was observed along the whole Al/C interface already after 24 hours, but the double layer was less evident after 24 hours. The areas of the second layer were found towards carbon material close to cracks or defects in the thin first layer, which is shown in the optical micrograph in Figure 7.3. These areas

were growing over time until they have connected together forming the compact second layer as shown in Figure 7.4.

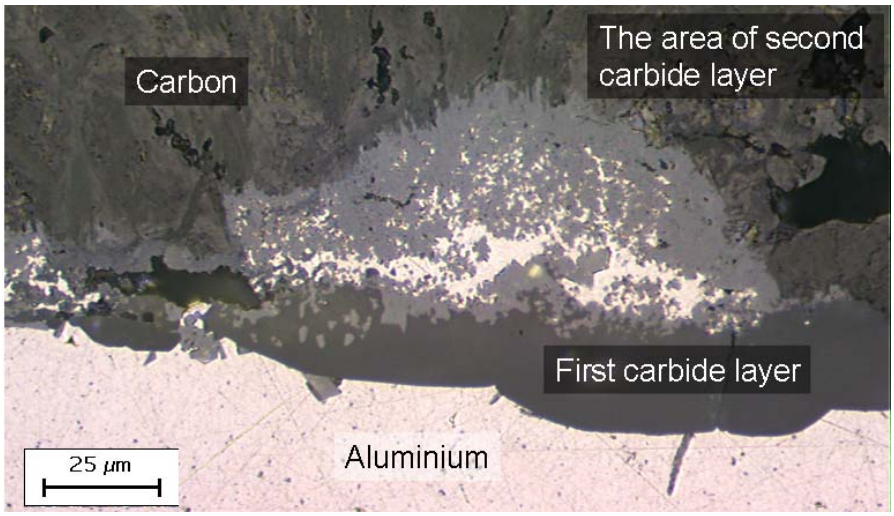

Figure 7.3: Optical macrograph of the Al/C interface after 24 h at 1200 °C. The diffusion couple was mounted in an alumina crucible and flushed with Ar during the experiment.

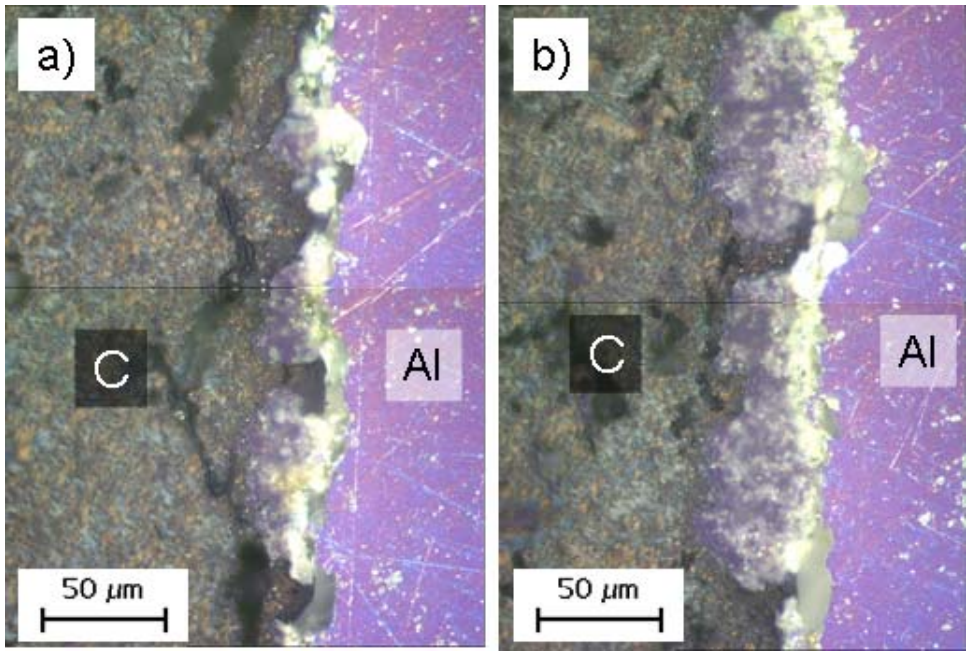

Figure 7.4: Optical micrograph of the development of the growth of the second layer at the Al/C interface. a) Discontinuous regions of the second layer, b) continuous compact second layer. Al was placed into the carbon crucible and the experiment was performed 6 days at 1200 °C in stagnant Ar atmosphere.

When the glass tube with the sample was cooled slowly after the experiment, large aluminium carbide crystals could easily be identified as shown in Figure 7.5. The precipitation of these large carbide crystals during cooling demonstrates clearly that a considerable amount of C was dissolved in molten Al at the annealing temperature.

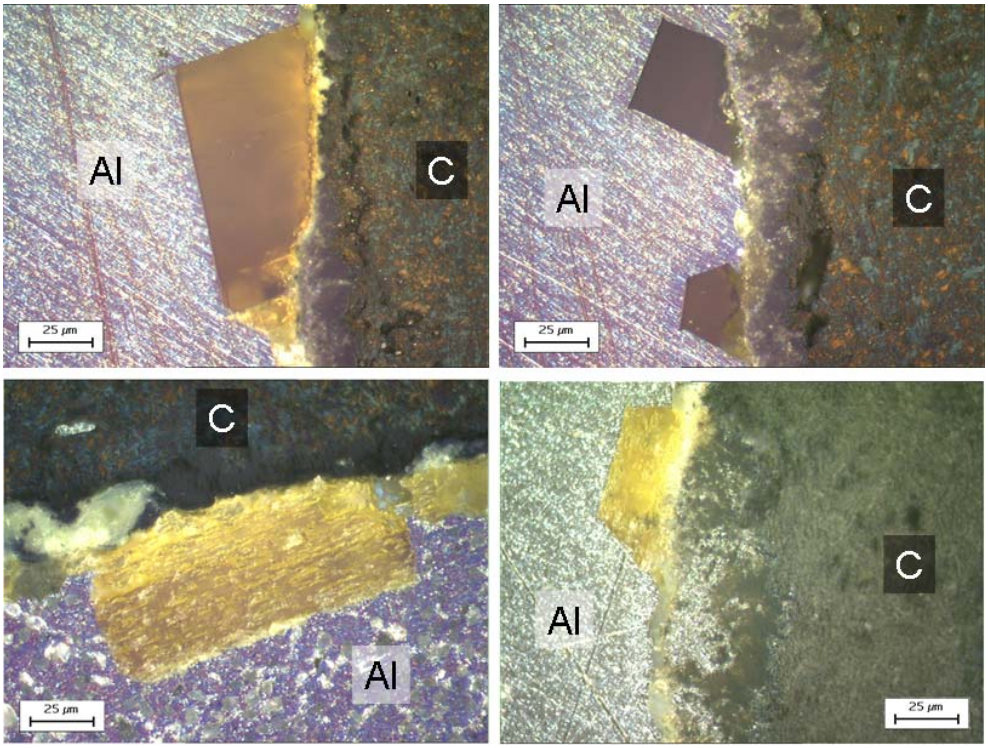

Figure 7.5: Optical images of aluminium carbide crystals precipitated in liquid aluminium at slow cooling rate.

Thermodynamic calculations using the program FactSage 6.2 [60] were performed to better understand the reaction between Al and C, and possible influence of O. The most important issue was to examine the potential involvement of oxygen in the reactions. However, the formation of oxycarbides was not included in the calculations due to lack of thermodynamic data for these compounds in the database used.

In general, the number of degrees of freedom of the system can be found by the Gibbs phase rule,

$$Ph + F = C + 2 \qquad (7.1)$$

where Ph is the number of phases in thermodynamic equilibrium, F is the degree of freedom, C is the number of components and 2 corresponds to pressure and temperature. When Al-O binary system is considered (C=2) at a constant

temperature, the total pressure of the system is fixed (F=0) when the gas is in equilibrium with Al_2O_3(s) and Al(l) since Ph+F=3 and Ph=3. Introduction of an inert gas as Ar will only influence the total pressure and not the partial pressures of Al_2O and Al. The equilibrium calculations gave the equilibrium composition of the gas with Al_2O(g) as the dominating gas species. The protective Al_2O_3 layer may be removed by the evaporation of Al_2O(g) as it was predicted by Laurent [35] by Equation (4.2). Figure 7.6 shows the vapour pressure of the sub-oxide Al_2O(g) increases with increasing temperature and reaches ~10^{-6} bar at around 1100 °C. It is empirically known form thermogravimetrical analysis that the weight loss can be detected when the vapour pressure exceeds ~10^{-6} bar [61]. The thin protective oxide layer can then be evaporated completely from the Al(l) surface at these temperatures. It also corresponds with the experimental observations, where aluminium carbide was found on the Al/C interface at temperatures higher than 1100 °C. The oxide scale on Al does therefore represent a kinetic hindrance for the direct reaction between Al and C.

The next step was to investigate the Al-C-O system and how carbon can change the composition of the gas phase and influence the volatility of the oxide scale. Here, an air leakage or oxygen impurities in stagnant argon, as mentioned above, were considered. If the oxygen in the system reacts with carbon to form CO(g), one may expect that the vapour pressure of Al_2O(g) will change. The ternary phase diagram of Al-C-O system can be divided into 3 subsystems, as shown in Figure 7.7. In triangle 1, aluminium carbide is in equilibrium with excessive, unreacted aluminium and aluminium oxide. The vapour composition is fixed according to Gibbs phase rule in the entire region of this triangle and is independent of the oxygen content in the system. Excessive oxygen always reacts with Al and ends up as Al_2O_3. Triangle 2 represents excess of carbon, and the vapour composition is again fixed according to the Gibbs phase rule. In triangle 3 excess amount of oxygen is present and CO and CO_2 are in equilibrium with Al_2O_3. In the diffusion couple experiments, carbon and aluminium are not completely consumed and the global equilibrium is never reached. Locally the vapour pressure can deviate substantially from the global equilibrium values. The subsystems 1 and 2 might represent the metastable conditions in the vicinity of aluminium and carbon. The vapour pressure in triangle 1 and 2 was calculated as a function of temperature, as shown in Figure 7.8. The vapour pressures increase nearly two orders of magnitude between 1000 °C and 1200 °C. The vapour pressure of aluminium sub-oxide (Al_2O) in triangle 1 is exactly the same as in Al-O system, which means that the presence of carbon in the system has no influence on the volatility of the aluminium oxide layer.

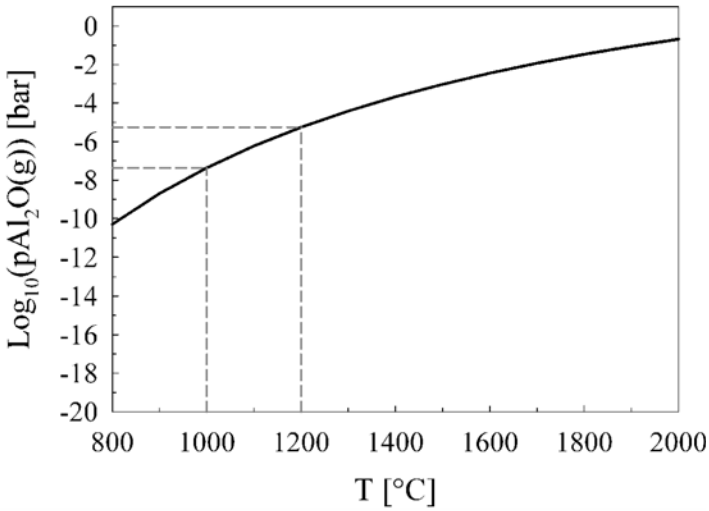

Figure 7.6: The calculated equilibrium vapour pressure of Al_2O sub-oxide as function of temperature in the system Al-O, corresponding to Reaction (5). The temperature range for experiments performed here is marked with dashed lines.

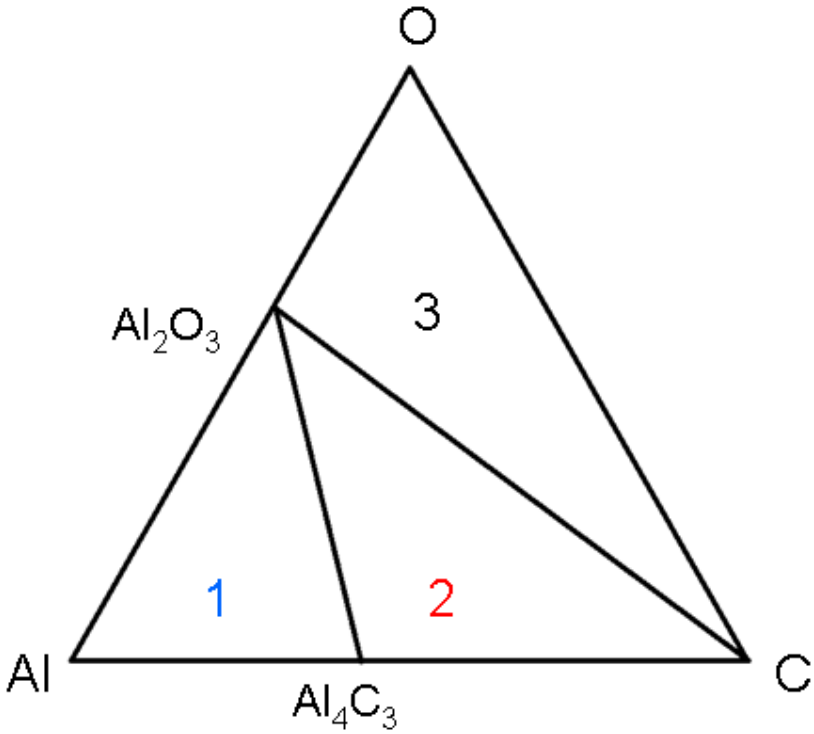

Figure 7.7: Phase diagram of Al-C-O ternary system with 3 subsystems.

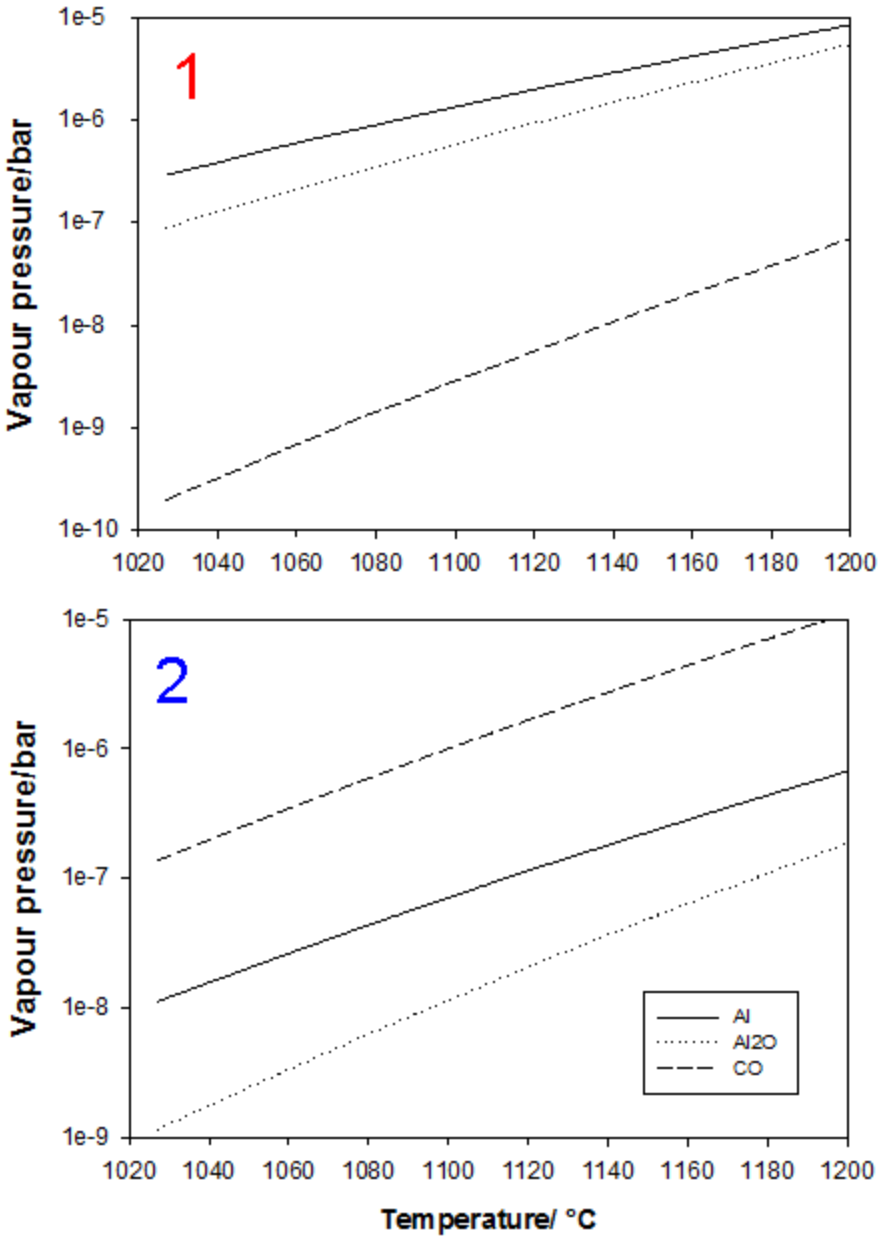

Figure 7.8: Partial pressures of Al, Al_2O and CO in Al-C-O ternary system. Subsystems 1 (Al, Al_2O_3, Al_4C_3) and 2 (C, Al_2O_3, Al_4C_3).

The oxide observed in the aluminium carbide may come from argon during the experiment and also from the air during sample preparation (cutting, polishing), handling and microscopy analysis. The sensitivity and reactivity of aluminium carbide with oxygen and water was treated in Chapter 5.1. Aluminium carbide reacts with oxygen and water according to Reactions (5.1) and (5.2). Aluminium hydroxide, the product of hydrolysis undergoes thermal decomposition at higher

temperatures (Reaction 7.2) and aluminium oxide is the only product of aluminium carbide oxidation at high temperatures. Aged samples oxidized by air moisture at room temperature have higher oxygen/aluminium ratio due to the presence of aluminium hydroxide.

$$2Al(OH)_3 \rightarrow Al_2O_3 + 3H_2O \qquad (7.2)$$

Taking into account the gas flow rate and the oxygen and water content in argon, these two species can oxidize a 1 μm layer of aluminium carbide per day in an argon flux of 1.6 l/h (carbon pellet diameter = 15 mm), which gives oxide content in relatively good correlation with the experimental data. The calculation has been done for the case of total oxidation. Attempt to minimize the oxidation of aluminium carbide during experiment was conducted by introduction of stagnant argon atmosphere and removal of alumina crucible. The concentration of oxygen in the carbide layers was reduced, but higher oxygen content in the first layer towards aluminium was still evident. When the experiment was flushed with argon, the higher oxygen content was visible also in the optical image using polarized light, shown in Figure 7.9, where the colours of the layers are yellow and grey.

When the oxidation by the impurities in argon and by the air is considered, aluminium carbide should be oxidized evenly. Higher oxygen content in the first carbide layer suggests the involvement of oxygen in the reaction. The second layer is most likely pure aluminium carbide formed by different mechanism without oxygen. The low oxygen amount found in this layer is probably originating from oxidation/hydration of the carbide layer.

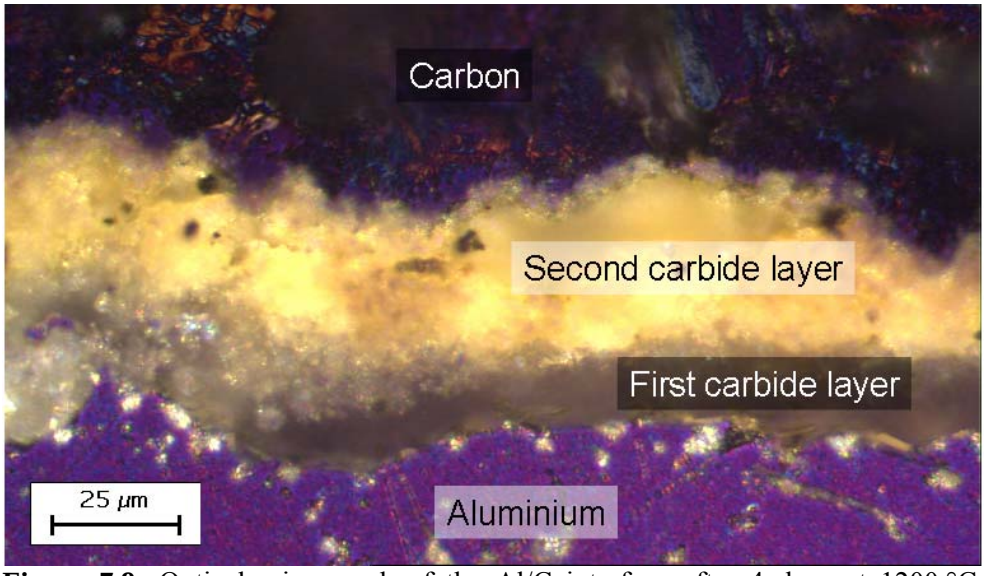

Figure 7.9: Optical micrograph of the Al/C interface after 4 days at 1200 °C. Alumina crucible was and flushed with Ar.

The most important result of the thermodynamic considerations is the relatively high vapour pressure of aluminium sub-oxide (Al_2O), which demonstrates that evaporation of the oxide layer is possible. Then aluminium carbide can be formed by direct contact between aluminium and carbon. The initial expectation was that the diffusion couples would provide evidence for the solid state diffusion through a carbide layer at the interface, but the experiments showed two different layers and the second layer was not growing evenly. Estimation of the diffusion coefficient by $D=4L^2/t$, where L is the thickness and t is the time, give diffusion coefficient of the order of 10^{-10} m^2/s. Such high diffusion coefficients are highly unlikely in the carbide crystal structure with strong covalent bonds, even if faster diffusion along the grain boundaries is considered.

Possible gas transport mechanism related to the growth is proposed in Figure 7.10. The protective Al_2O_3 layer is removed from the Al(l) surface, and the carbide can be formed by direct reaction between the two elements. The gaseous sub-oxide $Al_2O(g)$, the product of Al_2O_3 evaporation, can diffuse towards the carbon surface, enabling transport of Al through the gas phase and initiate aluminium carbide formation at the carbon surface. Aluminium vapour can also be involved in the reactions, and the thermodynamic calculations showed the high partial pressure of Al in the same order of magnitude as the vapour pressure of aluminium sub-oxide (Figure 7.8). At the carbon surface $Al_2O(g)$ reacts to form carbide and CO(g) (Reaction 7.3). Contrary, the released CO(g) may diffuse towards the aluminium surface where CO(g) can react to form $Al_4C_3(s)$ and $Al_2O_3(s)$ or oxycarbides (Reaction 7.4). The aluminium oxide will generate $Al_2O(g)$ again and oxygen can then circulate between both interfaces and act as a carrier of Al and C.

$$2\ Al_2O(g) + 5\ C(s) = Al_4C_3(s) + 2\ CO(g) \qquad (7.3)$$

$$\frac{1}{2}\ CO(s) + Al(l) = \frac{1}{6}\ Al_4C_3(s) + \frac{1}{6}\ Al_2O_3(s) \qquad (7.4)$$

According to the calculations, the partial pressure of Al_2O reaches $\sim 10^{-6}$ bar at 1100 °C, which means the oxide layer can evaporate and the formation of Al_4C_3 at the Al/C interface may proceed. The mechanism suggests that the evaporation of aluminium sub-oxide is necessary in order for the carbide formation to proceed. One would expect the removal of the protective layer as a breakthrough after which the reaction should proceed. One special experiment was performed, where the temperature 1200 °C was kept for the first hour and then was lowered to 1000 °C for the rest of the experiment (4 days). This experiment was an attempt to remove initially the oxide layer at higher temperature and then to form aluminium carbide at 1000 °C. Almost no carbide was found at the Al/C interface and that supports the gas transport mechanism, where the temperature higher than 1100 °C is needed in order to maintain higher vapour pressure of Al_2O. The partial pressure of CO in the vicinity of carbon is similar to the partial pressure of Al_2O in the vicinity of aluminium, but can be even higher. When the local equilibrium C-O is considered,

oxygen reacts quantitatively to CO, thus the partial pressure of CO is dependent on the oxygen concentration in argon.

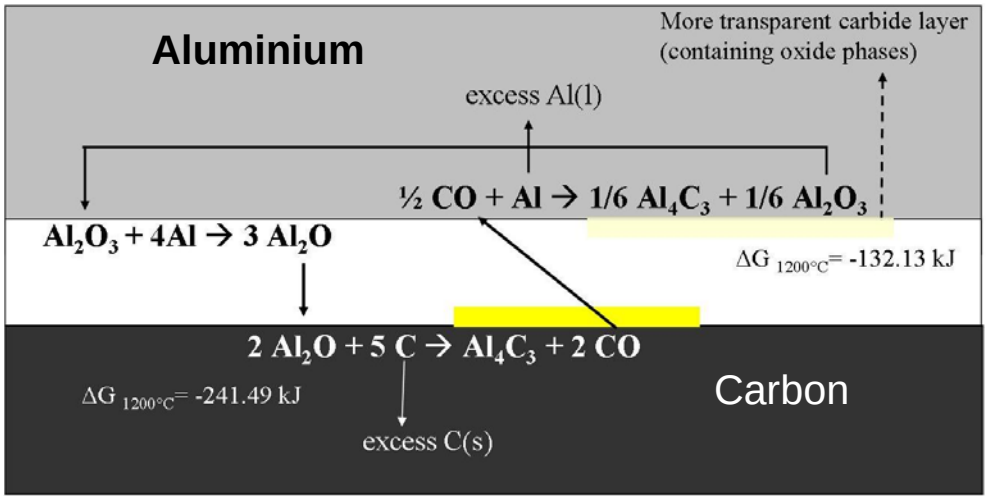

Figure 7.10: Proposed gas transport mechanism of the removal of Al_2O_3 layer and aluminium carbide formation.

One may imagine that the two reactions at the two different surfaces generate two different Al_4C_3(s) microstructures. This scenario can provide an explanation for the formation of the two different layers of carbide. It corresponds with experimental observations, where the layer towards aluminium has higher oxygen content and the layer towards carbon is almost pure carbide. It is assumed that aluminium carbide grows at both interfaces according to the sub-reactions (7.3) and (7.4). At the present stage the possibility of formation of oxycarbides (Al_2OC and/or Al_4O_4C) cannot be ruled out. The composition and appearance of the first layer suggest the presence of oxycarbide phases (Figure 7.1), because it is known from literature that aluminium oxycarbides have transparent colourless appearance [62, 63]. However it is not possible to make a conclusion because the EDS mapping gives only qualitative amounts of the elements. The oxycarbide phases can be detected by X-ray diffraction, but the low thickness of the carbide layers and strong interconnection of aluminium and carbon surfaces make the detachment and analysis challenging. Tschöpe et al. [64] performed X-ray diffraction of the interfacial powder after similar experiment and it has revealed pure aluminium carbide. The results of Tschöpe et al. are discussed further below.

The oxygen impurities in Ar and leakage in the vicinity of carbon surface (C-O local equilibrium) leads to CO formation, but not to Al_2O formation in the vicinity of aluminium surface, where oxygen will react to aluminium oxide. Higher partial pressure of CO may lead to more intensive formation of the oxygen rich carbide layer towards aluminium. This is not the case and the oxygen containing layer is always evidently thinner. However, it might be the reason why the oxygen rich layer towards aluminium is present from the very beginning and why the formation

of the second carbide layer with lower oxygen content needs longer time to develop. It takes some time for the protective oxide layer to evaporate and generate sufficient amount of $Al_2O(g)$ for the formation of the second layer, while formation of CO(g) on the carbon surface is relatively fast process. CO(g) may also oxidize aluminium carbide according to Reaction (7.5), but the stoichiometry of the Reactions (7.3) and (7.5) is showing that the aluminium carbide formation at the carbon surface (Reaction 7.3) does not generate enough CO for the oxidation of all the carbide.

$$Al_4C_3 + 6CO \rightarrow 2Al_2O_3 + 9C \qquad (7.5)$$

However, there are some arguments against these considerations. The carbide layer towards carbon is not fully developed and only some regions of carbide are formed initially. According to the proposed mechanism, both layers are growing at the same time, because the by- product of one reaction is the reactant for the second reaction. Thus the second layer should be present all over the interface from the very beginning. Recirculation of the oxygen from the oxygen rich first layer is also questionable. Thermodynamic calculations showed acceptable partial pressure of Al_2O (10^{-6}) above aluminium oxide, but this value is probably lower above the mixture of carbide and oxide, respectively oxycarbides. In this case all the oxygen in the system should accumulate in the oxygen rich layer and the mechanism is then valid only for the initial stage until aluminium oxide protective layer is evaporated completely. However, the oxygen in the argon and from the leakage in the vicinity of Al might generate oxide layer even after the original oxide layer is evaporated. Another alternative could be that the proposed gas transport mechanism is valid only for the first oxygen rich layer, which is formed from the protective oxide layer. After some time cracks are initiated in the oxide scale, which might be the pathways for liquid aluminium and the second layer is formed by direct contact of liquid aluminium and carbon.

The crystals of aluminium carbide observed after slow cooling are formed by precipitation of aluminium carbide in liquid aluminium. The solubility of carbon (as aluminium carbide) in aluminium is 40 ppm at 1000 °C, but significantly higher, around 250 ppm at 1200 °C [37]. These crystals were therefore growing during cooling showing that Al contained significant amount of carbon. Carbon is in direct contact with aluminium, but the aluminium oxide protective layer may represent a barrier against the dissolution. When a carbide layer is formed, the barrier between Al and C becomes more significant and the transport of solid carbon through the dense Al_4C_3 layer is not likely. However, formed aluminium carbide on the Al/C interface may also dissolve to liquid aluminium.

Tschöpe et al. observed aluminium carbide with different morphology after the same experiments in the same setup [64]. Typical two layers with different oxygen content were present, but another carbide layer was also found towards aluminium, as shown in Figure 7.11. The disordered, particle-like character of this layer

suggests the reaction of aluminium on the carbon surface followed by the detachment of formed aluminium carbide. The new carbon surface is periodically established and the disordered layer does not represent a diffusion barrier.

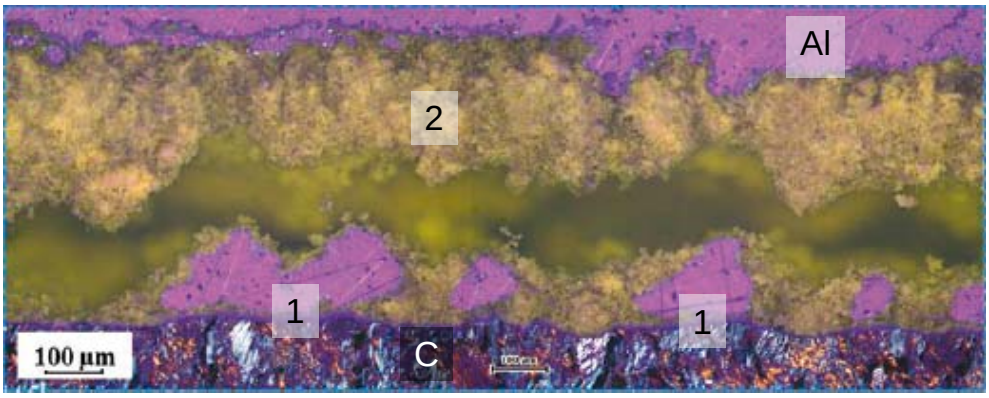

Figure 7.11: Optical image of Al/C interface after the experiment performed by Tschöpe (1200 °C, 10 days). Original layer is visible on some places of C surface (1). Disordered carbide layer was found more in the bulk of Al (2) [64].

Similar pattern was observed in one experiment, where the furnace was shut down accidentally after 1 day. The furnace was then restarted and the experiment continued another 3 days. The detachment of the carbide double layer was observed, which was followed by the formation of disordered carbide layer as shown in Figure 7.12. The detachment might have happened during cooling or heating up. The carbon surface was thereby renewed and enabled the formation of aluminium carbide with different morphology.

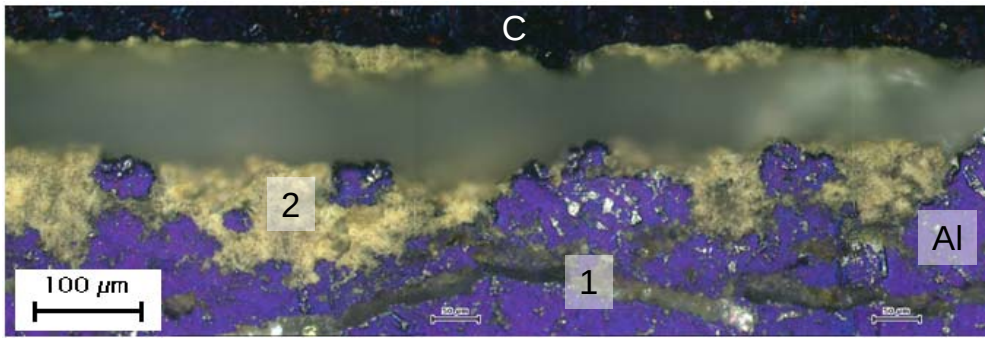

Figure 7.12: Optical image of an experiment restarted after accidental shut down slow cooling. Original layer has detached (1) and a new layer with different morphology was formed (2).

7.2 Al-C diffusion couples with cryolite

Introduction of cryolite at the Al/C interface had a significant influence on the formation of aluminium carbide. Aluminium carbide was found at the interface at 1030 °C. The thickness of the aluminium carbide layer was uneven along the interface reflecting the topography and variation in the local amount of cryolite. A typical Al/C interface after the experiment with small amount of cryolite introduced at the interface is shown in Figure 7.13.

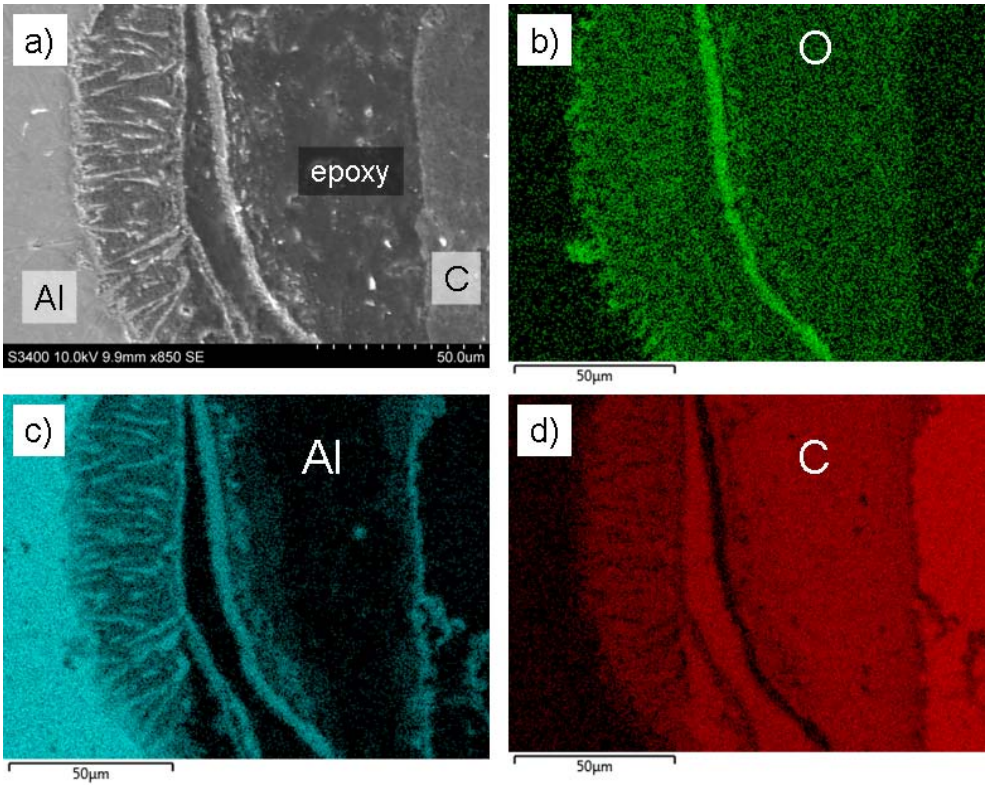

Figure 7.13: Al/C interface after 3 hours at 1030 °C with cryolite; a) SEM image and element maps of b) oxygen, c) aluminium and d) carbon.

The gap between Al and C due to the solidification of liquid Al during cooling became infiltrated with epoxy during sample preparation. Cryolite could not be found at the cross section of the diffusion couple after the experiment. A layer of aluminium carbide was found near the carbon surface, which is evident from the Al map in Figure 7.13c. A thick and relatively dense layer was usually observed at the interface and the thickness was varying from 10 to 20 µm. EDS analysis of this layer revealed high oxygen content, as demonstrated by the oxygen element map in Figure 7.13b. The layer was in this case detached from the carbon surface, but sometimes it was found also near the carbon surface.

Aluminium carbide grains with needle-like morphology were observed towards aluminium (Figure 7.13). These needles were always oriented perpendicularly to the Al/C interface regardless of the position in the crucible (bottom, top or sidewalls). The layer of the Al_4C_3 needles was observed only in some regions of the interface and the thickness was varying from 10 to 300 μm. A special experiment was performed, where thicker layer of cryolite (up to 500 μm) was introduced on the top of the crucible under the carbon lid. Figure 7.14 shows the long carbide needles found in this region, which confirmed the prediction that the length and occurrence of the needles is dependent on the local amount of cryolite initially present at the Al/C interface.

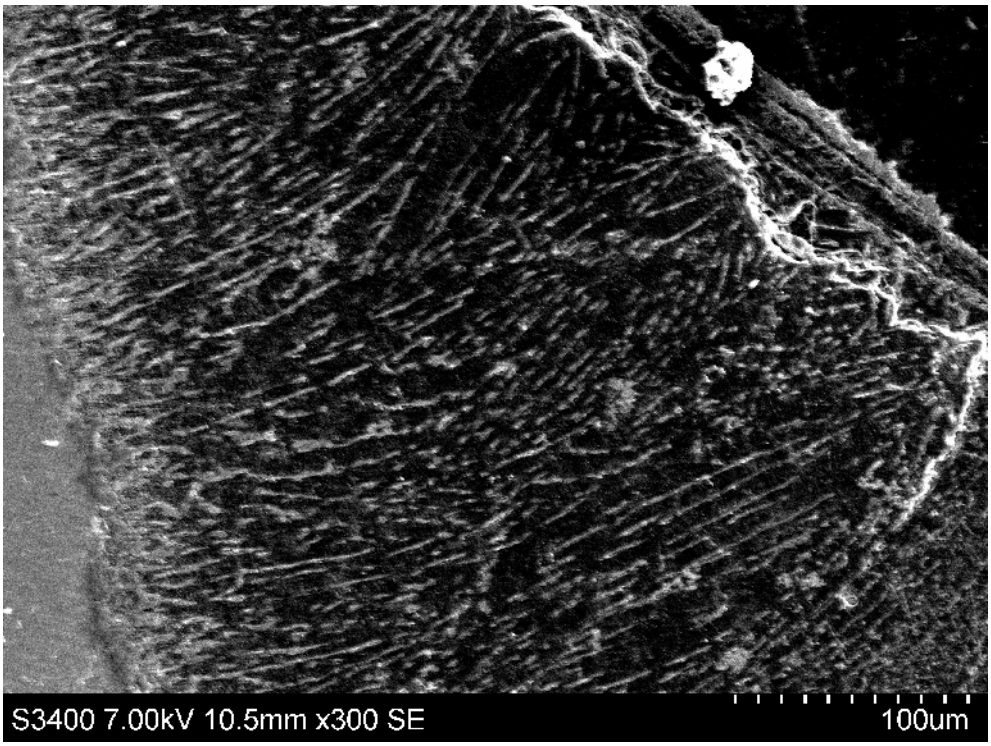

Figure 7.14: Optical image of relatively thick needle-like Al_4C_3 layer found on the place with high amount of introduced cryolite after 3 hours at 1030 °C.

The penetration of molten electrolyte into the pores was usually not observed, because the low amount of cryolite at the interface did not give sufficient amount of molten fluoride to fill the pores and the dense layer could act as a barrier on the carbon surface. In Figure 7.15 one special case of penetration was observed. The aluminium oxide layer was not found in contact with carbon and higher amount of cryolite was present locally, which made sufficient penetration to the pores possible. The element mapping suggests the presence of aluminium carbide in the pores. No fluorine or sodium could be detected, but cryolite had most likely penetrated to the pores in the initial stage before it has evaporated and enabled aluminium carbide formation.

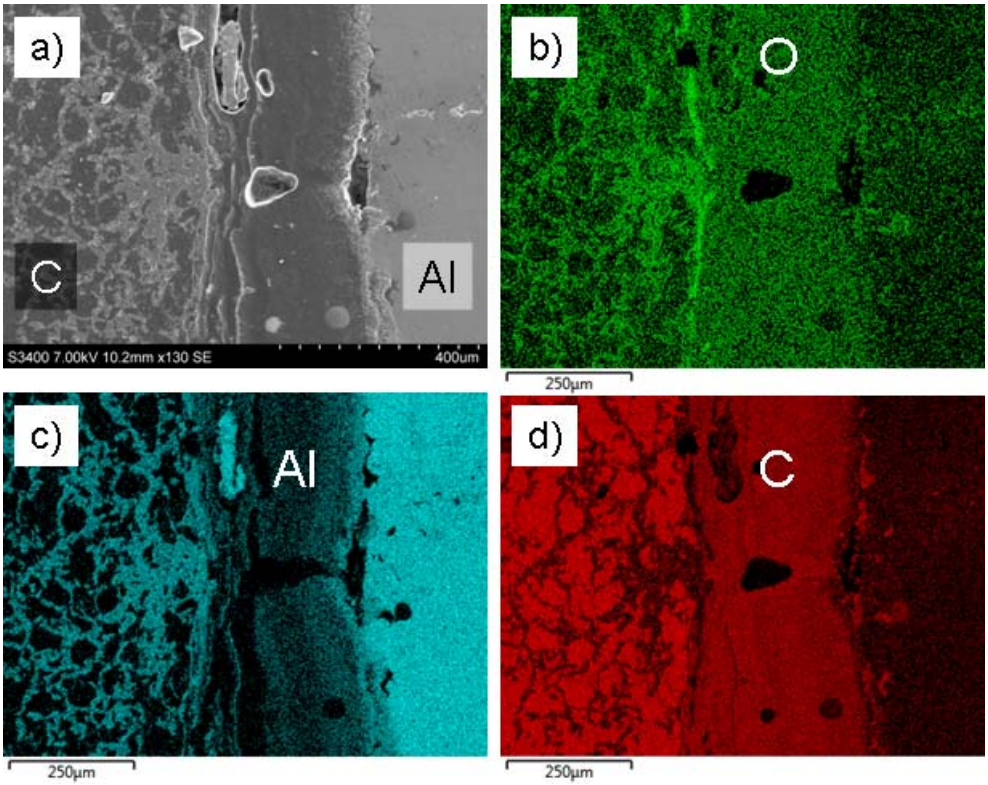

Figure 7.15: Aluminium carbide found in the pores of carbon after 3 days at 1100 °C; a) SEM image and element maps of b) oxygen, c) aluminium and d) carbon.

XRD of the aluminium and carbon surfaces confirmed the presence of aluminium carbide and aluminium oxide, but no oxycarbides could be found. The X-ray diffractogram of the interfacial region is shown in Figure 7.16. Cryolite or fluorides could not be detected in any of the experiments with small amounts of cryolite introduced at the Al/C interface. This was evident also by EDS mapping, where no fluorine or sodium could be detected.

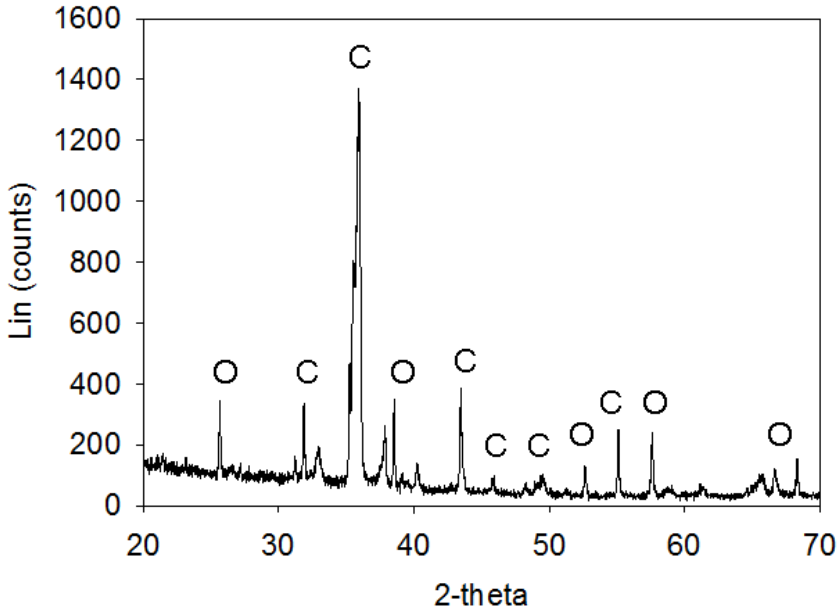

Figure 7.16: X-ray diffraction pattern of the Al surface (the contact surface with C). The reflections belong to aluminium carbide (C) and aluminium oxide (O).

The dense layer with relatively high oxygen content was typically observed close to the carbon surface. It is not possible to make a conclusion whether the layer is highly oxidized aluminium carbide, aluminium oxycarbide or aluminium oxide. EDS mapping gives only the element ratio and carbon coating of the sample, which is necessary for the SEM sample preparation, makes element mapping more challenging. The small amount of carbon in this layer may come from the carbon coating. Based on Figure 7.13 it is suggested that the dense, oxygen rich layer is aluminium oxide, which is formed by re-precipitation from the cryolite film present initially at the aluminium surface. The thin aluminium carbide layer is probably formed by direct contact of aluminium and carbon at the carbon surface. In the initial stage, before the cryolite has disappeared completely, aluminium could be transported relatively fast through the thin layer of liquid cryolite. Dissolution of aluminium carbide into cryolite can be neglected, because the small amount of cryolite does not have sufficient capacity for carbide dissolution. Cryolite was not detected after the experiment, but the initial presence before evaporation enabled Al/C contact and formation of aluminium carbide.

Thermodynamic calculations (FactSage 6.2) [60] were performed to determine the vapour composition in Al-C-O system in presence of cryolite at various conditions. The results revealed that introduction of cryolite have no influence on the vapour pressures of aluminium and aluminium suboxide. Vapour pressures of aluminium and aluminium suboxide were considerable at 1100 - 1200 °C (Figure 7.8), where the gas transport mechanism was proposed for Al/C reaction without cryolite (Figure 7.10). At the experimental temperature (1030 °C) these partial pressures are low ($\sim 10^{-7}$) and their involvement in aluminium carbide formation is less likely.

The layers were different compared to layers formed without cryolite, which also point to a different growth mechanism. The calculated vapour pressures of cryolite species when cryolite is in contact with Al and C and traces of Al_2O_3 are given in Table 7.1. The values given in Table 7.1 demonstrate the volatility of sodium and fluorine at these conditions. This supports the experimental findings where cryolite species were not found at the interface after the termination of the experiments. When the volume of the glass tube and the small amount of cryolite is considered, cryolite can be completely removed by evaporation. In addition, fluorides are attacking the glass-tube and thereby increasing the driving force of fluoride removal. Cryolite is therefore relatively quickly transported away from the Al-C interface during the experiment, but the initial presence is sufficient to initiate carbide formation. The effect of cryolite is suggested to be the dissolution of the protective oxide scale on the Al surface and improvement of the wetting properties between Al and C. The dissolution of aluminium oxide by cryolite is not included in the calculations, but cryolite is known to be a good solvent for aluminium oxide [9]. However aluminium oxide is reprecipitated due to the evaporation of cryolite and the oxide layer is then found near the carbon surface.

Table 7.1: Vapour pressures of cryolite species in Al-C-O system with cryolite at 1030 °C.

System	Excess Al	Excess C
	Partial pressure / bar	
Na	$4.2 \cdot 10^{-2}$	$1.4 \cdot 10^{-2}$
AlF	$1.05 \cdot 10^{-2}$	$1.2 \cdot 10^{-3}$
$NaAlF_4$	$6.2 \cdot 10^{-3}$	$6.2 \cdot 10^{-3}$

The reactions and processes taking place at Al/C interface with a thin film of cryolite are illustrated in Figure 7.17. Transport of aluminium to the carbon surface and the formation of aluminium carbide are possible after the oxide layer is dissolved. The morphology and occurrence of the carbide needles suggest that they are formed by precipitation from the bath. As cryolite is evaporating, the dissolved aluminium carbide precipitates and the carbide crystals grow. The presence of cryolite was shown to be a necessary requirement for the formation of the carbide needles.

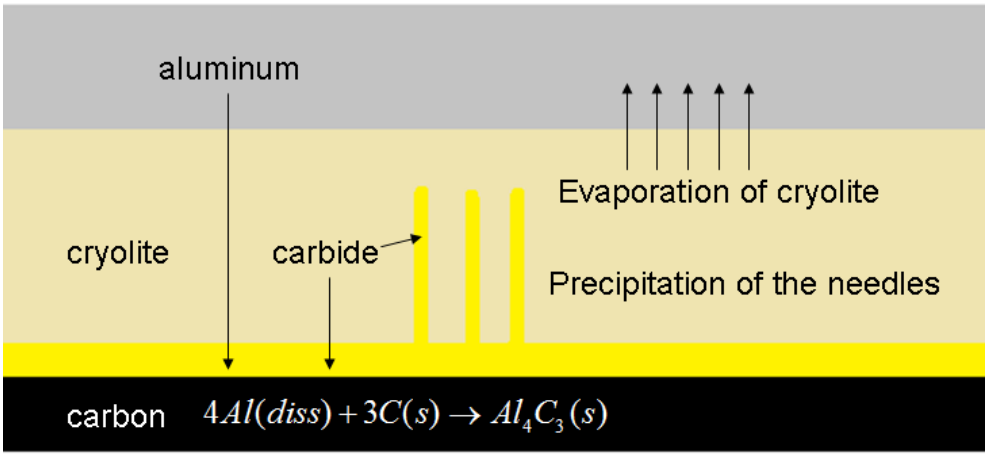

Figure 7.17: Reaction scheme on Al/C interface with thin film of cryolite.

The needle-like shape of the crystals is determined by the crystal structure and the growth is preferred to proceed in one direction. The orientation of the needles and their formation in cryolite environment points to a vapour-liquid-solid growth mechanism [58], which was described in Figure 5.2. The growth in the direction from aluminium towards carbon is less likely due to low vapour pressure of aluminium and aluminium suboxide. Liquid aluminium is not an appropriate substrate for the growth of the needles. The growth towards aluminium is more likely, as it is illustrated in Figure 7.18 and carbon might serve as a good substrate. Cryolite as a liquid phase is saturated with aluminium carbide (≈1 wt%) [41] and aluminium (≈0.1 wt%) [65]. The only carbon containing gas, which can be involved in the reaction with molten Al, is CO. The partial pressure of CO in the system is low (10^{-7} bar), but on the outside of the crucible (local equilibrium) the pressure is higher (10^{-5} bar) and depends on oxygen concentration in the system. When CO is introduced to cryolite, it reacts with dissolved aluminium (Reaction 17). Formation of aluminium carbide in saturated cryolite leads to precipitation of Al_4C_3(s). The precipitation can take place by further growth of the needles. This is determined by the anisotropy of the crystal, the growth is preferred to proceed in one direction. Solubility of Al_2O_3, the by-product of the reaction, is 10-20 times higher, therefore precipitation should not occur in the initial stage, but when cryolite is evaporated. Alumina content reduces aluminium carbide solubility in cryolite [25] and thereby enhances its further precipitation. If Al_4C_3 is formed by Reaction (7.6), the by product CO_2 can be transported back to carbon, react to CO and recycle the oxygen without accumulation. However, this reaction is not thermodynamically favoured ($\Delta G° = 28.6$ kJ (1030 °C)).

$$6CO(g)+4Al(diss)=Al_4C_3(s)+3CO_2(g) \qquad (7.6)$$

Evaporation of cryolite also leads to Al_4C_3 precipitation, which might contribute to the growth of the needles. These two mechanisms (evaporation-precipitation and v-l-s) can actually work together.

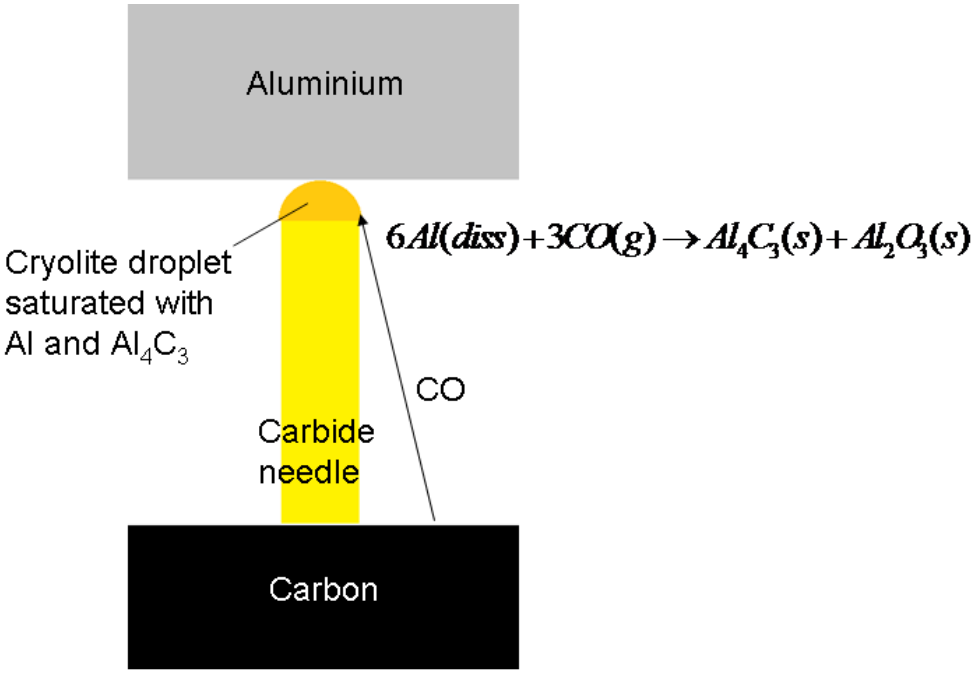

Figure 7.18: Illustration of the growth of aluminium carbide needles by vapour-liquid-solid mechanism.

The experiments showed that small amount of cryolite changes the reaction between Al and C dramatically. However the evaporation of cryolite and formation of carbide needles is not likely to happen in industrial cell, where large amount of cryolite is present, and mass transport in the gas phase is less likely.

The experiments with larger amounts of cryolite showed different results compared to experiments with only a thin film of cryolite. The cross section of the Al/C interface on the bottom of a crucible after 3 hours of experiment is shown in Figure 7.19. The gap between Al and C is caused by the shrinkage of aluminium during cooling. Aluminium carbide was not found at the interface, only a layer of the fluoride bath was observed. The molten salt had also infiltrated the pores of the carbon material, which can be seen in the Na and F element maps shown in Figure 7.19. However, a thin layer of aluminium carbide, which is not visible in the resolution of the images, cannot be ruled out. Aluminium carbide might also be dissolved in the bath, but the low concentration at this temperature does not allow identification from the element maps.

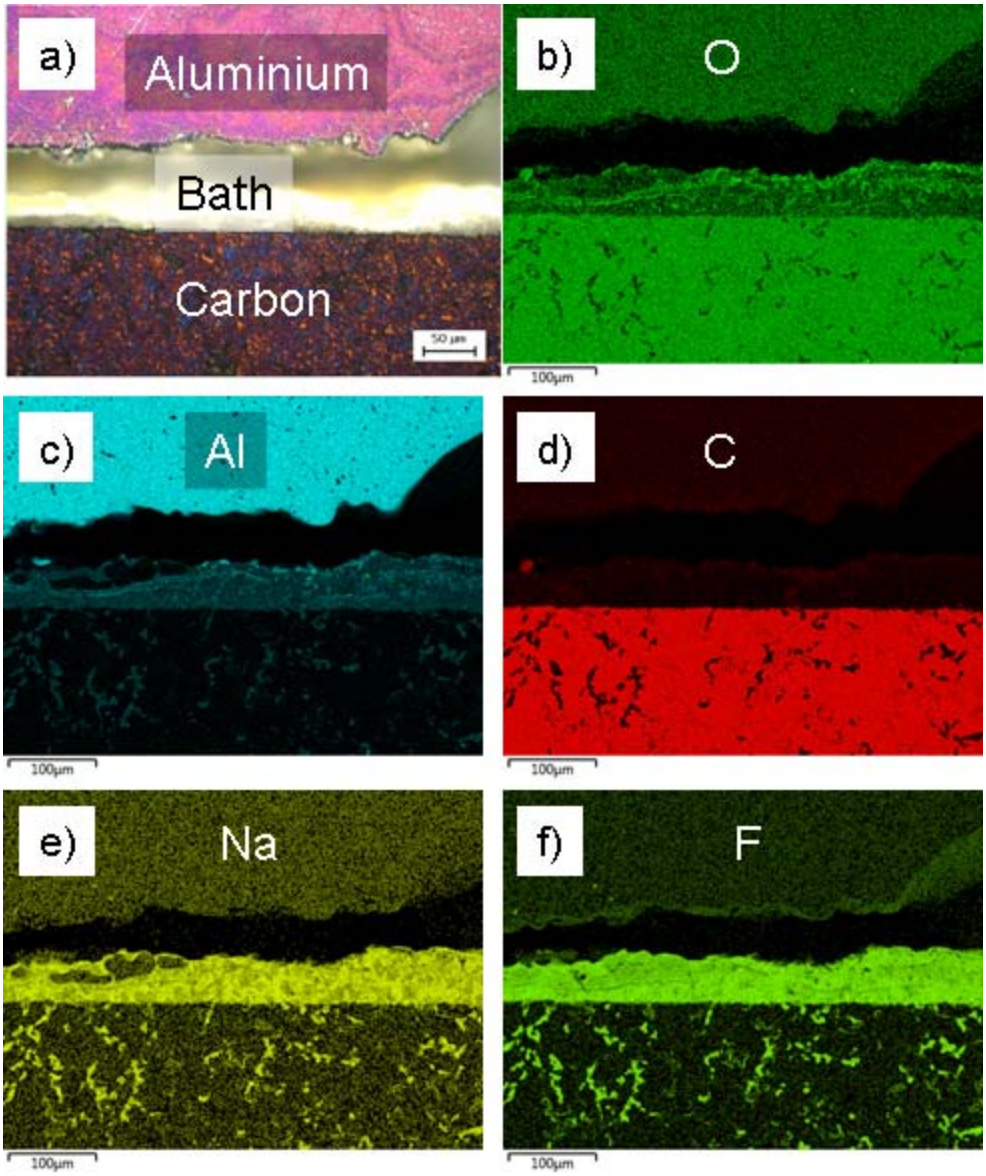

Figure 7.19: Al/C interface after 3 hours experiment with proper amount of cryolite, 980 °C, a) SEM image and element maps of b) oxygen, c) aluminium, d) carbon, e) sodium and f) fluorine.

A layer of aluminium carbide could also be observed at the carbon surface after the experiment with duration of 3 days. Figure 7.20a shows aluminium carbide layer, which is recognizable by the characteristic purple/pink colour in the optical images using polarized light. The layer is porous and the pores were filled with the molten bath, as shown in Figure 7.20b. In some regions the aluminum carbide layer was observed to detach from the carbon material, which was followed by the formation

of a new layer and the delaminated layers of aluminum carbide could be observed in Figure 7.20c.

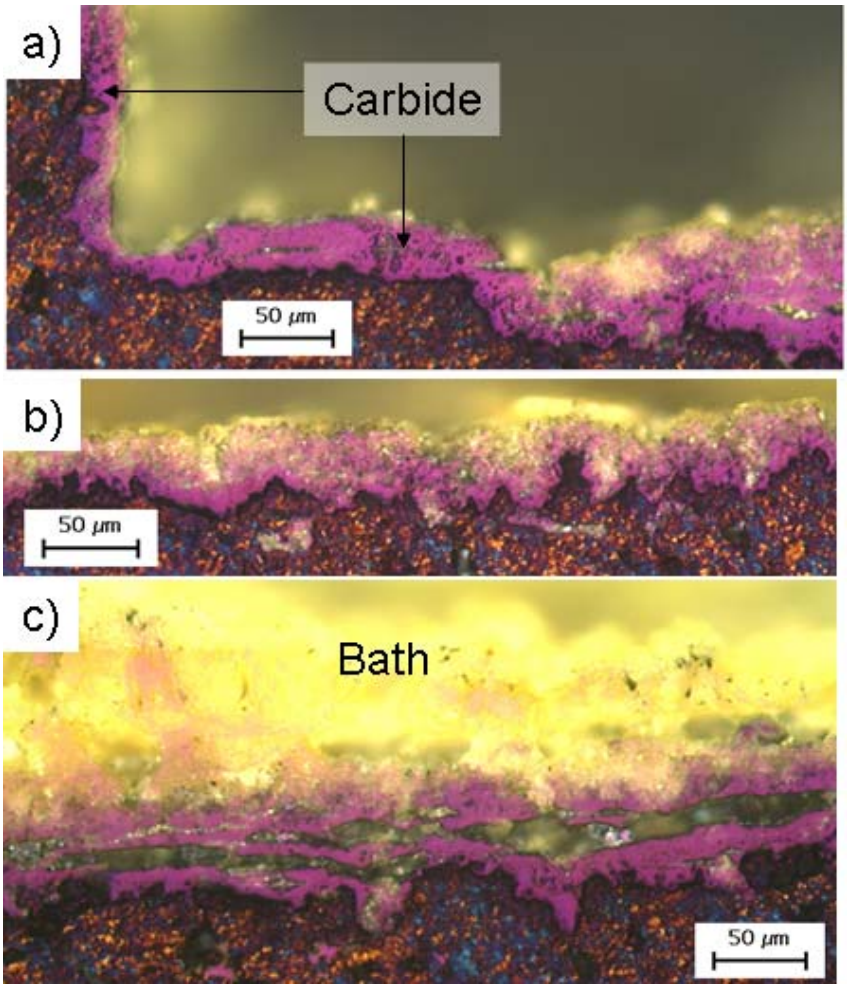

Figure 7.20: Optical images of aluminium carbide layer after 3 days at 980 °C, a) compact layer all over the interface, b) porous layer filled with bath, c) delaminating of carbide layers.

The experiments showed that longer time is needed for the formation of aluminium carbide layer, when higher amount of cryolite is present. These results are in line with the experiments performed by Grjotheim [42], which were described in Chapter 4.2. Aluminium carbide formation and dissolution into the bath proceeds until saturation and the saturation time depends on several factors such as bath composition and amount, aluminium-carbon contact surface and convection in the system and removal of carbide from the vicinity of the interface. The reaction becomes slowed down as a carbide layer is formed at the carbon surface, which acts as a diffusion barrier for further growth. However the analysis of aluminium carbide layer revealed a porous layer, which allows faster mass transfer through the

pores (Figure 7.20). Therefore it was challenging to determine the critical thickness for further growth of the layer. In some regions relatively thin and dense Al_4C_3 layer without pores was found as shown in Figure 7.21. The thickness was around 10 μm and that might be considered as a critical thickness.

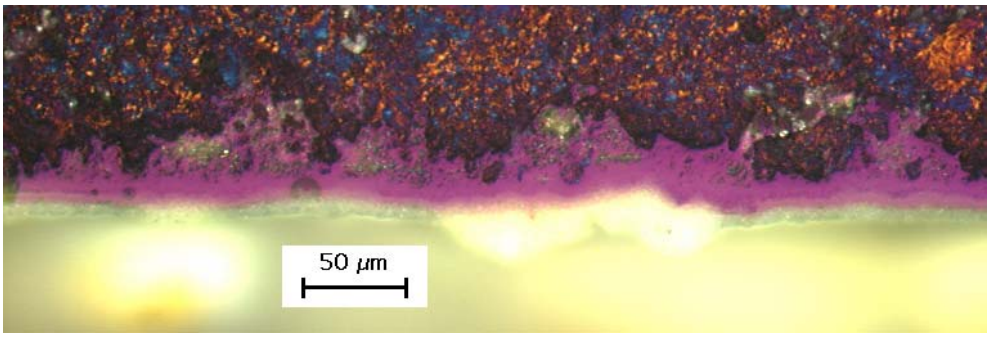

Figure 7.21: Optical image of relatively thin and dense layer of aluminium carbide, proper amount of cryolite, 3 days, at 980 °C.

Grjotheim observed also strong correlation between the amount of the carbide formed and the porosity of the carbon material [42]. The morphology of the aluminium carbide reflects the topography of the carbon material and higher porosity means larger contact surface, where the reaction takes place. Carbon particle detachment is also more likely to happen in more porous materials.

7.3 Al-C diffusion couples in an electrical field

Experiment with current going through the pure Al/C interface was performed at 1030 °C for 1 day. During the first 2 hours the cell voltage was rising continuously from 0.3 V to 1V, followed by periodical oscillations as shown in Figure 7.22a. Sometimes the oscillation peaks were reaching high values (more than 10V), but the most typical oscillations were between 0.2 and 0.8V as shown in Figure 7.22b. The typical period of the oscillations was around 3 minutes and the voltage was rising exponentially within this period. Analysis of the carbon cathode/aluminium interface did not show any sign of an aluminium carbide layer. Aluminium was in poor contact with carbon and the gaps were filled with epoxy during sample preparation as shown in Figure 7.23. The cell voltage during the experiment at 1100 °C was similar to the experiment at 1030 °C. The voltage was rising the first 2 hours and then similar oscillations were observed as displayed in Figure 7.24. In this case, the character of these oscillation periods was a bit different. The height of the peaks was usually higher, the voltage was not always rising exponentially and the duration of the period was varying more. Figure 7.25 shows the cross section of the interface. A layer of aluminium carbide layer could not be observed, but aluminium was found in relatively good contact with carbon.

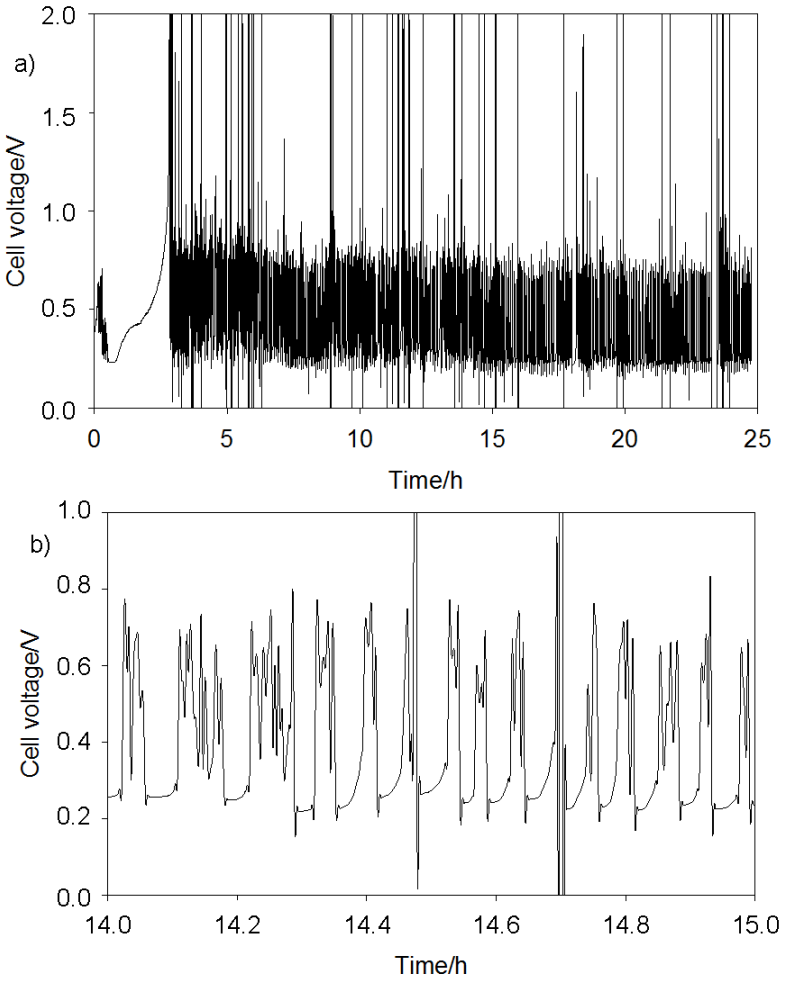

Figure 7.22: Cell voltage during Al/C diffusion couple experiment with an electrical voltage over the interface, 1030 °C, 1 day; a) cell voltage during all electrolysis, b) zoom of cell voltage, periodical oscillations.

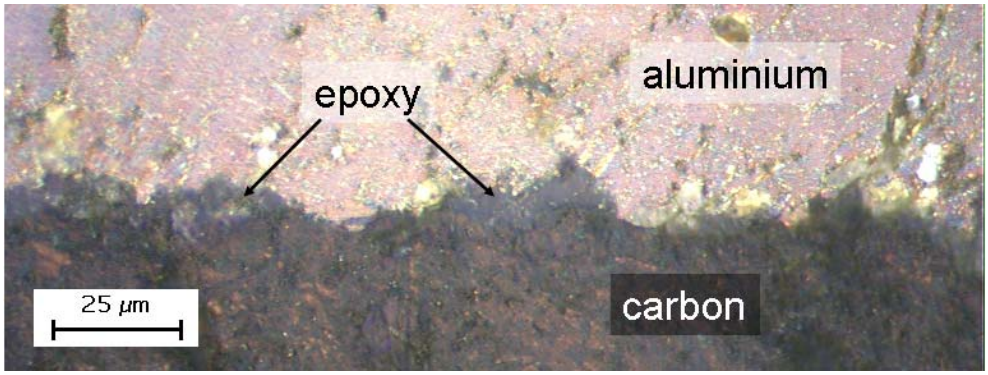

Figure 7.23: Aluminium/carbon interface after Al/C diffusion couple experiment with an electrical voltage over the interface, 0.2 A/cm^2, 1030 °C, 1 day.

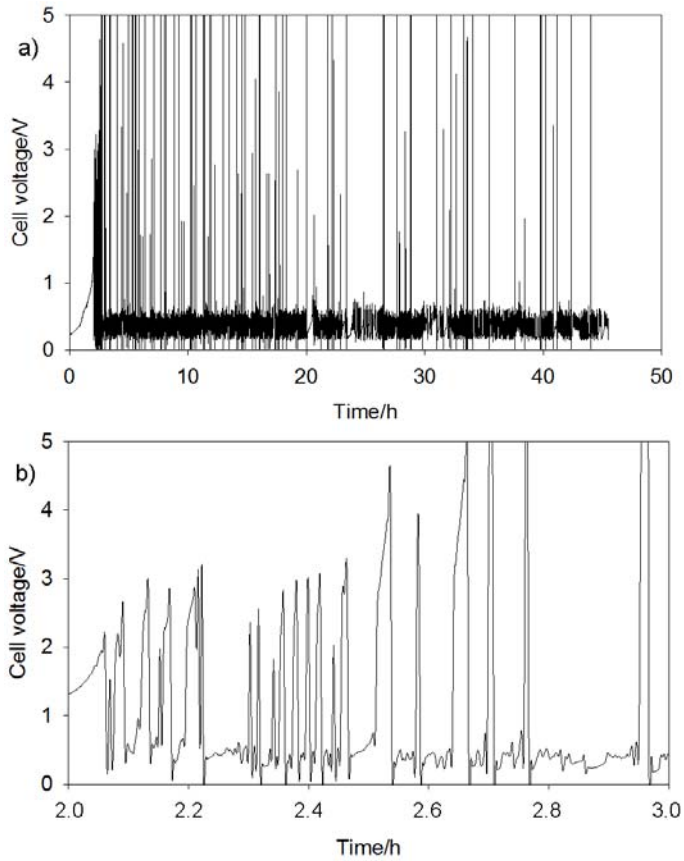

Figure 7.24: Cell voltage during Al/C diffusion couple experiment with an electrical voltage over the interface, 1100 °C, 2 days; a) cell voltage during all electrolysis, b) zoom of cell voltage, periodical oscillations.

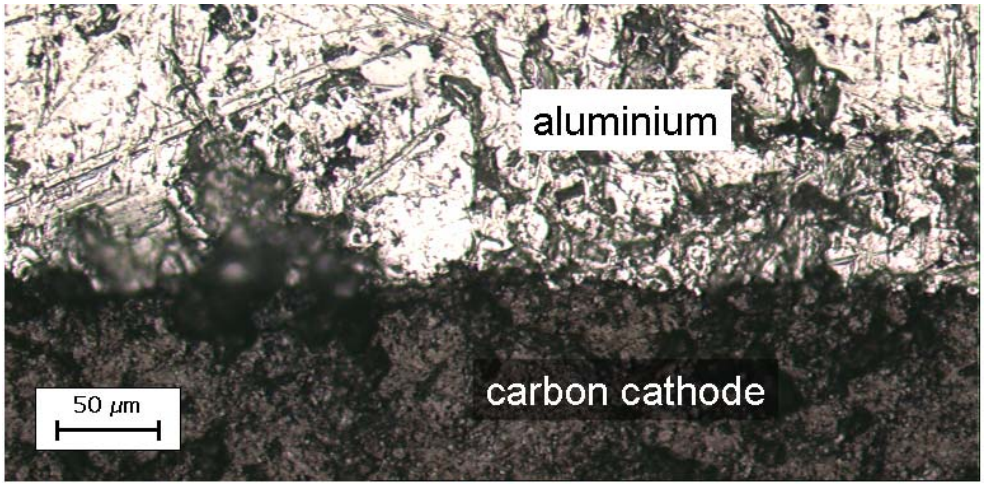

Figure 7.25: Aluminium/carbon interface after Al/C diffusion couple experiment with an electrical voltage over the interface, 0.2 A/cm^2, 1100 °C, 2 days.

When cryolite was introduced at the Al/C interface, the cell voltage versus time displayed a quite similar pattern as in the experiments without cryolite, as shown in Figure 7.26. The voltage was rising during the first hour and then the oscillations started.

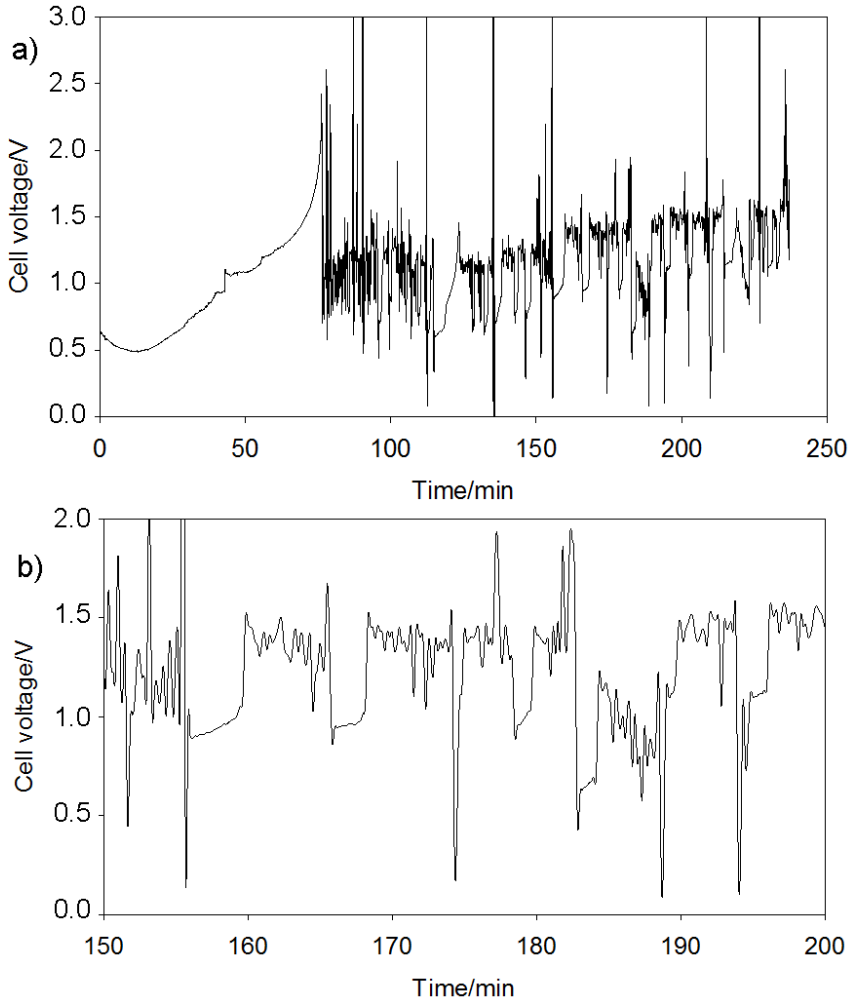

Figure 7.26: Cell voltage during Al/C diffusion couple experiment with film of cryolite and an electrical voltage over the interface, 1030 °C, 4 hours; a) cell voltage during all the experiment, b) zoom of cell voltage, periodical oscillations.

Figure 7.27 shows the cross section of the Al/C interface, which is similar to the diffusion couples without current as shown in Figure 7.13. Cryolite was not found at the Al/C interface after the experiment and the needles of aluminium carbide were found towards aluminium. The thickness of the needle layer of aluminium carbide was dependent on the local amount of cryolite.

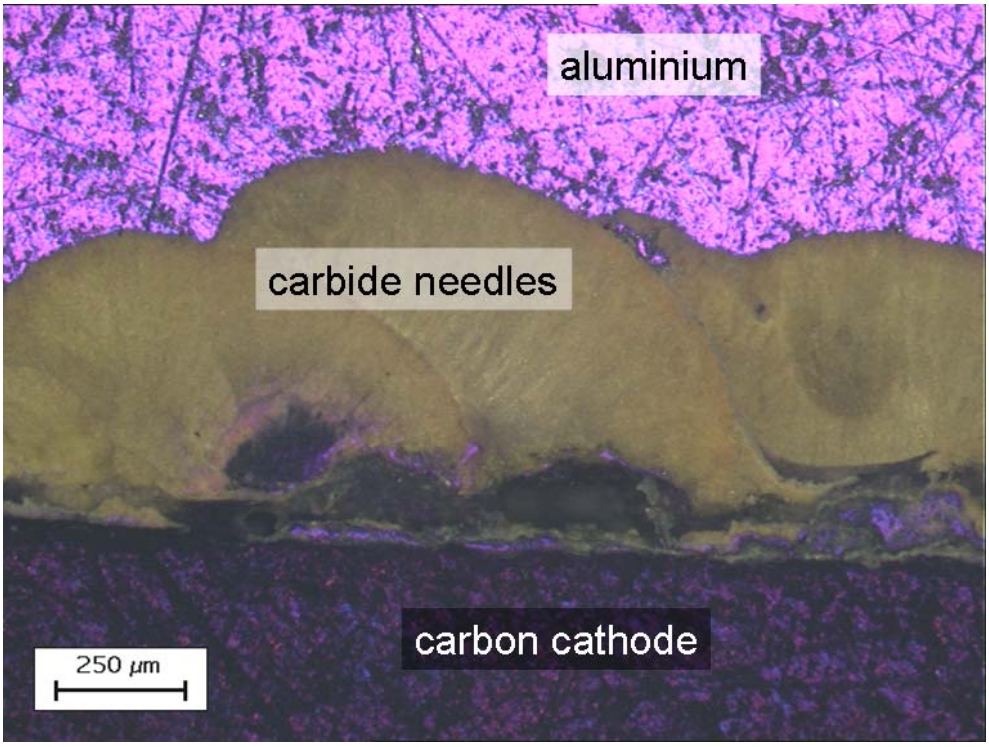

Figure 7.27: Optical image of aluminium/carbon interface after Al/C diffusion couple experiment with a film of cryolite and an electrical voltage over the interface, 0.2 A/cm^2, 1030 °C, 4 hours.

The detail of the Al/C interface (Figure 7.27) with EDS element maps is shown in Figure 7.28. The amount of aluminium carbide was however higher when current had passed through the diffusion couple. Aluminium carbide was found in a good contact with the carbon surface, but not always as a compact layer. The detached fragments of aluminium carbide were usually observed along the interface and the space between them and the gap caused by the shrinkage of liquid aluminium due to the solidification were filled with epoxy.

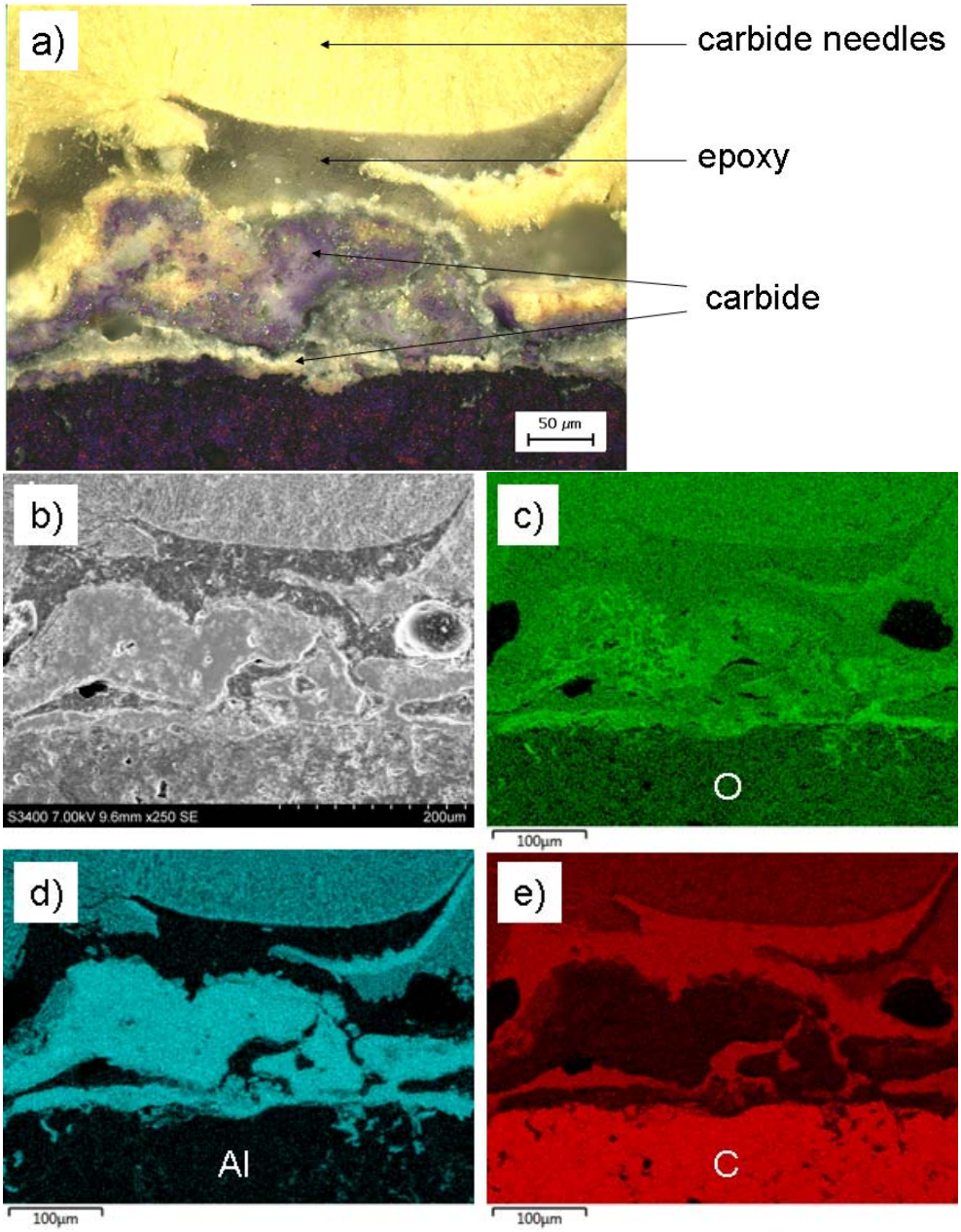

Figure 7.28: The detail of aluminium/carbon interface after Al/C diffusion couple experiment with a film of cryolite under polarization, 0.2 A/cm^2, 1030 °C, 4 hours, a) optical image (polarized light), b) SEM image and element maps of c) oxygen, d) aluminium and e) carbon.

It was shown in the previous experiments (Chapter 7.1) that a visible aluminium carbide layer did not form at 1030 °C without the presence of cryolite at the interface. The oscillations in the cell voltage can be explained by the formation of a

thin carbide layer, not detectable by the resolution of the image. Aluminium carbide is an electrical insulator and a thin, compact layer on the interface will increase the cell voltage. High resistivity of the layer may lead to local overheating and the reaction kinetics is enhanced. The cell voltage is rising until a critical value where the carbide layer is fractured, the Al/C contact is renewed and the cell voltage drops. Aluminium carbide on the carbon surface improves the wetting properties and the contact of aluminium and carbon was probably changing during the experiment as the layer was forming and detaching. Local contacts of Al and C were observed after the experiment in Figure 7.23. No electrochemical reactions are expected on the electrodes, only ohmic resistance. However, aluminium cations are suggested to be present in the system from the dissociation of Al metal, but ohmic conduction should be the dominant contribution.

A dense layer of aluminium carbide was observed at 1100 °C in the diffusion couple experiments without the application of an electrical current. Such a layer may represent a barrier with high electrical resistivity and its occurrence after the experiment with an electrical voltage is unlikely. The oscillations in the cell voltage are suggesting a periodical formation and fracture of a dense carbide layer. As the layer grows, the resistivity of the cell is rising, which is reflected by increased cell voltage. The thickness of the layer and the cell voltage reach a critical value, which might lead to fracture and formation of new Al/C interface. Higher oscillation peaks compared to experiment at 1100 °C and more irregularities in cell voltage can be explained by faster formation of aluminium carbide, which is probably formed by a direct reaction between the two elements. Relatively good contact of Al and C after the experiment is pointing to formation of a thin layer of carbide at the interface.

The needles of aluminium carbide in experiment with cryolite were probably formed by precipitation from the evaporating cryolite, as it was suggested in diffusion couple experiments. The oscillations in cell voltage may also be explained by the formation and fracture of the resistive carbide layer. The amount of aluminium carbide formed on the carbon surface was higher compared to diffusion couple experiment, which suggests that formation of aluminium carbide is enhanced by electrolysis. Increased cell voltage during oscillation periods was enhancing the electrochemical formation. Fractured aluminium carbide in the vicinity of carbon was observed due to low amount of cryolite and the evaporation of the cryolite, which did not allow sufficient dissolution of the resistive carbide layer.

7.4 Formation of Al_4C_3 in electrochemical cells

Electrolysis with a cell setup corresponding to real industrial cell was performed. A dramatic increase in cell voltage occurred after about 35 min as shown in Figure 7.29, where the experiment was terminated. The cell voltage during the initial 30

min of the experiment was 2.4±0.2 V. The electrochemical reaction, proposed to take place will be discussed further below.

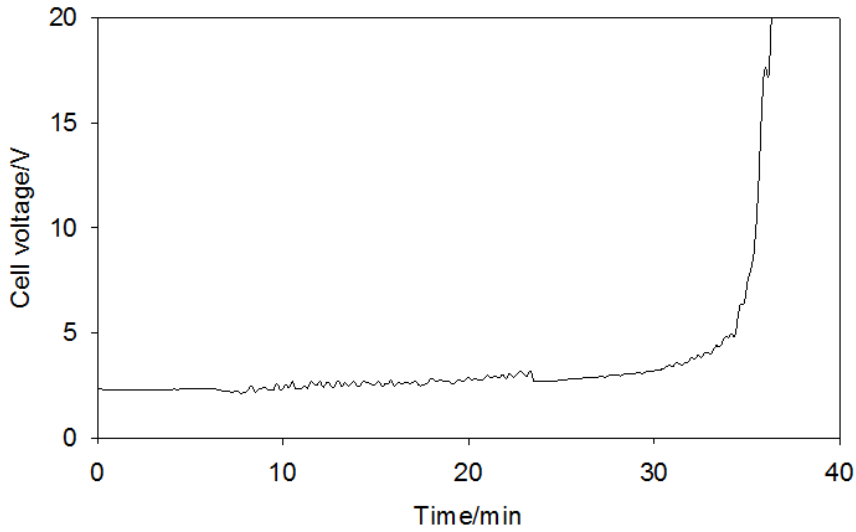

Figure 7.29: The recorded cell voltage during electrolysis at 980 °C in a cell setup corresponding to an industrial cell.

An aluminium carbide layer at the carbon surface was observed after the experiment, which is evident from the optical image and the C and Al element maps displayed in Figure 7.30. A thin film of the bath was present between aluminium and carbon. The thickness of the carbide layer is relatively even all over the cathode surface, but locally the layer has small gaps and the layer appears as an agglomerate of smaller carbide grains. The formation of aluminium carbide due to the electrolysis reaction is clearly much faster relative to the situation where no current was going through the cell.

The electrolyte bath had clearly penetrated into the porous carbon material in this experiment. An SEM image and element map of the interior carbon material is shown in Figure 7.31. The pores of the carbon cathode were filled with the bath and aluminium carbide was also observed to be formed on the walls of the pores. The Al_4C_3 layer is visible on the aluminium element map in Figure 7.31c. No aluminium metal could be detected in the interior of the carbon material.

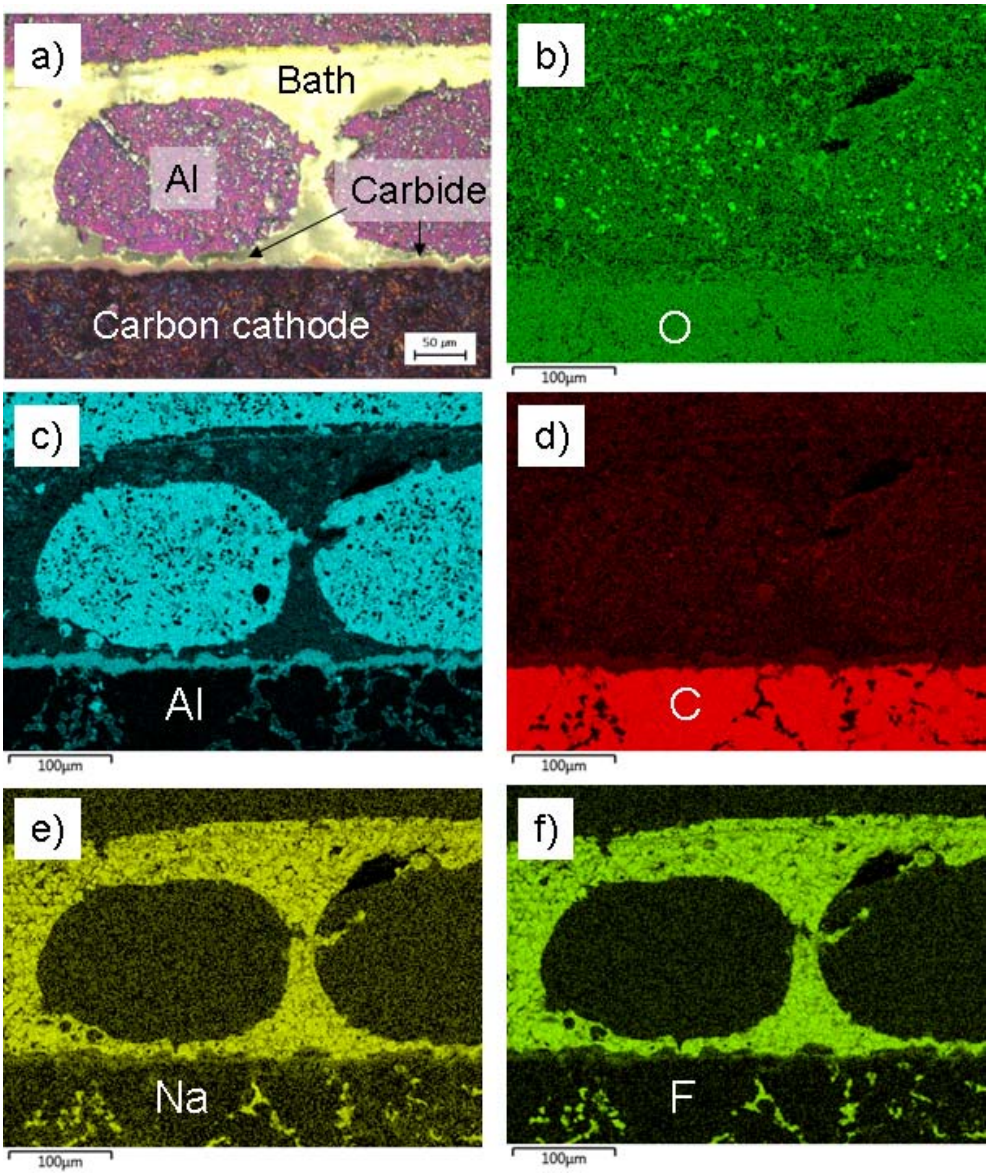

Figure 7.30: Al/C interface after 35 min of electrolysis in the conventional cell setup, 980 °C, a) Optical image and element maps of b) oxygen, c) aluminium, d) carbon, e) sodium and f) fluorine.

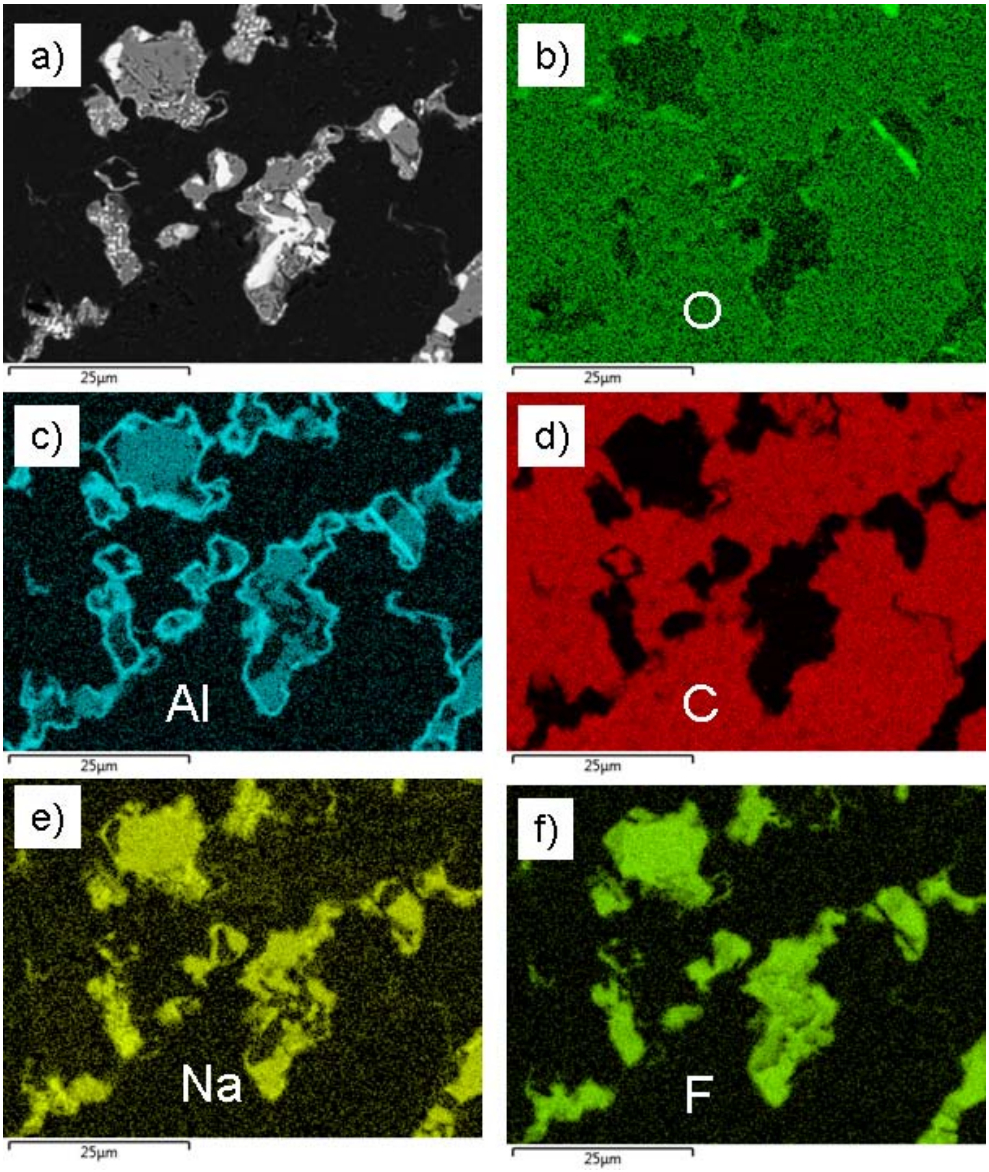

Figure 7.31: Pores of carbon after 35 min of electrolysis in the conventional cell setup, 980 °C, a) SEM image and element maps of b) oxygen, c) aluminium, d) carbon, e) sodium and f) fluorine.

During the experiment in the inverted cell the cell voltage was relatively stable, around 0.3 V, as shown in Figure 7.32. The cell voltage of about 0.25-0.35 V was significantly lower compared to electrolysis experiment conducted in the conventional cell. When the electrolysis was performed at higher current density 1 A/cm^2, the cell voltage was higher, around 1.3 V.

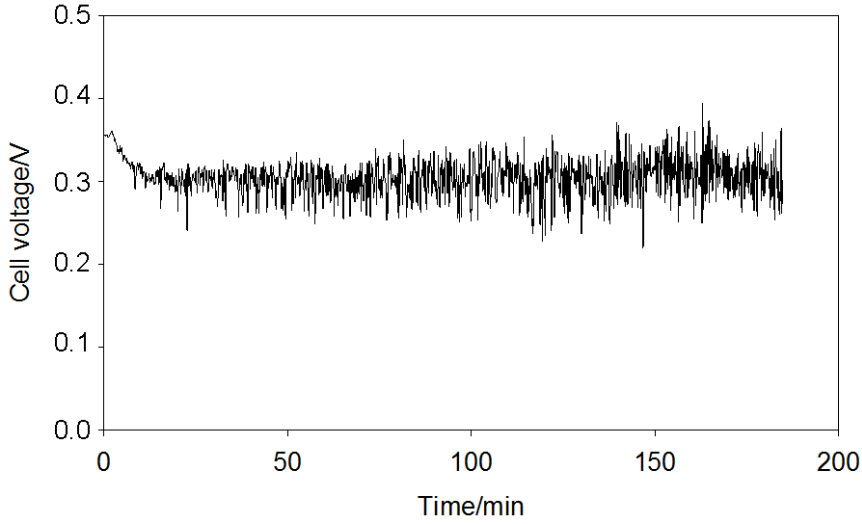

Figure 7.32: Cell voltage during electrolysis in the inverted cell setup at 980 °C.

An optical image and element maps of the bottom of the inverted cathode on the top of the cell is shown in Figure 7.33. Aluminium carbide could be observed at the surface of the cathode and on the pore walls inside the cathode material. The morphology of the carbide layer is comparable with the morphology of the carbide layer formed in the conventional cell (Figure 7.30). During this experiment aluminium was not intended to be in contact with the cathode at the initial stage and the aluminium observed in the bath close to the cathode is suggested to be cathodically deposited aluminium. The molten aluminium formed at the cathode should drop down through the bath to the Al pool, which is on the anode. However, the distance between the Al pool and the cathode was not large and the materials might have come into contact during the electrolysis. Analysis of the pores of the cathode material revealed the same result as in the conventional cell, which is shown in Figure 7.31, where the bath and aluminium carbide were found. Analysis of the anode, which was in this case in contact with aluminium, is shown in Figure 7.34. The bath film was present between the anode and aluminium, but no aluminium carbide layer was found. The bath has also penetrated into the pores of anode, but no carbide was found on the pore walls of the anode.

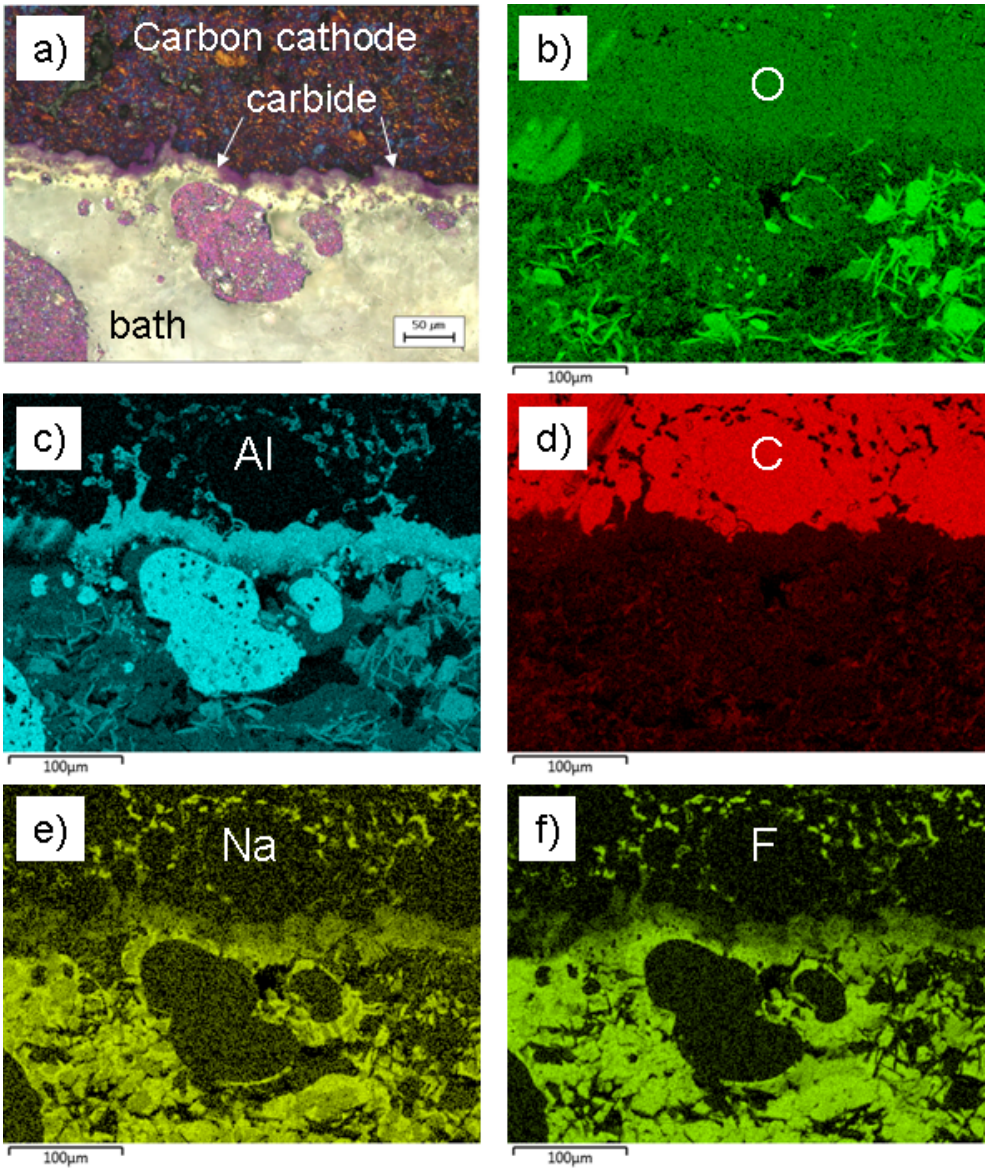

Figure 7.33: Cathode surface after electrolysis in the inverted cell setup, 3 hours, 980 °C, a) optical image and element maps of b) oxygen, c) aluminium, d) carbon, e) sodium and f) fluorine.

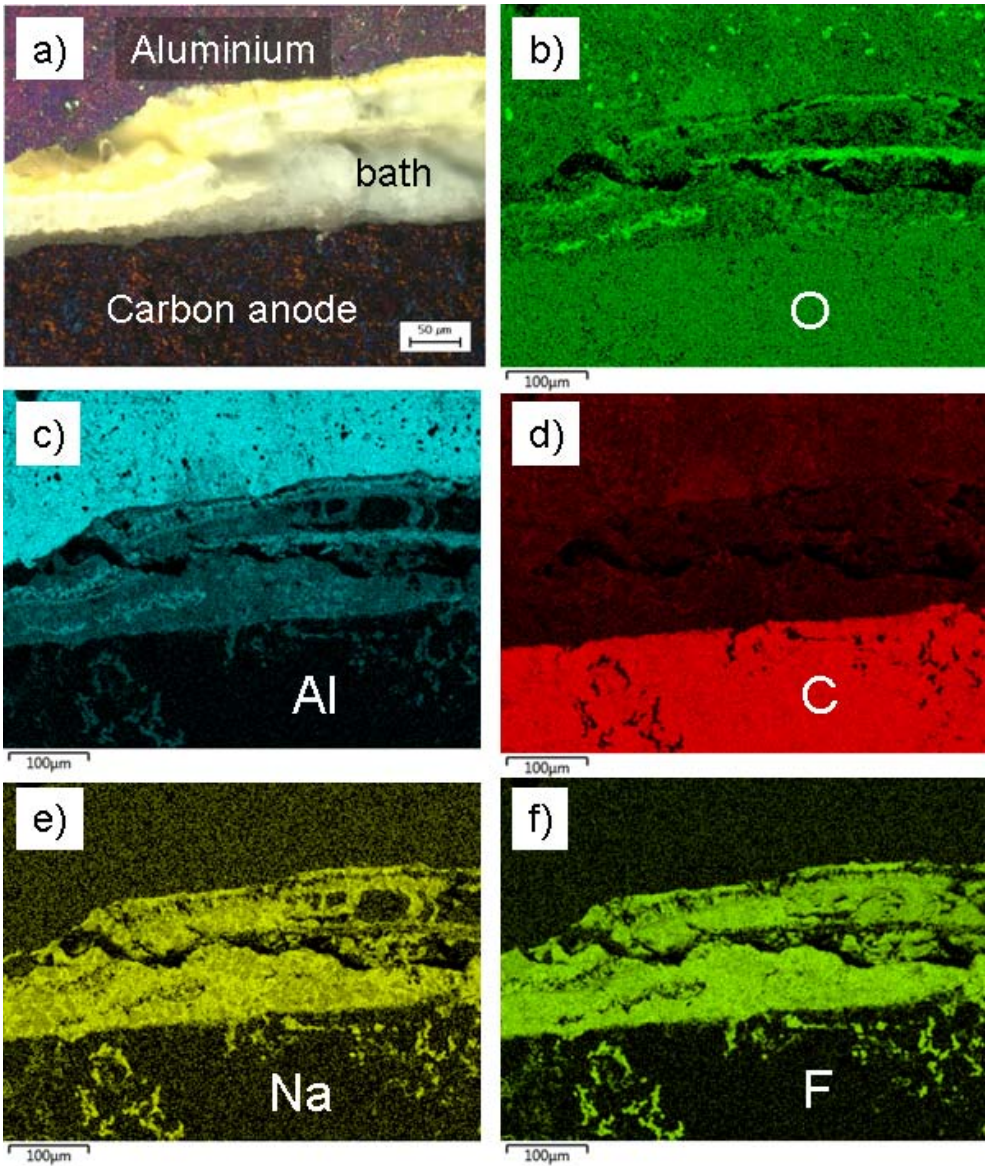

Figure 7.34: Anode surface after electrolysis in the inverted cell setup, 3 hours, 980 °C, a) optical image and element maps of b) oxygen, c) aluminium, d) carbon, e) sodium and f) fluorine.

The experiment using an inverted cell without aluminium present initially had similar cell voltage as the voltage observed in the conventional cell setup. The initial cell voltage was about 2.2 V, as displayed in Figure 7.35. This cell voltage suggests that alumina decomposition is the main reaction as discussed further below. A dramatically increased cell voltage was also observed, in this case after 60-80 min.

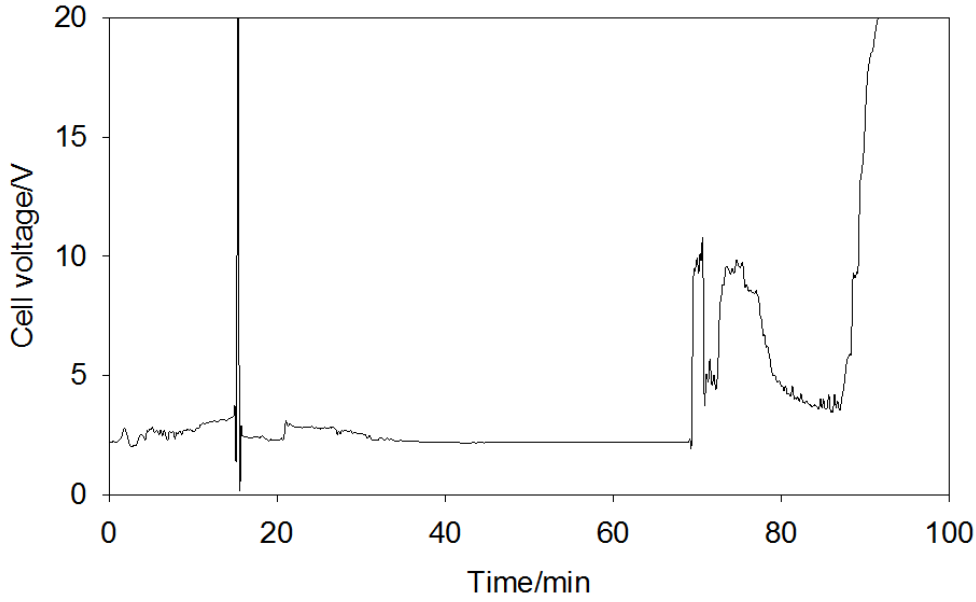

Figure 7.35: Cell voltage during electrolysis in the inverted cell setup at 980 °C without aluminium present initially.

An optical image and the element maps of the surface of the carbon cathode are shown in Figure 7.36. An aluminium carbide layer was also found on the carbon surface in this case, but the thickness was lower compared to the real and the inverted cell. The morphology of the carbide layer was similar to the other experiments. The layer was porous and the pores were filled with bath. Aluminium carbide was also observed in the pores, which is visible in Al element map in Figure 7.36c. Some aluminium was found in the bath in the vicinity of the cathode surface. This aluminium must have been formed on the cathode during electrolysis since no aluminium was present initially. Analysis of the anode revealed that there was no aluminium pad established. No carbide layer was found on the anode surface.

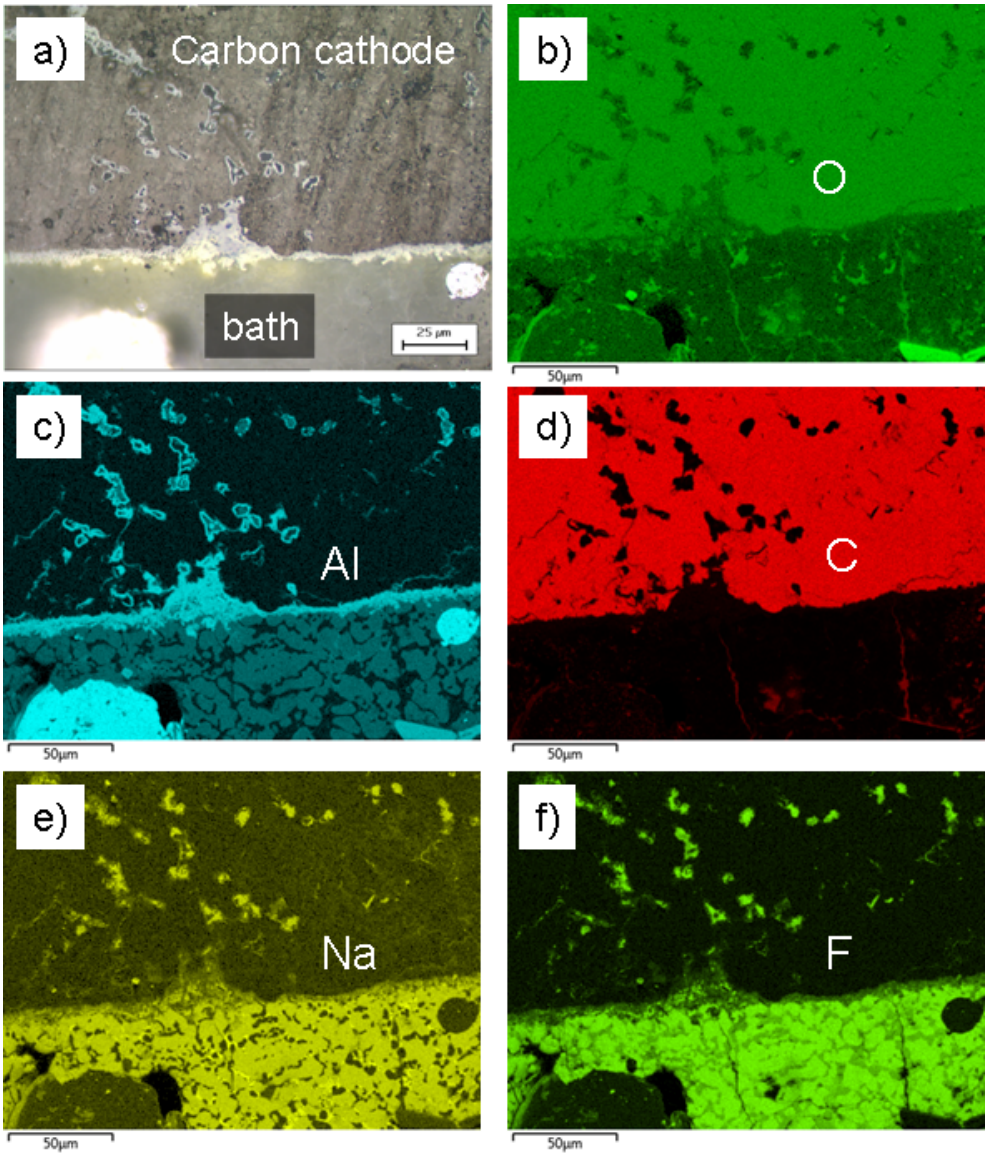

Figure 7.36: Cathode surface after 90 min of electrolysis in the inverted cell setup without Al, 980 °C, a) optical image and element maps of b) oxygen, c) aluminium, d) carbon, e) sodium and f) fluorine.

After the electrolysis in the setup corresponding to the conventional industrial cell aluminium carbide layer was found already after 35 minutes. Experiment with the same setup without electrolysis did not show aluminium carbide layer after 3 hours, which means that the electrochemical formation of aluminium carbide is much faster than the simple chemical reaction between the elements. The morphology of the layer was similar compared to chemical formation, where the carbide layer had pores filled with the bath. The character of the layer corresponds with carbide layers observed in industrial cells by Østrem [51].

This gives support to the mechanism suggested by Solheim [50], where aluminium carbide layer is proposed to act as a current shield on the carbon cathode. Areas, which are not covered with carbide, should have significantly higher current densities and excessive wear, especially on the edges of these "carbide islands". However, the carbide layer is probably dynamically changing and the thickness is a result of the equilibrium between aluminium carbide formation and dissolution. Faster formation and slower dissolution means carbide layer growth, but the formation is continuously slowed down as the layer grows and becomes a diffusion barrier. This suggests that the areas, which are or are not covered with aluminium carbide are periodically changing. Stable cell voltage also suggests that porous carbide layer does not represent significant electrical resistivity in terms of the overall voltage of the cell, but may play a role as a local current shield.

The cell voltage during the electrolysis in conventional cell was more than 2V and was increasing dramatically after about 35 minutes. Electrode reactions were expected to be the same as in industrial cell:

Cathode: $$AlF_4^- + 3\bar{e} \rightarrow Al + 4F \qquad (7.7)$$

Anode: $$AlOF_x^{1-x} + C \rightarrow CO_2 + AlF_x^{3-x} + 2\bar{e} \qquad (7.8)$$

The calculation from Faraday's law confirmed that the amount of alumina introduced to the bath was for 35 minutes of electrolysis when alumina decomposition (Reaction 1.1) is considered as the only reaction. It also means there was only negligible dissolution of alumina crucible, which could be a source of alumina for the electrolysis. The reversible voltage for alumina decomposition is 1.2 V (Reaction 1.1) and the rest of the cell voltage (2.4 V) is the ohmic resistivity of the bath and of the other cell components. Anodic and cathodic overvoltages are probably small contributions because of low current densities. Analysis of the pores suggested electrochemical deposition of carbide layer directly from the bath (Reactions 4.4 and 4.5). The carbide layer was observed on the walls, but no aluminium metal was found in the pores. However it is difficult to evaluate the involvement of aluminium metal in the formation of aluminium carbide, because even in the areas with no direct contact between carbon and Al metal, the main reaction is aluminium deposition. The formation of aluminium carbide may proceed in two steps, electrochemical deposition of Al (Reaction 2.1) and then chemical formation of Al_4C_3 (Reaction 4.1). This mechanism is however not likely, because the second step, chemical formation of aluminium carbide layer, was shown to be very slow when larger amount of bath is present in the cell.

The electrolysis experiment in the inverted cell had a lower cell voltage, only 0.3 V compared to more than 2.0 V in the conventional cell setup. There was no alumina decomposition taking place, but only cyclic reduction and oxidation of aluminium (Reactions 7.9 and 7.10). The reversible voltage of the inverted cell is 0 V and the measured cell voltage represents only the resistivity of the cell. The cathode reaction is the same as in the conventional cell (Reaction 7.7) and on the anode

there is no CO_2 evolution, but only the oxidation of aluminium, which is in this case in contact with the anode.

Cathode: $$Al^{3+} + 3\bar{e} \rightarrow Al \quad (7.9)$$

Anode: $$Al \rightarrow Al^{3+} + 3\bar{e} \quad (7.10)$$

The cell voltage in the electrolysis without aluminium was more than 2V, which suggests that alumina decomposition (Reaction 1.1) is the main reaction. One might expect that an aluminium pad is established on the anode after short time of electrolysis, which would then result in the Reactions (7.9) and (7.10) with a low cell voltage comparable to the inverted cell. However, this was not the case and the reason is the high efficiency of the back reaction. Aluminium formed on the cathode at the top of the cell is falling down towards the anode bottom and at the same time, CO_2 formed on the anode bottom is moving upwards meeting the aluminium in the bath as illustrated in Figure 7.37.

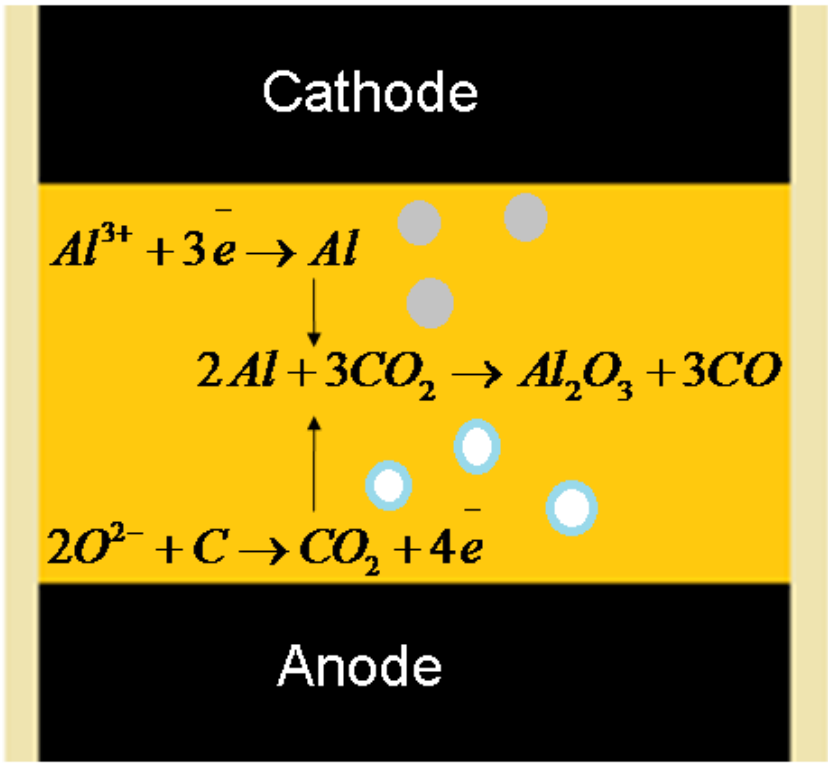

Figure 7.37: Schematic illustration of electrode reactions and the back reaction during electrolysis in the inverted cell setup without aluminium present initially.

The product of this back reaction, aluminium oxide can undergo electrochemical decomposition and this main reaction can proceed without additional alumina feeding longer than the time predicted by Faraday's law. The calculation from Faraday's law showed that alumina added initially is sufficient for 90 minutes of

electrolysis, which correspond well with time when the cell voltage increased dramatically. Needles of β-alumina were found in the bath, which is visible in Figure 7.38. These needles may explain why alumina formed by the back reaction does not undergo electrolysis, but accumulates in the bath. β-alumina is a modification of alumina with intercalated sodium and the formation is therefore more likely in more basic cryolitic bath with higher cryolite ratio. The thinner aluminium carbide layer compared to real and inverted cell with aluminium may be explained by the faster dissolution of carbide into the bath. The cathode surface was not protected by Al metal and there was also higher amount of bath in the vicinity of the carbon cathode.

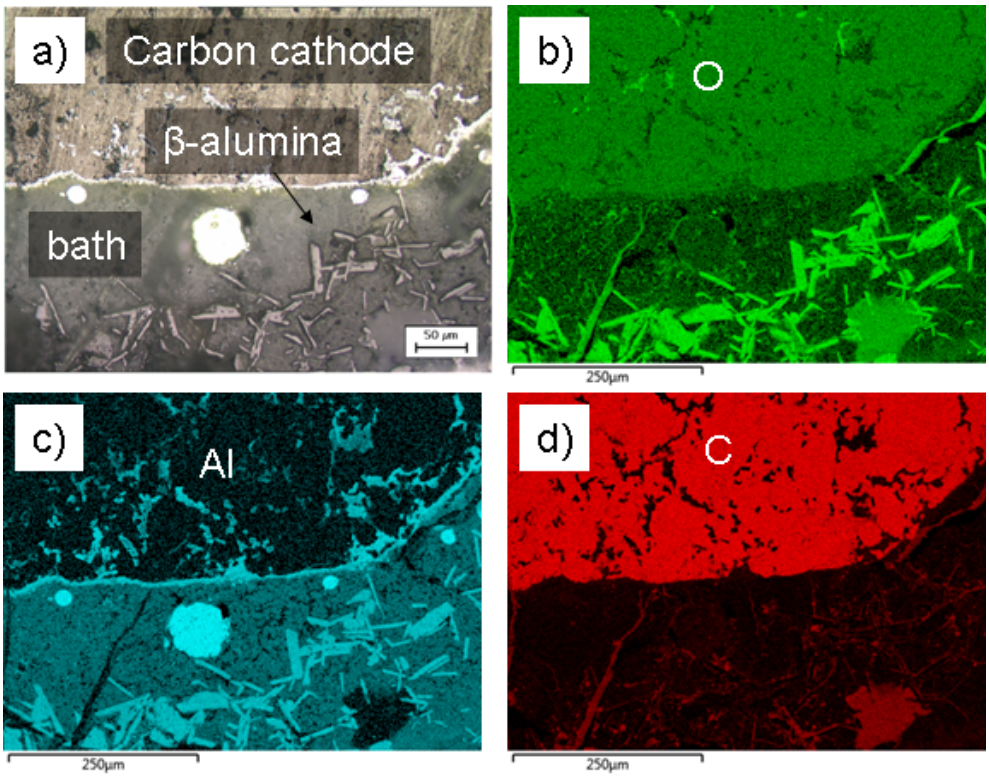

Figure 7.38: β-alumina needles found in the bath after electrolysis in inverted cell setup without aluminium present initially, a) optical image and element maps of b) oxygen, c) aluminium and d) carbon, 90 min, 980 °C.

Analysis of the anodes showed the same pattern for all 3 cell setups. The molten bath had penetrated into the pores of carbon anode, but no aluminium carbide could be found on the carbon surface or in the pores. Cryolite does not wet carbon very well (wetting angle around 90°), but when carbon is anodically polarized, the wetting properties are improved (wetting angle around 20°) [14]. When aluminium is in contact with carbon and cryolite is present, aluminium carbide can be formed without cathodic polarization, but it is a slow process. This might be the case of

inverted cell where chemical formation of aluminium carbide in principle could take place. However, aluminium carbide undergoes oxidation on the anode:

$$Al_4C_3 + 12NaF \rightarrow 4AlF_3 + 3C + 12Na^+ + 12\bar{e} \qquad (7.11)$$

When oxidation of carbon is the main anodic reaction, as it is in the case of conventional cell and inverted cell without Al, aluminium carbide can be oxidized by the anode gases:

$$Al_4C_3 + 6CO_2 \rightarrow Al_2O_3 + 3C + 6CO \qquad (7.12)$$

Anodic oxidation of aluminium carbide is a fast process and it might explain why aluminium carbide could not be found on the anode. Even if there is slow chemical formation of aluminium carbide on the anode of inverted cell, it would undergo oxidation.

No significant differences in the structure of aluminium carbide layers from various electrochemical cells were observed. This also suggests the formation of aluminium carbide electrochemically by the reaction of ionic species from the bath with the carbon cathode. Aluminium cations from the bath undergo reduction at the cathode. There are two possible reactions, the reduction of Al cation to Al metal (Reaction 7.9) and the reduction to aluminium carbide (Reactions 4.4 and 4.5). The reactions at the cathode are illustrated in Figure 7.39.

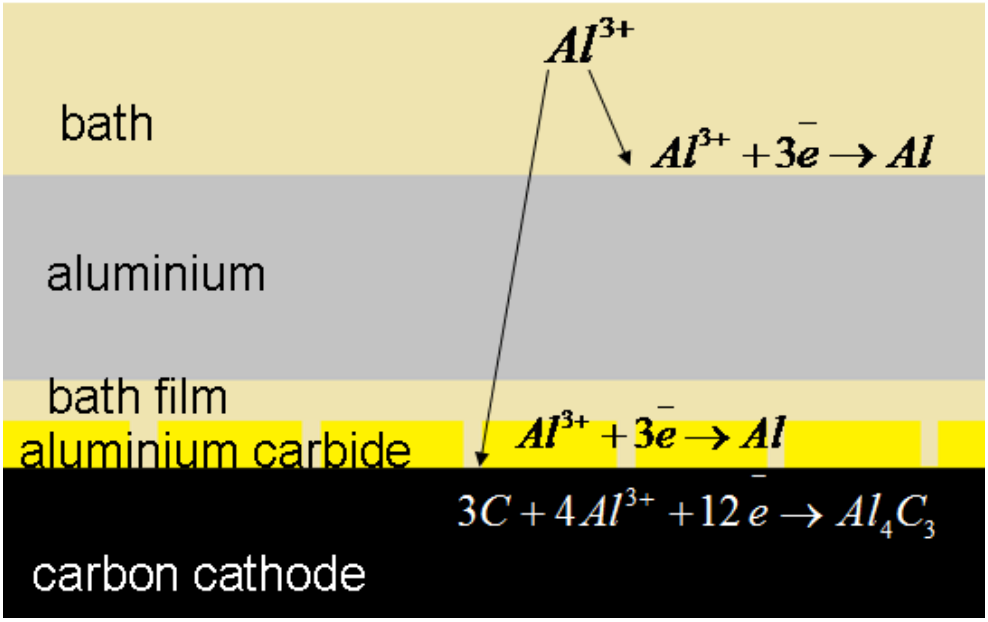

Figure 7.39: Illustration of the main electrochemical reactions at the cathode.

Aluminium carbide can be formed only at the carbon surface, where Al cations come in contact with carbon, while Al metal may be deposited also on the Al pad. Limited access of the molten bath at the carbon surface may reduce the aluminium carbide formation and increase the current efficiency of the aluminium deposition. The aluminium pad and the carbide layer protect the carbon cathode surface from the bath. The bath is the source of Al^{3+} ions, which are the reactants for the electrochemical carbide formation. Another role of the bath is being a solvent of the aluminium carbide formed at the cathode.

8 Outlook

The diffusion couple experiments without the presence of cryolite revealed that the direct reaction between aluminium and carbon is relatively slow. The formation of aluminium carbide was clearly observed at temperatures 1100 °C and higher, which is significantly higher than the temperature in industrial electrolysis cells. The aluminium oxide protective layer on the aluminium surface will evaporate at these temperatures and the reaction between the two elements becomes more pronounced. Formation of aluminium carbide was not observed when current was applied through the diffusion couple, but the voltage was oscillating pointing to local formation of carbide at the interface. These experiments were considered as blank experiments for the conventional cells and the effects of cryolite and current could be studied separately. The scenario without cryolite and with a protective oxide layer at the Al surface does not correspond to the situation in an industrial cell. However, these observations may be relevant if wettable carbon cathodes are introduced. The purpose of this innovation is to improve the wetting of aluminium pad on carbon cathode and to reduce the height of the metal pad. Thin metal pad will be calmer and it will be possible to reduce the interpolar distance and thereby reduce the power consumption. Improved contact between the aluminium pad and the carbon cathode might lead to elimination of the molten bath film, which is present in conventional electrolysis cells used today. In absence of the electrolyte film the aluminium carbide formation will be restricted to the relatively slow chemical reaction between the pure elements Al and C. The lack of bath film would slow down the removal of aluminium carbide from the carbon surface, which may result into oscillations of the cell voltage. The formation of aluminium carbide would be even slower at operation temperature of industrial cells, but improved wetting properties will enhance the reaction. In reality the bath film will not be eliminated completely, because the wetting will not be perfect and also the reduced height of the aluminium pad will support the transport of the bath between the Al/C interface and the bulk of the bath. The exchange rate of the bath film will be probably only reduced, which will also slow down the cathode wear.

The experiments carried out in the inverted cells, where the cathode was exposed directly to the bath without the contact with aluminium, resulted in an aluminium carbide layer with basically the same morphology as the experiments in the cell with a setup corresponding to the conventional cell. Aluminium carbide is therefore suggested to be deposited electrochemically directly from the bath and the aluminium metal is not involved in the electrochemical reaction. The experiment performed with the inverted cell without Al present initially showed a relatively thinner carbide layer and the result was explained by higher amount of bath in the vicinity of the cathode surface and faster dissolution of the carbide layer into the bath. The carbon consumption was not studied, but it was expected to be higher in this case. These results are relevant for the laboratory test cells with the inverted

cathode cell design [2,46]. The aluminium carbide formation mechanism in these cells is expected to be the same as in industrial cell and the lack of aluminium at the cathode surface does not change the reaction mechanism. Aluminium serves only as shield protecting the carbon surface from the contact with the bath.

After the experiments in all 3 types of electrochemical cells aluminium carbide was observed to be formed on the walls of the pores inside the carbon cathode. The pores were filled with the bath, but no aluminium metal was found. This also supports that deposition of aluminium carbide take place directly from the bath without involvement of Al metal. Aluminium does not wet carbon and is known not to penetrate into the pores of the cathode. The electrolyte has lower electrical conductivity than carbon and lower current density is expected in the pores compared to the current density at the cathode surface. Despite the lower current density, the dissolution and the transport of aluminium carbide formed in the pores are suggested to be very slow, and this is most likely the reason why sufficient amount of carbide is always found at the pore walls.

The electrolysis experiments showed that electrical current enhances the formation of aluminium carbide. The amount of the molten bath in the vicinity of the cathode is controlling the dissolution and the transport of the carbide formed at the cathode surface. These two factors are also mostly accepted [3] as the wear rate determining steps. The significantly higher current density in industrial cell induces faster metal pad movement and the areas with the highest wear rate have the highest current densities and at the same time the highest local velocity of the aluminium pad. Therefore it is difficult to evaluate which factor is more important. The results of the experiments did not give quantitative results of the wear rate since this study was more focused on the mechanism of the formation of aluminium carbide. However, the amount of the bath present in the system was suggested to be more important than the current density. The wear rate in laboratory inverted cells is more than ten times higher compared to industrial cells [2, 46]. All these observations suggest that the amount of the bath and the convection give larger variations of the wear rate compared to the current density.

Industrial innovations for reducing the specific power consumption as wettable cathodes and innovative cathode design with special topography are beneficial also for the lifetime of the cathode. In order to reduce the interpolar distance it is necessary to stabilize the metal pad, which means also lower exchange rate of the bath. The possible influence of wettable carbon cathodes on cathode wear was already discussed above. The wear of the cathodes with special topography is still not known, because these cathodes has been introduced very recently and are still in operation. The topography suggests faster wear rate, especially on the edges of the ridges where the convection is higher, but it can be balanced by calmer metal pad and lower exchange rate of the bath.

9 Conclusions

The aluminium/carbon diffusion couple experiments demonstrated that two distinct layers of aluminium carbide were formed at the interface. EDS analysis of the two layers revealed a higher oxygen content in the carbide layer towards aluminium and a lower oxygen content in the layer towards carbon. The formation of aluminium carbide was observed only at temperatures 1100 °C and higher. The layer of aluminium carbide was found already after 24 hours of annealing, but the compact double layer was developed after several days. The removal of aluminium oxide protective layer by evaporation was shown to be the most important step for the initiation of the reaction. The partial pressure of Al_2O at 1100 °C and higher temperatures makes quantitative evaporation of the oxide scale on aluminium possible. Gas transport mechanism for the reaction was proposed, where Al_2O contribute to transport Al to C, while CO can transport C to Al.

The presence of cryolite has a pronounced effect on the formation of aluminium carbide. Introduction of catalytic amount (10-20 mg) at the Al/C interface changed the reaction and aluminium carbide was found at the carbon surface at lower temperatures already after 3 hours. The layer of aluminium carbide was found at the carbon surface and needle-like crystals of aluminium carbide were found towards aluminium. The carbide needles were found only in some regions and the occurrence and the length was shown to be dependent on the local amount of cryolite present. In case of only small amount of cryolite, the fluorides evaporated from the interface and could not be detected after the experiment. The high volatility of cryolite was shown by thermodynamic calculations, which could give a qualitative explanation of the evaporation. The aluminium carbide layer at the carbon surface was suggested to be formed by the reaction of carbon with aluminium transported through the layer of cryolite. The needles of aluminium carbide were suggested to be precipitated from cryolite. The vapour-liquid-solid mechanism of precipitation and growth was suggested as a plausible mechanism for the formation of the carbide needles.

The formation of the carbide layer by direct chemical reaction between Al and C was shown to be dependent on the amount of cryolite, which serves as a solvent of aluminium carbide. No aluminium carbide was found on the Al/C interface after 3 hours when larger amount of cryolite (2.5 g) was present in the crucible. Compact aluminium carbide layer was found on the carbon surface after 3 days of experiment. Aluminium carbide formation and dissolution proceeded until saturation of the bath and then the layer was formed on the carbon surface. The layer reflected the topography of the carbon material. The morphology of the layer was porous and the pores were filled with the bath. The layer may represent a diffusion barrier, but the porous structure allowed transport of aluminium and further growth of the carbide layer.

Applying electrical current through the Al/C diffusion couples did not cause formation of a visible aluminium carbide layer at the interface. The cell voltage was however oscillating, which suggested periodical formation and detachment of a carbide layer at the contact points. Similar experiment with cryolite present at the interfaces resulted in aluminium carbide at the carbon surface and formation of needles of aluminium carbide towards aluminium, which is similar to the experiments without electrical current. The higher amount of carbide at the carbon surface suggests that the formation of aluminium carbide is enhanced by the polarization induced by the voltage across the diffusion couple.

The formation of aluminium carbide in the electrochemical cells was shown to be significantly faster than compared to the experiments without electrolysis. The aluminium carbide layer was observed already after 30 minutes of electrolysis. The layer was found along the entire cathode surface and on the pore walls inside the carbon cathode, while no aluminium metal was found inside the pores. The experiments performed using in inverted cell and in the cell without aluminium present initially, gave qualitatively very similar results. Aluminium carbide was therefore suggested to be deposited electrochemically from the bath without the involvement of Al metal in the electrochemical reaction. The aluminium pad and the carbide layer protect the carbon surface from the bath, which also acts as a reactant and a solvent of aluminium carbide formed. The thinner carbide layer found in the experiment using in inverted cell without aluminium present initially was explained by the faster dissolution of aluminium carbide into the bath. The thickness of the carbide layer was proposed to be the result of a dynamic equilibrium between aluminium carbide formation and dissolution into the bath. The stable cell voltage during the experiments suggested that the compact aluminium carbide layer did not completely block the electrical current going through the cell, but may play the role as a local current shield at the carbon cathode surface.

References

1. Thonstad, J., Fellner, P., Haarberg, G.M., Híveš, J., Kvande, H.and Sterten, Å., Aluminium Electrolysis, 2nd edition, Aluminium- Verlag, 2001

2. Patel, P., On the Effect of Formulation and Porosity on Cathode Performance in Modern Aluminum Reduction Cells, PhD Thesis, The University of Auckland, July, 2009

3. Sørlie M. and Øye H., Cathodes in Aluminium Electrolysis, 3rd edition, Aluminium- Verlag (2010)

4. McClung, M. and Zerkle, R., Autopsy Procedures and Results at Century Aluminum of West Virginia, *Light Metals*, 213-218 (2004)

5. Skybakmoen, E., Rørvik, S., Solheim, A., Holm, K. R., Tiefenbach P., and Østrem, Ø., Measurement of Cathode Surface Wear Profiles by Laser Scanning, *Light Metals*, 1061-1066 (2011)

6. Severo, D., Gusberti, V., Schneider, A. F., Pinto, E.C.V. and Potocnik, V., Comparison of Various Methods for Modeling the Metal-Bath Interface, Light Metals, 413-418 (2008)

7. Fourcault, R. and Samanos, B., 2nd Australasian Aluminium Smelter Technology Course, Sydney, 1987

8. Pietrzyk, S. and Palimaka, P., Testing of Aluminium Carbide Formation in Hall-Heroult Electrolytic Cell, Materials Science Forum, 2438-2441. (2010)

9. Skybakmoen, E., Solheim, A. and Sterten Å. Alumina Solubility in Molten Salt Systems of Interest for Alumina Electrolysis and Related Phase Diagram Data, Met. Mat. Trans. B., 28B, 81-86 (1997)

10. Dorward, B.C., Energy Consumption of Aluminium Smelting Cells Containing Solid Wetted Cathodes, J. Appl. Electrochem., 13, 569-575 (1983)

11. Thonstad, J. and Rolseth, S., On the Cathodic Overvoltage on Aluminium in Cryolite-Alumina Melts, Electrochimmica Acta, 23, 223-241 (1978)

12. Peng, J., Feng, N., Feng, S., Liu, J., Qi, X., Development and Application of an Energy Saving Technology for Aluminium Reduction Cells, Light Metals, 1023-1027 (2011)

13. Martin, O., Allano, B., Barrioz E., Caratini, Y., Escande, A., Favel, N., Low Energy Cell Development on AP Technology, Light Metals, 569-574 (2012)

14. Ransley, C.E., "Refractory Carbides and Borides for Aluminium Reduction Cells", Journal of Metals, 14 (2), 129-135 (1962)

15. Finch, N.J., Met. Trans., The Mutual Solubilities Of Titanium And Boron in Pure Aluminum 3, 2709-2711 (1972)

16. Sekhar, J.A., de Nora, V., Liu, J. and Duruz, J.J., Critical Analysis of Sodium Membranes to Prevent Carbon Cathode Damage in the Hall-Heroult Cell, Light Metals, 271-276 (1996)

17. Brown, G.D., Hardie, G.J., Shaw, R.W. and Taylor, M.P., Proc. 6th Aust. Al. Smelting Workshop, eds. James, Skyllas-Kazakos, Welch, Queenstown, New Zealand, 499-508 (1998)

18. Atkins, P.W., Overton, T.L., Rourke, J.P., Weller, M.T. and Armstrong, F.A., Shriver and Atkins' Inorganic Chemistry, 5th edition, Oxford University Press, 2010

19. Housecroft, C.E. and Constable E.C., Chemistry, 2nd edition, Pearson Education Limited, 2002

20. Marsh, H. and Griffiths, J., Int. Symp. on Carbon, Toyohashi, Japan, , 81 (1982)

21. Wilkening, S., Erdöl Kohle Erdgas Petrochem. Verein. Brennst.-Chem., **39** 551. (1986)

22. Welch, B. J. and May, A. E., Proc. 8th Int. Light Metals Congress, Loeben-Vienna 120. (1987)

23. Tabereaux, A.T., Brown, J.H., Eldridge, I.J. and Alcorn, T.R., Erosion of Cathode Blocks in 180 kA Prebake Cells, *Light Metals* 187-198. (1999)

24. Gray, P.Y., Welch, B.J. and Homsi, P., *Light Metals*, 541-546 (2001)

25. Ødegard, R., Sterten, Å. and Thonstad, J.,On the Solubility of Aluminium Carbide in Cryolitic Melts – Influence on Cell Performance, *Light Metals*, 295-302 (1987)

26. Øye, H.A. and Welch, B., Cathode performance: The Influence of Design, Operations and Operating Conditions JOM, 50 (2) 18-23 (1998)

27. Pardo, J., da Silva Pontes, P., Finotti, T. and Lima, A., Cathode Performance Evaluation at Votorantim Metaís – CBA, *Light Metals*, 1241-1246. (2012)

28. Solheim, A., Some Hypothesis Concerning Cathode Wear in Aluminium Reduction Cells, *COM*, (2012)
29. Dell, M.B., Peterson, R.W. and Rumble, J.N., J.Metals 20 (9) 55. (1968)

30. Al-Jallaf, M.M.K., Mohammed, A.H.A. and Antony, J., Cathode Hot Patching to Prolong Cell Life at Dubal, *Light Metals*, 993-996 (2008)

31. Worell, W.L., Can.Met.Quart. **4** 87. (1965)

32. Wang, Z., Liu, X., Zhang, J. and Bian, X., Study of the Reaction Mechanism in Al-C Binary System through DSC and XRD, Journal of Materials Science, **39** 2179-2181. (2004)

33. Etter, T., Schulz, P., Weber, M., Metz, J., Wimmler, M., Löffler, J.F., Uggowitzer, P.J., Aluminium Carbide Formation in Interpenetrating Graphite/Aluminium composites, *Materials Science and Engineering*, A 448 1–6. (2007)

34. Landry, K., Kalogeropoulou, S. and Eustathopoulos, N., Materials Science and Engineering A254, 99 (1998)

35. Laurent, V., Chatain, D., Chatillon, C. and Eustathopoulos, N., Wettability of Monocrystalline Alumina by Aluminium between its Melting Point, *Acta Metallurgica*, 36 7 1797-1803. (1988)

36. Dorward, R.C., Reaction between Aluminum and Graphite in the Presence of Cryolite, Metallurgical Transactions, **4** 386-388 (1973)

37. Rødseth, J., Rasch, B., Lund, O. and Thonstad, J., Solubility of Carbon in Aluminium and its Effect upon the casting process, *Light Metals*, 883-888. (2002)

38. Taylor, M.P., Welch, B.J. and Keniry, J.T., Influence of Changing Process Conditions on the Heat Transfer During The Early Life of an Operating Cell, *Light Metals*, 437-442. (1983)

39 Motzfeldt, K., Kvande, H., Schei, A. and Grjotheim, K., Carbothermal Production of Aluminium, Aluminium-Verlag, Düsseldorf, Germany, 1989

40. Frolov, A.V., Gusev, A.O., Shurov, N.I., Kulik, N.P., Sitnikov, L.V., Babushkina, L.M., Stepanov, V.P., Zaikov, Y.P., Khramov, A.P. and Malkov, V.B., Wetting and Cryolite Bath Penetration in Graphitized Cathode Materials, *Light metals*, 645-649. (1987)

41. Ødegard, R., Sterten, Å. and Thonstad, J., "On the Solubility of Aluminium Carbide in Cryolitic Melts - Influence on Cell Performance", *Light Metals*, 295. (2006)

42. Grjotheim, K., Næumann, R., Øye, H.A., Formation of Aluminium Carbide in the Presence of Cryolite Melts, *Light metals*, 233-238. (1977)

43. Grjotheim, K., Herstad, O., Næumann, R. and Øye, H.A., *Light Metals*, 107 (1978)

44. Lihrmann, J.M., Thermodynamics of the Al2O3-Al4C3 System I. Thermochemical Functions of Al Oxide, Carbide and Oxycarbides between 298 and 2100 K, *Journal of the European Ceramic Society*, **28** 633-642. (2008)

45. Vasshaug, K., The Influence of the Formation and Dissolution of Aluminium Carbide on the Cathode Wear in Aluminium Electrolysis Cell, PhD. Thesis, NTNU, Norway, March 2008

46. Tschöpe, K., Støre, A., Skybakmoen, E., Solheim, A., Grande, T. and Ratvik, A.P., Critical Reflections on Laboratory Wear Tests for Ranking Commercial Cathode Materials in Aluminium Cells, *Light Metals*, 1251-1256. (2013)

47. Liao, X. and Øye, H.A., Carbon Cathode Corrosion by Aluminium Carbide Formation in Cryolitic Melts, *Light Metals,* 621-627. (1999)

48. Gudbrandsen, H., Sterten, Å. and Ødegård, R. "Cathodic Dissolution of Carbon in Cryolitic Melts", *Light metals*, 521-528. (1992)

49. King, W.R. and Dorward, R.C., Electrical Resistivity of Aluminium Carbide at 990-1240 K, *J. Electrochem. Soc*.,132, 388-389 (1985)

50. Solheim, A. and Tschöpe, K., Model for Excessive Cathode Wear by a „Carbon Pump" at the Cell Bottom, *Light Metals*, 1257-1262. (2013)

51. Østrem, Ø., Cathode Wear in Hall-Héroult Cells, PhD. Thesis, February 2013

52. Liao, X. and Øye, H.A., Physical and Chemical Wear of Carbon Materials, *Light Metals*, 667-674. (1998)

53. Chauke, L. and Garbers-Craig, A.M., Reactivity between Carbon Cathode Materials and Electrolyte Based on Industrial and Laboratory Data, *Carbon*, **58** 40-45. (2013)

54. Tschöpe, K., Støre, Rørvik, S., A., Skybakmoen, E., Solheim, A., Grande, T. and Ratvik, A.P., Investigation of the Cathode Wear Mechanism in a Laboratory Test Cell, *Light Metals*, 1349-1354. (2012)

55. Tschöpe, K., Støre, A., Skybakmoen, E., Solheim, A., Grande, T. and Ratvik, A.P., Electrochemical Wear of Carbon Cathodes in Electrowinning of Aluminium, *JOM*, (2013)

56. Bird, R.B., Steward, W.E. and Lightfoot, E.N., Transport Phenomena, 2nd edition, John Wiley & Sons, Inc., 2007

57. Maier, J., Physical Chemistry of Ionic Materials, John Wiley & Sons, Ltd., 2004

58. Wagner, R.S. and Ellis, W.C., Vapor-Liquid-Solid Mechanism of Single Crystal Growth, *Applied Physics Letters* 4, 89-90. (1964)

59. Grande, T. and Stølen, S., Chemical Thermodynamics of Materials, John Wiley & Sons, Ltd., 2004

60. Bale, C.W., Bélisle, E., Chartrand, P., Decterov, S.A., Eriksson, G., Hack, K., Jung, I.-H., Kang, Y.-B., Melançon, J., Pelton, A.D., Robelin, C. and Petersen, S., FactSage Thermochemical Software and Databases – Recent Developments, *Calphad: Computer Coupling of Phase Diagrams and Thermochemistry*, **33** 2 295-311, (2009)

61. Grande, T., Sommerset, H., Hagen, E., Wiik, K. and Einarsrud, M., Effect of Weight Loss on Liquid-Phase-Sintered Silicon Carbide, *Journal of the American Ceramic Society*, **80** 1047-1052. (1997)

62. Tchistyakov, A.A., Gavrish, A.M. and Ustitchenko, V.A. *Neorganitcheskie materially,* **27**, N8, 1657-1659, (1991)

63. Grass, V., Personal communication, March, 2011

64. Tschöpe, K., Skybakmoen, E., Solheim, A. and Grande, T., Cathode wear in Hall-Héroult cells, *Aluminium* 1-2, 40-43. (2013)

65. Ødegard, R., Sterten, Å. and Thonstad, J., "The Solubility of Aluminium Cryolitic Melts", *Light Metals*, 389-394, (1987)

Appendix

Papers

1. B. Novak, K. Tschöpe, A.P. Ratvik and T. Grande, “Fundamentals of Aluminum Carbide Formation”, *Light Metals,* 2012, pp. 1343-1348

2. B. Novak, K. Tschöpe, A.P. Ratvik and T. Grande, “The Effect of Cryolite on the Formation of Aluminum Carbide at the Carbon Aluminum Interface”, *Light Metals,* 2013, pp. 1245-1250

Light Metals 2012 *Edited by: Carlos E. Suarez*
TMS (The Minerals, Metals & Materials Society), 2012

FUNDAMENTALS OF ALUMINIUM CARBIDE FORMATION

B. Novak, K. Tschöpe, A.P. Ratvik and T. Grande
Department of Materials Science and Engineering
Norwegian University of Science and Technology, N-7491 Trondheim, Norway

Keywords: Aluminium carbide, reaction mechanism, gas transport

Abstract

The fundamentals of formation of aluminum carbide were studied by aluminum-carbon diffusion couple experiment. The diffusion couples consisted of liquid aluminum and graphitized carbon, and the diffusion couple experiments were performed at temperatures 1000-1200°C in stagnant argon atmosphere. The formation of aluminum carbide layer at the solid-liquid interface was confirmed by X-ray diffraction and electron and optical microscopy. The kinetics of the formation of the carbide layer was investigated in detail and formation of carbide by solid-gas reactions is discussed.

Introduction

One of the most common reasons for the shut down of aluminum cells is the wear of the cathode lining. In modern electrolysis technology the lifetime of the pot is mainly determined by cathode wear, which has been shown to depend on the carbon material and is now known to be faster for graphitized carbon materials compared to anthracitic carbon materials [1]. The cathode wear mechanism has recently received considerable attention, but there are no consensus regarding the mechanism [2]. The wear has been related to pure mechanical wear, to the formation of aluminum carbide (Al_4C_3), which may dissolve in the aluminum pad, and finally electrochemical wear, which can be related to the current density [3].The wear in industrial cell is uneven, it varies from place to place. Typical is double-w wear profile [4]. Despite the importance of aluminum carbide formation in the cathode lining, the mechanism is not known in detail.

Aluminum may react directly with carbon to form aluminum carbide according to reaction,

$$4Al(l) + 3C(s) \rightarrow Al_4C_3(s) \quad (1)$$

The reaction is thermodynamically favored at the temperature corresponding to the operation of the cell ($\Delta G°$= -147 kJ (970°C)) [5], but the lack of direct contact between liquid aluminum and the carbon cathode hinders the reaction to proceed. It is not possible to form detectable amounts of the carbide below 1000°C without the presence of the bath [6]. It is also well known that liquid aluminum does not wet carbon. The surface of aluminum is covered by a thin protective layer of aluminum oxide [7], which can be removed by the following reaction,

$$Al_2O_3(s) + 4Al(l) \rightarrow 3Al_2O(g) \quad (2)$$

The wetting of aluminum and carbon has been studied by Landry et al. [7]. At an early stage, the interaction is characterized by high wetting angle (θ_0) between Al/Al_2O_3 [7]. During the evaporation, reaction (2), the wetting angle is decreasing and when the oxide layer is removed, the contact between aluminum and carbon is enabled. The interaction is then characterized by the wetting angle between Al/C. At elevated temperatures it has been shown that the reaction between Al and C takes place on the interface, where aluminum carbide is directly formed. The wetting angle decreases during the reaction and the final wetting angle between Al/Al_4C_3 is reached. The Al-C wetting properties depend also on the type of carbon material. The higher the atomic density of carbon substrate in contact with aluminum, the higher the adhesion energy and the lower the contact angle. Roughness is also important, and a polished surface is better wetted than a rough surface [7]. In an aluminum electrolysis cell the cryolite bath serves as a wetting agent, it dissolves the oxide layer and changes the surface properties of carbon [2]. However, the bath wets Al better than the carbon material and hinders direct contact between molten aluminum and the cathode. In addition, intercalation of Na in carbon changes the wetting angle between the bath and carbon cathode [1]. In this paper initial results on the fundamentals of aluminum carbide formation are reported. The direct reaction between molten aluminum and carbon is studied in the temperature range 1000-1200°C, significantly higher than the operation temperature of aluminum cells, but these temperatures are necessary in order to study the kinetics of the reaction.

Experimental

The interaction of molten aluminium and carbon was studied by using diffusion couple experiments. Initial experiments were performed by pressing pellets of Al and C together in an alumina crucible (Haldenwanger), see Fig 1c. The crucible was placed into a fused silica-liner, which was flushed with Ar gas as shown in Fig 2. Ar 5.0 (Yara Praxair) contains 2 ppm of oxygen and 3 ppm of water. In order to reduce the possible effect of the oxygen impurities, similar experiments were also performed, in stagnant argon atmosphere. In this case the silica-liner was evacuated down to 2 mbar and kept at 2 mbar or re-filled with Ar to 0,8 bar total pressure. A modification of the set-up was conducted by removal of the alumina crucible, which might influence the reaction and made polishing of the diffusion couple more difficult. In this case a carbon crucible from the tested material was prepared, see Fig. 1b. The aluminum cylinder (super purity of 99.99 %) was forced into the crucible and covered with a carbon pellet, as illustrated in Fig. 1c. Extra load (alumina cylinder) on the top was applied to improve the contact at elevated temperatures.

Two different carbon materials were used in the study. The first experiments were conducted using electrode graphite (Svensk specialgrafit AB) with a density of 1.54 g/cm^3. Later, fully graphitized carbon IG-15 (Toyo Tanso, graphitization temperature of 3000°C with a bulk density of 1.9 g/cm^3) was chosen because of its high degree of graphitization.

Experiments were performed in a temperature range of 1000-1200°C, and the duration of the experiments was varying from 1 to 10 days. For some tests the temperature was kept at 1200°C for

one hour and afterwards lowered to 1000°C for the rest of the experiment. The initial first hour was introduced in an attempt to remove the protective oxide layer at the Al(l) surface. The heating rate was 300°C per hour and the glass-liner with the sample was quenched in water or gaseous nitrogen at the end of the experiments.

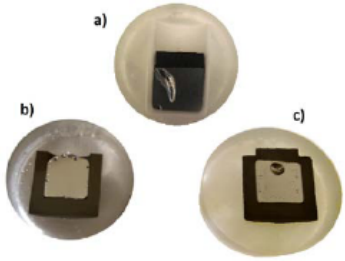

Fig. 1: Diffusion couples embedded in epoxy; a) diffusion couple in alumina crucible b) diffusion couple in graphite crucible c) diffusion couple in a graphite crucible and carbon lid.

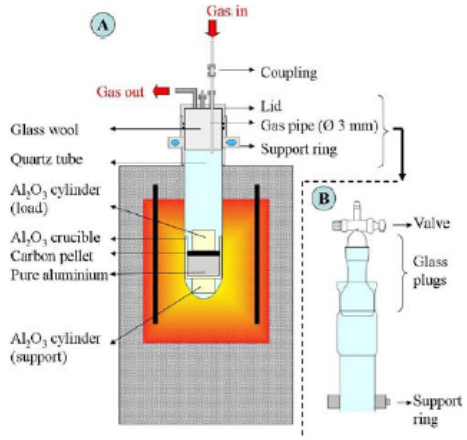

Fig. 2: Experimental set-up with alumina crucible and flux of Ar (A) and top of the glass tube for experiments with stagnant Ar (B).

Characterization of the diffusion couples

After the experiment the diffusion couple was embedded in epoxy resin and cut in two to get a cross section. The cross section was then grinded by a silicon carbide abrasive paper and polished using diamond sprays down to ¼ µm on polishing cloth (Struers). 100 % ethanol was used as a lubricant for grinding and polishing, because aluminium carbide reacts with water. The Al-C interface was analyzed by optical microscope using a polarizing filter (polmet), electron microscopy (LV-SEM HITACHI S-3500N), energy dispersive spectroscopy (EDS) (HITACHI-S 3400) and X-ray diffraction (Bruker D8 Focus). Thermodynamic calculations have been performed using FactSage 5.0.

Results

Typical cross sections of the aluminum/carbon interface at various conditions are shown in Figs. 3-9. Formation of aluminum carbide took place at the Al/C interface at temperatures between 1100 and 1200°C. The thickness and microstructure of the layer was observed to be dependent on the reaction conditions (time, temperature, stagnant or flowing Ar and total pressure). The Al_4C_3 layer appeared inhomogeneous along the C-Al interface, but in most of the diffusion couples it was possible to measure an average thickness. Large single crystals of aluminum carbide could also be observed in the Al layer.

In the experiments, where the diffusion couple was mounted in an alumina crucible and with argon flux through the liner, a thin, uneven layer, with accumulation of carbide shown as large crystals/polycrystalline areas, was already observed after 1 day at 1200°C as shown in Figs. 3 and 5. Beside a thin initial layer, voids or pores in the inhomogeneous carbon material seams to be filled with the reaction product during the initial reaction. With increasing time the reaction product continue to grow and become more even in thickness over time, see Fig 5b and c. The thickness was 40-50 and 80-100 µm after 4 and 16 days, respectively. The micrographs provide evidence that the layer is not homogeneous and consist of two layers, the first containing both O and C, indicating formation of an oxycarbide and a second layer towards the carbon materials with a low O-content. The two layers are shown in Fig. 4. The carbide layer in the vicinity of the carbon surface is more yellowish as compared to the transparent layer towards the aluminum surface. The presence of O and C was confirmed by EDS, but a quantitative determination of the O and C content is difficult due to the porous nature of the layer and possible influence of hydration/oxidation of Al_4C_3 during sample preparation. The origin of the oxygen in one of the layers cannot be ruled out, it might be impurity in Ar or from the alumina crucible.

The thickness of the carbide layer formed after 4 days at 1000°C were difficult to determine. In this experiment the diffusion couple was initially heated for 1 h at 1200°C in order to possibly remove the oxide scale at the Al surface. A thin polycrystalline layer of carbide could be observed, see Fig. 6

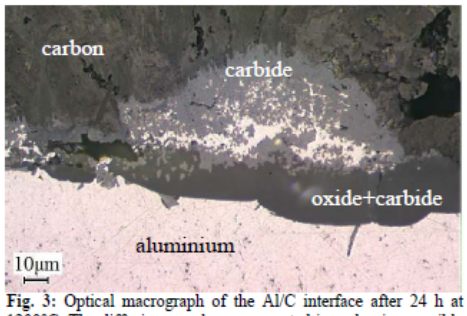

Fig. 3: Optical macrograph of the Al/C interface after 24 h at 1200°C. The diffusion couple was mounted in a alumina crucible and Ar was flushed during the experiment.

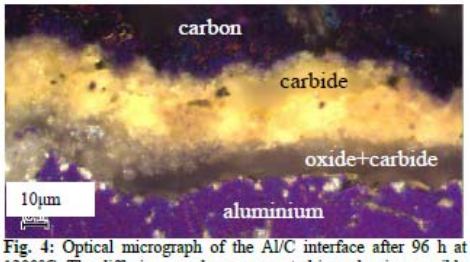

Fig. 4: Optical micrograph of the Al/C interface after 96 h at 1200°C. The diffusion couple was mounted in a alumina crucible and Ar was flushed during the experiment.

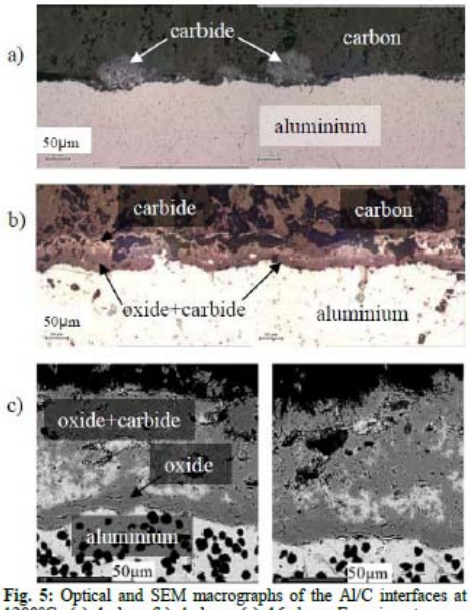

Fig. 5: Optical and SEM macrographs of the Al/C interfaces at 1200°C. (a) 1 day, (b) 4 days, (c) 16 days. Experiments were performed an alumina crucible and flushing Ar. All phases are labeled, the black spots in the aluminium layer are diamonds from polishing.

The experiments in stagnant Ar atmosphere showed lower oxygen content in the first layer near the aluminum surface in comparison with experiments performed in flux of Ar. An example is shown in Fig. 7. A higher content of oxygen was confirmed by EDS in the more transparent grains.

Large apparently single crystals of Al_4C_3 were observed inside the Al layer in most of the diffusion couples. A typical example is shown in Fig. 8, where a ~ 60x120 µm large Al_4C_3 crystal can be recognized. This crystal has most likely been formed during cooling and has precipitated from C dissolved in Al(l). C has clearly been dissolved into Al(l) during the experiments.

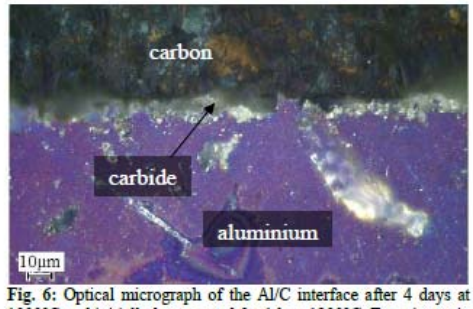

Fig. 6: Optical micrograph of the Al/C interface after 4 days at 1000°C and initially heat treated for 1 h at 1200°C. Experiment in alumina crucible and flushing Ar.

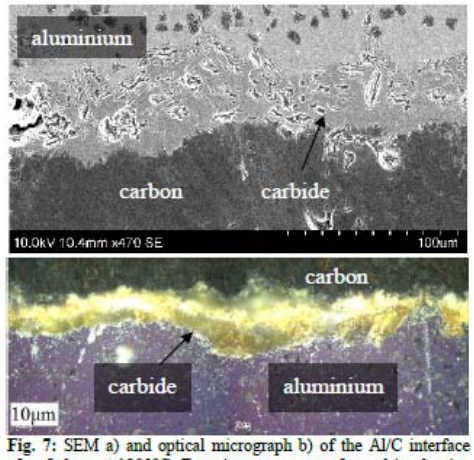

Fig. 7: SEM a) and optical micrograph b) of the Al/C interface after 5 days at 1200°C. Experiments were performed in alumina crucible and stagnant Ar atmosphere.

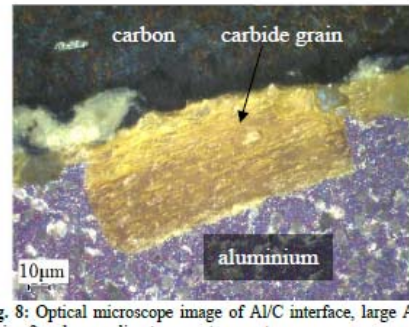

Fig. 8: Optical microscope image of Al/C interface, large Al_4C_3 grain after slow cooling to room temperature.

A diffusion couple using carbon crucible and stagnant Ar atmosphere is shown in Fig. 9. Qualitatively the results are comparable to the ones with the alumina crucible in terms of general carbide formation, but more experiments are needed to get a quantitative comparison.

The experiments using the graphite crucible were performed in stagnant Ar, while most of the experiments using the alumina crucible was performed using Ar flux. In these experiments the type of carbon materials has also not been varied in a systematic way, hence, it is yet not possible to compare the carbide growth rate using two analyzed carbon materials. The carbide thickness in Ar flux was typically 50-80 µm after 8 days and in stagnant argon 80-100 µm after 16 days.

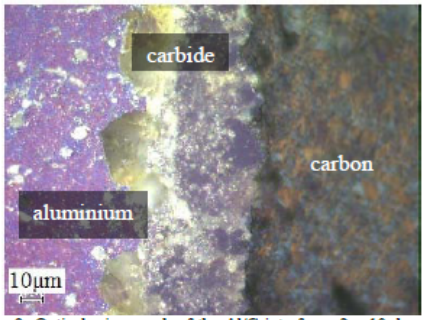

Fig. 9: Optical micrograph of the Al/C interface after 10 days at 1150°C. Graphite crucible (IG-15) and stagnant Ar atmosphere.

In some experiments using the same set-up poor reproducibility of the thickness of the Al_4C_3 layer was observed. An example is shown in Fig. 10 where a porous 500 µm thick layer of Al_4C_3 could be observed. It was also possible in this case to confirm that the layer was Al_4C_3 by X-ray diffraction, see Fig. 11. The explanation for the poor reproducibility is not clear at the present stage, and will be followed up in future work. The porous nature of the layer is, however, strongly suggesting that the majority of the Al_4C_3 is formed from the gas phase and not due to a direct reaction between Al and C.

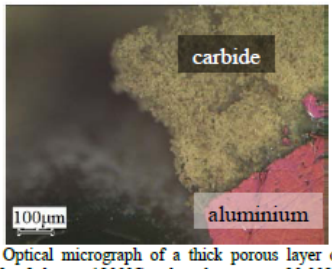

Fig. 10: Optical micrograph of a thick porous layer of Al_4C_3, formed after 3 days at 1200°C and total pressure of 0.002 bar Ar.

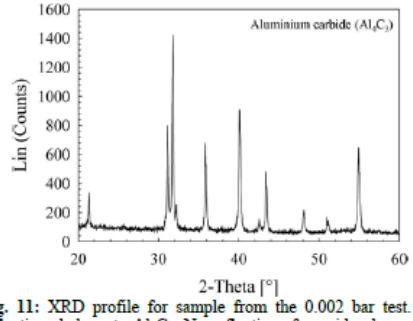

Fig. 11: XRD profile for sample from the 0.002 bar test. All reflections belong to Al_4C_3. No reflections for oxide phases like Al_2O_3, Al_4O_4C or Al_2OC are present.

Discussion

In an ideal diffusion couple experiment with a good and flat contact between the two reactants, the solid state reactions are either controlled by diffusion through the intermediate layer formed at the interface or controlled by the reactions if transport through the layer is not controlling the kinetics. In the Al-C diffusion couple there is several factors which challenge the interpretation of the data. First, one of the reactants is a liquid, and transport of the product through the liquid cannot be ruled out. However, in the last version of the set-up, liquid Al is completely surrounded by liquid C and transport of C through Al is not important when Al become saturated by C. The large carbide crystals precipitated during cooling (Fig. 8) give clear evidence that C has dissolved in Al during the experiment. Secondly, the carbon material is relatively inhomogeneous with large variations in the grain size and with pores of different size. Due to this the first reaction layer appears inhomogeneous during the first 3 days as shown in Fig. 5. It was not straight forward to determine an average thickness, because the layer is only some µm thick and the second layer is not developed. However, after 4 days the second layer starts to appear and an average thickness is measurable.

The first experiments were performed with argon flux containing 2 ppm O_2 and 3 ppm H_2O. If one assume that these traces of oxygen will be involved in the reaction between Al and O one must take into consideration the possibility to form Al oxycarbides in addition to pure carbide. The presence of oxygen in the initial (first) layer was confirmed by EDS, and this layer was also recognizable with the optical microscope (Figs. 3 and 4). According to calculations, oxygen and water present in argon can oxidize 1 micron layer of aluminium carbide per day in an argon flux of 1.6 l/h (carbon pellet diameter = 15 mm), which corresponds to the experimental observations. The calculation has been done for the case of total oxidation. To avoid oxygen, the experimental setup with no flux was introduced (closed system) as shown in Fig. 1b, where it was possible to run experiments in vacuum or stagnant atmosphere. EDS analysis of the carbide layer formed in stagnant argon at 0.8 bar showed specific oxidized areas (corresponding with transparent grains), but the content of oxygen was lower compared to flux of argon. Since the aluminum is initially covered with an oxide layer, complete elimination of the influence of oxygen is impossible in these experiments.

In order to understand the influence of oxygen, several thermodynamic calculations have been performed using the software package FactSage 5.0. In these calculations, formation of oxycarbide was not possible due to lack of thermodynamic data.

In general, the number of degrees of freedom of the system can be found by the Gibbs phase rule,

$$Ph + F = C + 2 \quad (3)$$

where Ph is the number of phases in thermodynamic equilibrium, F is the degree of freedom, C is the number of involved components and 2 corresponds to pressure and temperature. Let us first consider the binary Al-O system with Ar as an inert gas (C=3) at a constant temperature. The total pressure of the system is fixed (F=0) when the gas is in equilibrium with $Al_2O_3(s)$ and Al(l) since Ph+F=3 and Ph=3. The equilibrium composition of the gas is then fixed with $Al_2O(g)$ as the dominating gas species, as predicted in equation (2). It is suggested that the protective Al_2O_3 layer at the aluminium surface is removed or cracked either mechanically, due to the expansion of aluminium at elevated temperatures, or chemically through the evaporation of $Al_2O(g)$. The latter will be discussed further below.

Fig.12 shows that the vapor pressure of the sub-oxide $Al_2O(g)$ increases with increasing temperatures, and reaches 10^{-6} bar at temperatures above 1100°C, where the oxide layer evaporates thermally away from the Al(l) surface. This explains observations made by Landry et al. [7] and explain why it is so difficult to get direct contact between Al and C and formation of carbide. Carbide was only found at temperatures above 1100°C. The partial pressure of $O_2(g)$ in the Al-O system at 1100-1200°C is 10^{-34} and 10^{-31}, respectively, demonstrating the reducing conditions due to the presence of Al(l).

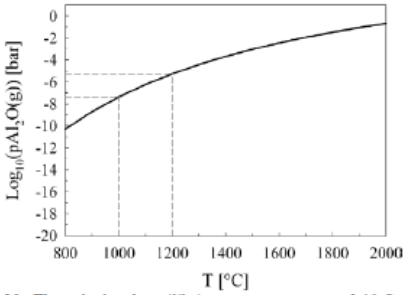

Fig. 12: The calculated equilibrium vapor pressure of Al_2O sub-oxide as function of temperature in the system Al-O, corresponding to reaction (2). The temperature range for experiments performed here is marked with dashed lines.

The next step was to investigate what may contribute to a change in volatility of the oxide scale. Here, an air leakage or oxygen impurities in stagnant argon, as mentioned above, were considered. If the oxygen in the system reacts with carbon to form CO(g), one may expect that the volatility of aluminium increases, which changes the vapor pressure of $Al_2O(g)$. This is however not the case. The partial pressure of $Al_2O(g)$ remains constant according to reaction (2) as long as $Al_2O_3(s)$ is present. Equilibrium calculations have shown that additions of small amounts of C to the Al-O system increases the CO(g) pressure until $Al_4C_3(s)$ starts to form. In this case the gas composition is fixed again (constant pressure of $Al_2O(g)$) according to Gibbs phase rule. This scenario does not change until one of the condensed phases is consumed or disappears. Any excess of carbon (after the formation of CO(g)) will react with Al(l) to form $Al_4C_3(s)$. This proceeds until Al(l) is consumed and an equilibrium between $Al_2O_3(s)$, $Al_4C_3(s)$ and C(s) is established. Here the formation of oxycarbides is neglected, but the main conclusion that the volatility of $Al_2O(g)$ would not be greatly influenced by the presence of C is valid. The removal of the alumina scale from Al(l) is therefore most likely controlled by temperature and the diffusion of $Al_2O(g)$ away from the Al surface.

In Fig. 13, possible mechanism is proposed, how the protective Al_2O_3 layer is removed from the Al(l) surface and how the carbide formation may take place. The the gaseous sub-oxide $Al_2O(g)$ can diffuse towards the carbon surface, enabling transport of Al through the gas phase. At the carbon surface $Al_2O(g)$ reacts to form carbide (or oxycarbide) and CO(g). Contrary, the released CO(g) transports C to the aluminium surface, where CO(g) can react to form $Al_4C_3(s)$ and generate $Al_2O(g)$. Oxygen can then circulate between both interfaces, and one may imagine that the two reactions at the two different surfaces generate two different $Al_4C_3(s)$ microstructures.

From this scenario, a possible explanation for the formation of two different layers, as shown in Fig. 4, is proposed. It is assumed that aluminium carbide grows at both interfaces according to the sub-reactions (4) and (5). Reaction (5) leads to an oxide rich carbide layer in the vicinity of the aluminium surface. At the present stage the possibility of formation of oxycarbides (Al_2OC and/or Al_4O_4C) cannot be ruled out. This will be followed up in future work, including these species in the thermodynamic analysis. From literature it is known that aluminium oxycarbides appear transparent [8, 9]. In Figs. 4, 8 and 9 it is evident that the first layer consists of transparent grains and EDS measurements have shown the presence of oxygen in this layer. However, reaction (4) may explain the oxide free carbide layer at the carbon surface.

$$2\,Al_2O(g) + 5\,C(s) = Al_4C_3(s) + 2\,CO(g) \quad (4)$$

$$\frac{1}{2}CO(s) + Al(l) = \frac{1}{6}Al_4C_3(s) + \frac{1}{6}\,Al_2O_3(s) \quad (5)$$

In initial experiments it was not possible to identify the original position of the C/Al interface in order to elucidate the growth rate by these two proposed reaction mechanisms. Both reactions are heterogeneous, involving both a gas and condensed phases. The presence of liquid Al is expected to have a strong detrimental effect on the microstructure of the layer formed at the Al interface. Dissolution - precipitation due to the solubility of $Al_4C_3(s)$ in Al(l) may also influence the microstructure and destabilization of the oxycarbide due to the low O solubility in Al(l). On the other surface the microstructure of carbon material is expected to influence the microstructure of the carbide form. Here both grain orientation (graphite like grains), grain and pore size are expected to be important. These effects will be followed up in future studies.

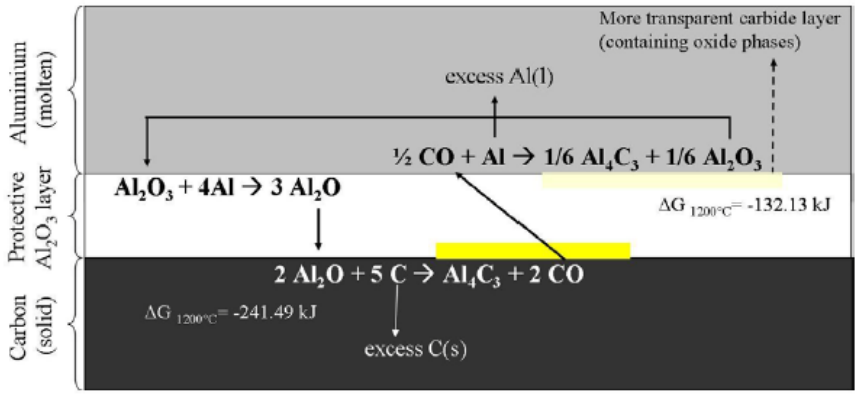

Fig. 13: Proposed gas transport mechanism of aluminium carbide formation.

The initial expectation was that the diffusion couples would provide evidence for the solid state diffusion through a carbide layer at the interface. Estimation of the diffusion coefficient by $D=4L^2/t$, where L is the thickness and t is the time, give diffusion coefficient of the order of 10^{-10} m^2/s. Such high diffusion coefficients are highly unlikely in the carbide with strong covalent bonds, which strongly supports the preliminary conclusion that gas diffusion is involved in the growth. For gas assisted diffusion, higher temperatures are necessary throughout the experiment to produce Al_2O sub-oxide (see Fig. 12), and finally aluminium carbide. The attempt to remove the oxide layer at 1200°C for 1 hour and lowering the temperature to 1000°C in the course of the experiment in argon flux was show the presence of a carbide layer, but quantitative determination of the thickness was challenging after only 4 days of reaction.

The large single crystal like grains, with regular shape (Fig. 7) were observed on the interface only after slow cooling (4h), not after quenching in water or gaseous nitrogen flow. It is proposed that their formation is due to nucleation and growth from the molten aluminum during cooling. The solubility of carbon (as aluminum carbide) in liquid aluminium is approximately 200-250 ppm at 1200°C, 40 ppm at 1000°C and less than 10 ppm at 800°C [10]. The carbide deposition from dissolved carbon in aluminium proceeds continuously during cooling, where the cooling rate influences the microstructure of the precipitate.

Conclusion

Initial experiments using Al/C diffusion couples have shown that aluminum carbide is formed at the interface. The reaction was influenced by several factors such as the atmosphere and the presence of solid alumina. The reaction rate has been shown to be retarded initially due to the oxide scale on molten aluminum, and thick layers of carbide were only observed at 1200°C. The microstructure of the layer formed at the interface showed evidence of two different layers between Al and C, and in one of the layers the presence of oxygen was confirmed by EDS, suggesting that this layer contained oxycarbide. A possible reaction mechanism was suggested involving mass transport between the Al and C surface by $Al_2O(g)$ and CO(g). The two different heterogeneous reactions at the two surfaces could possibly explain the two layers formed in the diffusion couples.

References

1. X. Liao and H.A. Øye, "Physical and Chemical Wear of Carbon Cathode Materials", Light Metals (1998), 667-674.
2. M. Sørlie and H.A. Øye, Cathodes in Aluminium Electrolysis, 3rd edition, Aluminium- Verlag, (2010).
3. P. Patel, "On the Effect of Formulation and Porosity on Cathode Performance in Modern Aluminium Reduction Cells", PhD Thesis, The University of Auckland, July, 2009
4. E. Skybakmoen, S. Rørvik, A. Solheim, K. R. Holm, P. Tiefenbach and Ø. Østrem, "Measurement of Cathode Surface Wear Profiles by Laser Scanning", Light Metals (2011), 1061-1066
5. W.L. Worell, "Carbothermic Reduction of Alumina. A Thermodynamic Analysis", Can.Met.Quart. 4 (1965), 87-95.
6. S. Pietrzyk and P. Palimaka, "Testing of Aluminium Carbide Formation in Hall-Heroult Electrolytic Cell", Materials Science Forum (2010), 2438-2441.
7. K. Landry, S. Kalogeropoulou, N. Eustathopoulos, "Wettability of Carbon by Aluminium in Aluminium Alloys" Materials Science and Engineering A254, (1998), 99-111.
8. A.A. Tchistyakov, A.M. Gavrish and V.A.Ustitchenko Neorganitcheskie materialy 27 (1991), N8, 1657-1659.
9. V. Grass, Personal communication, March, 2011
10. J. Rødseth, B. Rasch, O. Lund and J. Thonstad, "Solubility of Carbon in Aluminium and its Effect upon the casting process", *Light Metals* (2002), 883-888.

Light Metals 2013 *Edited by: Barry Sadler*
TMS (The Minerals, Metals & Materials Society), 2013

THE EFFECT OF CRYOLITE ON THE FORMATION OF ALUMINUM CARBIDE AT THE CARBON ALUMINUM INTERFACE

B. Novak[1], K. Tschöpe[1, 2], A.P. Ratvik[1] and T. Grande[1]
[1]Department of Materials Science and Engineering
[1]Norwegian University of Science and Technology, N-7491 Trondheim, Norway
[2]SINTEF Materials and Chemistry, N-7465 Trondheim, Norway
Keywords: Aluminum carbide, reaction mechanism, cryolite, thermodynamics

Abstract

The effect of cryolite on the formation of aluminum carbide was studied by an aluminum-carbon diffusion couple experiment. The interface between the aluminum and carbon was coated by a thin layer of cryolite, and the diffusion couple experiments were performed at 1030 °C in stagnant argon atmosphere. The microstructure of the relatively thick and porous aluminum carbide formed at the solid-liquid interface was investigated by optical and scanning electron microscopy. It was shown that the presence of cryolite has a pronounced effect on the formation of carbide, although fluorides could not be found at the interface after the experiment. The porous and needle like morphology of the carbide layer suggests the mass transport during growth is through the gas or liquid phase. The stability of cryolite and possible gas species involved in the growth process have been analyzed thermodynamically to identify possible gaseous species present at both global equilibrium and metastable conditions.

Introduction

One of the most common reasons for the shut down of aluminum electrochemical cells is the degradation of the cathode lining [1]. In modern aluminum electrolysis technology the lifetime of the pot is mainly determined by cathode wear, which has become more significant with the use of graphitized cathode blocks [2]. The cathode wear mechanism has received increasing attention because aluminum producers are increasing the amperage of the cells and the tendency to shift to graphitized cathodes with higher electrical conductivity. The wear has been related to pure mechanical wear or to the formation of aluminum carbide (Al_4C_3), which might be formed chemically or electrochemically. Aluminum carbide may dissolve into the bath. [3]. Despite the importance of cathode wear, the wear mechanism(s) is still not fully understood [1].

Aluminum may react directly with carbon to form aluminum carbide according to reaction (1),

$$4Al(l) + 3C(s) \rightarrow Al_4C_3(s) \quad (1)$$

The reaction is thermodynamically favored at the temperature corresponding to the operation of the cell ($\Delta G° = -147$ kJ (970 °C)) [4], but poor wetting between liquid aluminum and carbon materials hinders the reaction to proceed [5]. In diffusion couple, the surface of aluminum is covered by a thin protective layer of aluminum oxide. This layer can be removed and aluminum carbide can be formed at temperatures higher than 1100 °C [6]. The protective oxide is removed thermally by the following reaction (2),

$$Al_2O_3(s) + 4Al(l) \rightarrow 3Al_2O(g) \quad (2)$$

but the reaction (2) is known not to occur at temperatures relevant for the electrolysis [7]. The removal of the oxide layer and the initial stage of aluminum carbide formation were studied in recent work by the authors [6]. The vapor pressure of aluminum suboxide in reaction (2) reaches the value ~10^{-6} bar at temperature 1100 °C, which allows the evaporation of the thin oxide layer at atmospheric conditions. Then Al_4C_3 may form by the reactions between aluminum suboxide and carbon (3), and CO and Al (4).

$$2\,Al_2O(g) + 5\,C(s) = Al_4C_3(s) + 2\,CO(g) \quad (3)$$

$$\frac{1}{2}CO(g) + Al(l) = \frac{1}{6}Al_4C_3(s) + \frac{1}{6}Al_2O_3(s) \quad (4)$$

Here, the formation of aluminum oxycarbide is neglected for simplicity. In the previous study two layers of aluminum carbide were observed at temperatures higher than 1100 °C [6]. The first layer towards aluminum was shown to contain more oxygen, possibly due to formation of oxycarbides (Figure 2). The second layer growing towards carbon had lower oxygen content and was regarded as almost pure aluminum carbide.

In aluminum electrolysis cell the cryolite bath dissolves the oxide layer and improves the wetting of liquid Al on carbon materials [8]. Molten cryolite is also a solvent of Al_4C_3 and can thereby reduce the diffusion barrier between Al and C induced by a layer of Al_4C_3(s) [9]. The influence of cryolite on the interfacial reaction between molten aluminum and carbon is investigated in the temperature range 1030-1100 °C in this paper. The experimental findings are analyzed with support from a thermodynamic analysis of possible reactions and vapor pressures at global equilibrium and metastable conditions.

Experimental

The influence of cryolite on the interaction of molten aluminum and carbon was studied by performing diffusion couple experiments. Cryolite was introduced by submerging of an Al cylinder into the suspension of fine cryolite powder and 100% ethanol. A small amount of cryolite (10-20 mg) was introduced in order to serve only as a wetting agent, not as a solvent of aluminum carbide. The coated Al cylinder was cast into the carbon crucible and dried. The aluminum cylinder was made of aluminum with high purity (99.99 %). Fully graphitized carbon IG-15 (Toyo Tanso, graphitization temperature of 3000 °C with a bulk density of 1.9 g/cm^3) was chosen because of its high degree of graphitization. Natural cryolite was used for the initial experiments, but was later replaced with synthetic cryolite (Sigma-Aldrich) in order to reduce the agglomeration of fine fluoride particles. A carbon pellet was placed on the top to improve the contact between the reactants (Figure 1). The crucible was placed into a fused silica-liner [6] and experiments were

performed in a stagnant argon atmosphere. The liner was evacuated down to 2 mbar and re-filled with Ar gas (-5.0 Yara Praxair, 2 ppm O_2 and 3 ppm H_2O) to 0.8 bar to reach less than 1 bar total pressure. The diffusion couples were heat treated at 1030 °C (the melting point of cryolite is 1012 °C), and the duration of the experiments was from 3 hours to 3 days. The heating rate was 300 °C per hour and the glass-liner with the sample was quenched in water at the end of the experiments.

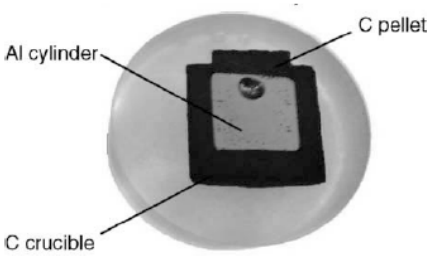

Figure 1: Cross section of the aluminum carbon diffusion couple embedded in epoxy.

Characterization of the diffusion couples

After the experiment the diffusion couple was embedded in epoxy resin and cut into two to get a cross section (Figure 1). The cross section was then ground using silicon carbide abrasive paper and polished using diamond sprays down to ¼ µm on polishing cloth (Struers). 100 % ethanol was used as a lubricant for grinding and polishing, to reduce reaction of the reaction layer with humidity. The Al-C interface was analyzed both by optical microscope using a polarizing filter (polmet) and electron microscopy (LV-SEM HITACHI S-3500N). Scanning electron microscopy (SEM) and element mapping was done by energy dispersive spectroscopy (EDS) using a HITACHI-S 3400 SEM. The interface of the diffusion couples after the reaction was analyzed by X-ray diffraction (Bruker D8 Focus).

Results

In the previous work two layers of aluminum carbide were observed at temperatures higher than 1100 °C [6]. An example of the two layers formed at the Al-C interface is shown in Figure 2.

A typical Al/C interface with small amount of cryolite at the interface is shown in Figure 3. Aluminum carbide was found on the interface already after 3 hours. The thickness of the aluminum carbide layers was uneven along the interface reflecting the variation in the local amount of cryolite. A gap between Al and C due to the solidification of $Al_{(l)}$ during cooling became infiltrated with epoxy during sample preparation. EDS analysis of the layers showed the formation of aluminum carbide, with considerable amount of oxygen present (Figures 3 and 8). XRD of the aluminum and carbon surfaces confirmed the presence of aluminum carbide. Aluminum oxide was also present according to XRD, but no oxycarbides could be found (Figure 4). Cryolite or fluorides could not be detected by EDS or XRD at any of the interfaces.

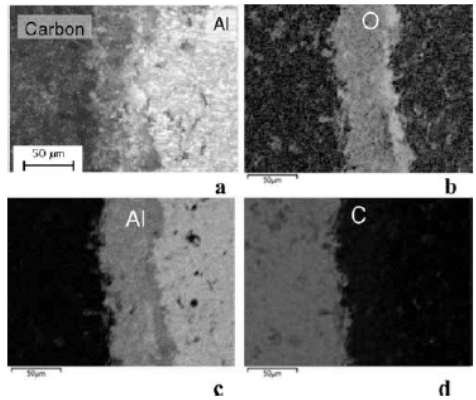

Figure 2: a) Optical image of two layers of aluminum carbide at the liquid aluminum solid carbon interface without cryolite, 1200 °C, 10 days The first layer with higher oxygen content towards Al and the second layer with lower oxygen content towards C. Element mapping of b) oxygen, c) aluminum and d) carbon.

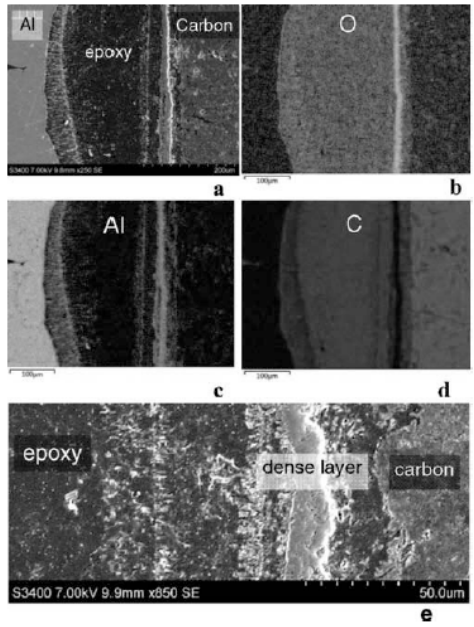

Figure 3: a) SEM image and element maps of b) oxygen, c) aluminum and d) carbon of a typical Al/C interface after 3 days at 1030 °C with cryolite. e) SEM image; the detail of more compact denser layer towards the carbon material.

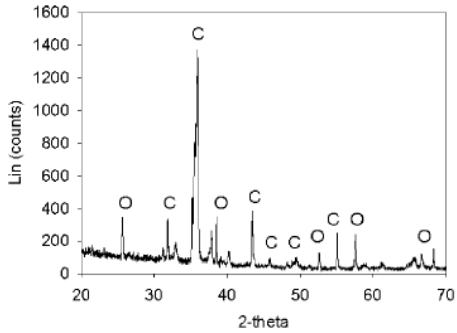

Figure 4: XRD spectrum of Al surface (the contact surface with C). The peaks belong to aluminum carbide (C) and aluminum oxide (O).

The aluminum oxide found at the interface originates either due to oxidation of the carbide after exposure to air, from oxygen impurities in the Ar gas or the initial oxide layer on Al. No significant difference between the experiments performed for 3 hours and 3 days experiments were observed, which suggests that the reaction is fast and the layers are formed during first hours.

Al_4C_3 grains with needle-like morphology could always be observed towards aluminum (Figures 3- 8). The layer of Al_4C_3 needles was observed at all the interfaces, but the thickness varied, from 10 to 300 μm. The occurrence and length of the aluminum carbide needles depended on the local amount of cryolite. In some experiments, an excessive amount of cryolite was introduced onto the top of aluminum cylinder, which resulted in thicker layer with long carbide needles (Figure 5).

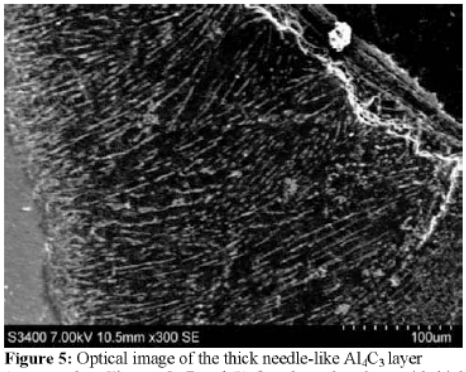

Figure 5: Optical image of the thick needle-like Al_4C_3 layer (compared to Figures 3, 7 and 8) found on the place with high amount of introduced cryolite after 3 hours.

Towards the carbon materials a relatively denser layer was observed (Figures 3, 7 and 8). The thickness is varying from 10 to 20 μm. The oxygen content in this denser layer was always higher than in the layer with needles (Figure 3).

Aluminum or aluminum carbide were usually not observed in the pores of the carbon material, because of its low porosity and the dense layer, which acts as a diffusion barrier. In some special cases however, when the layer was found not in contact, aluminum carbide was found in the pores of carbon (Figure 6).

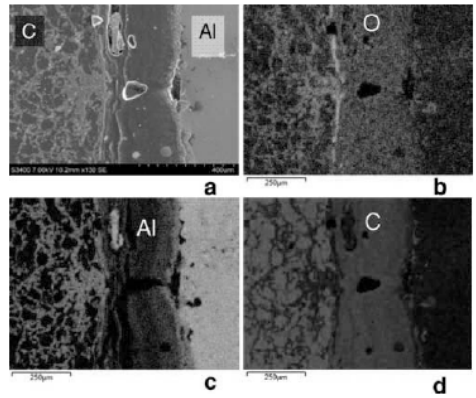

Figure 6: a) SEM image of aluminum carbide penetration into the pores of carbon. Element mapping of b) oxygen, c) aluminum and d) carbon.

There were also regions which displayed a somewhat different microstructure than these two characteristic layers. EDS analysis of the reaction product in these cases showed aluminum carbide with very high carbon content, which reflects the mixture of epoxy with carbide. The molten aluminum shrunk during cooling, and the significant volume reduction caused usually fracture of the layers with the carbide needles. Some carbide particles that had detached from both layers were found in the resulting gap in the diffusion couple, which became surrounded by epoxy and appear like an extra layer (Figure 3).

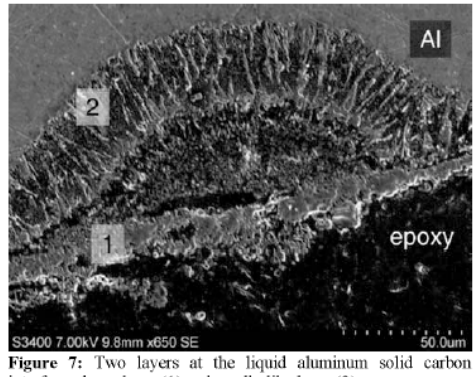

Figure 7: Two layers at the liquid aluminum solid carbon interface; dense layer (1) and needle-like layer (2).

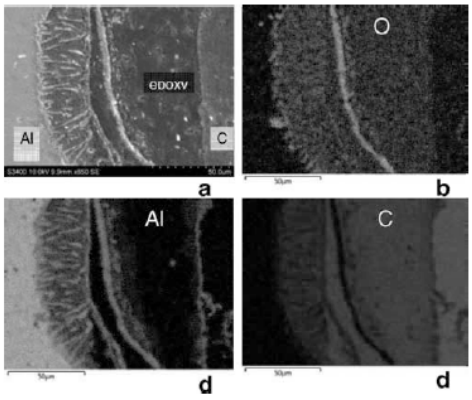

Figure 8: a) SEM image and element maps of b) oxygen, c) aluminum and d) carbon of a typical Al/C interface after 3 hours at 1030 °C with cryolite.

Discussion

Thermodynamic calculations (FactSage 6.2) were performed to determine the vapor composition in Al-C-O system with cryolite at various conditions. Aluminum oxycarbide phases were not included in the calculations due to lack of thermodynamic data. The partial pressures of the gaseous species are helpful for understanding the mechanism of aluminum carbide formation and the influence of cryolite. The ternary phase diagram of Al-C-O system can be divided into 3 subsystems (Figure 9). In triangle 1, aluminum carbide is in equilibrium with excessive, unreacted aluminum and aluminum oxide. The vapor composition is fixed according to Gibbs phase rule in the entire region, independent of oxygen content in the system. Triangle 2 represents excess of carbon, and the vapor composition is again fixed according to the Gibbs phase rule. In triangle 3 excess amount of oxygen is present and the only gaseous species is CO and CO_2 in equilibrium with Al_2O_3. In the diffusion couple experiments, carbon and aluminum are not consumed and global equilibrium is not reached. Locally the vapor pressure can deviate substantially from the global equilibrium values. The three subsystems represent the metastable conditions in the vicinity of excess carbon, aluminum and oxygen.

The partial pressures in two subsystems with excess aluminum and carbon are rising with the temperature (Figure 10). They are fixed within the region and oxygen content does not influence the vapor composition according to the Gibbs phase rule. The vapor pressures increase with nearly two orders of magnitude by increasing the temperature to 1200 °C.

The calculated vapor pressures of volatile species when cryolite is in contact with Al and C and traces of Al_2O_3 are given in Table 1. These calculations demonstrate the volatility of sodium and fluorine, in line with the experimental findings, where any of cryolite species were not found at the interfaces after the termination of the experiments. Cryolite will be therefore relatively quickly being transported away from the C-Al interface during the experiment. The main effect of cryolite is therefore to dissolve the oxide scale on the Al surface and to facilitate reactions between Al and C, either through the gas phase or by the direct contact between the two phases as discussed further below.

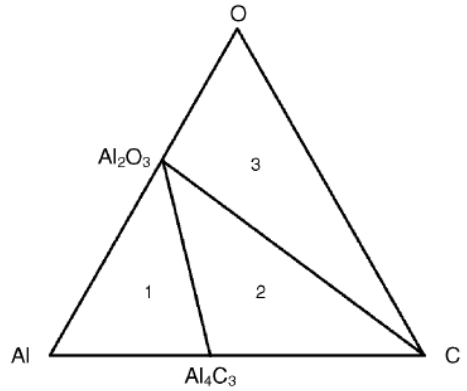

Figure 9: Phase diagram of Al-C-O ternary system with 3 subsystems.

Table 1: Partial pressures of species above cryolite in Al-C-O system at a temperature of 1030 °C.

System	Excess Al	Excess C
	Partial pressure / bar	
Na	$4.2 \cdot 10^{-2}$	$1.4 \cdot 10^{-2}$
AlF	$1.05 \cdot 10^{-2}$	$1.2 \cdot 10^{-3}$
$NaAlF_4$	$6.2 \cdot 10^{-3}$	$6.2 \cdot 10^{-3}$

The gas transport mechanism was proposed in previous work [6]. The protective oxide layer can be evaporated at temperatures higher than 1100 °C and can initiate aluminum carbide formation (Reactions 3-4). Vapor pressures of aluminum and aluminum suboxide reach the value 10^{-6} at 1100 °C in the vicinity of aluminum and CO pressure reaches this value at 1100 °C in the vicinity of carbon (Figure 10). Al vapor and Al_2O can transport aluminum to carbon and CO can transport carbon to aluminum. The presence of cryolite has no influence on the vapor pressures of Al, Al_2O and CO. The partial pressures are low ($\sim 10^{-7}$) at experimental temperature 1030 °C and their involvement in aluminum carbide formation is less likely than in the previous study at 1200 °C [6].

Aluminum carbide was formed already at 1030 °C and has different morphology than the carbide observed after the experiment without cryolite at higher temperatures. Cryolite is generally considered as a wetting agent and solvent of the aluminum oxide protective layer and aluminum carbide [8]. Experimentally cryolite was shown to disappear, explained by the estimated high vapor pressures when cryolite is in equilibrium with $Al_{(l)}$. The dissolution of Al and Al_2O_3 in molten cryolite will reduce the vapor pressures but not sufficiently to hinder the evaporation. The dissolution was not included in the calculations, but cryolite is known as a good solvent of aluminum oxide [10]. Thus in the initial stage of the reaction the aluminum oxide layer can dissolve in cryolite and dissolution re-precipitation of the oxide may occur before the cryolite is evaporated. Then the transport of aluminum to the carbon can be fast through the liquid layer of cryolite. However, formation of a dense aluminum

carbide layer can slow down the reaction, which can be then diffusion controlled. Grjotheim et al. studied Al_4C_3 formation with a large amount of cryolite [11]. The reaction and dissolution proceeded until saturation, which was reached after a couple of hours. The solubility of aluminum carbide in cryolite is around 1 wt. % [9]. Then the diffusion controlled growth of a carbide layer was suggested on the carbon surface.

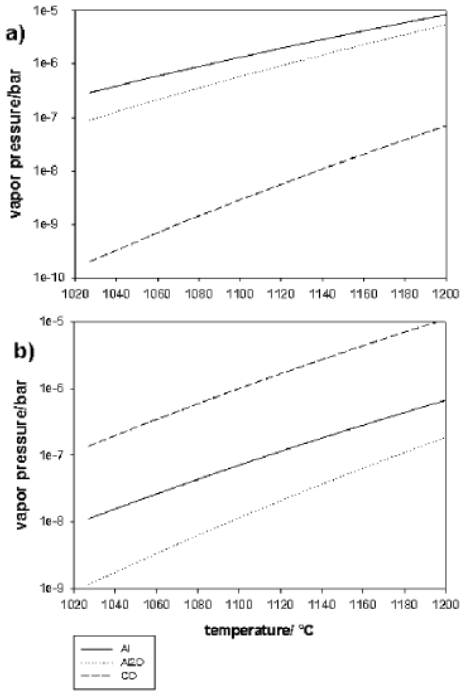

Figure 10: Vapor pressures of selected species in two subsystems: a) excess Al (triangle 1) and b) excess C (triangle 2).

Needle-like aluminum carbide, which was found towards the aluminum, suggests precipitation and growth from a liquid or gas phase. Precipitation from liquid aluminum at cooling was observed in experiments without cryolite, large aluminum carbide grains with regular shape were formed [6]. At 1030 °C the solubility of carbon in aluminum is low and the precipitation is not likely [12]. Discussed gas transport mechanisms from the previous work are less likely at lower temperatures. They are also independent of the presence of cryolite, but the differences between aluminum carbides observed with and without cryolite are evident. Occurrence and length of the needles have been shown to be dependent on the local amount of cryolite (Figure 5). Thus the effect of cryolite and its involvement in the reaction is believed to be very important. Aluminum carbide needles might have precipitated from cryolite. The needles were always oriented perpendicular to Al/C interface, regardless of the position in the crucible (bottom, top, and sidewall). The deposition could proceed by vapor-solid-liquid growth mechanism [13]. The direction of the growth is suggested to be towards aluminum. The dense carbide layer might act as a good substrate for the growth of the needles. Cryolite as a liquid phase is saturated with aluminum carbide (≈1 wt. %) [9] and aluminum (≈0,1 wt. %) [14]. The only carbon containing gas, which can be involved in the reaction with dissolved Al, is CO. The partial pressure of CO in the system is low, but on the outside of the crucible (local equilibrium) the pressure is higher (10^{-5} bar) and depends on oxygen concentration in the system. When CO is introduced to the cryolite, it reacts with dissolved aluminum (Reaction 4). Formation of aluminum carbide in saturated cryolite leads to precipitation of $Al_4C_3(s)$. The precipitation can take place by further growth of the needles. This is determined by the anisotropy of the crystal, the growth is preferred to proceed in one direction. Solubility of Al_2O_3, the by product of the reaction, is 10-20 times higher, therefore precipitation should not occur in the initial stage. Alumina content reduces aluminum carbide solubility in cryolite [9]. Evaporation of cryolite also leads into Al_4C_3 precipitation, which might contribute to the growth of the needles. When cryolite is evaporated, the formation of the needles stops. Oxygen content in the system is limited and will in the end cause formation of Al_2O_3. If Al_4C_3 is formed by reaction (5), the by product CO_2 can be transported back to carbon, react to CO and bring the carbon back.

$$6CO(g) + 4Al(diss) = Al_4C_3(s) + 3CO_2(g) \quad (5)$$

This reaction is however not thermodynamically favored according to the calculations ($\Delta G° = 28{,}6$ kJ (1030 °C)).

The dense layer towards carbon has relatively high oxygen content and it is not clear to identify from EDS mapping whether it is highly oxidized aluminum carbide or aluminum oxide. The small amount of carbon in this layer might have come from the carbon coating of the sample. On the Figure 8 the dense, relatively thick and oxygen rich layer is detached from the carbon surface and thinner, aluminum carbide layer is towards carbon. This suggest the dense, oxygen rich layer to be aluminum oxide, which might be formed by precipitation from cryolite either by evaporation or from the reaction (4) as a by product of the formation of carbide needles. The thin aluminum carbide layer is probably formed by direct contact of aluminum and carbon on the carbon surface. In the initial stage, before cryolite was evaporated completely, aluminum could be transported relatively fast through the layer of liquid cryolite. Formed aluminum carbide can be dissolved into the bath. The experiment with duration of 3 hours showed, that saturation of cryolite with carbide and the formation of the carbide layer towards carbon are very fast processes.

The proposed mechanisms for formation of aluminum carbide at the carbon aluminum interface is illustrated Figure 11.

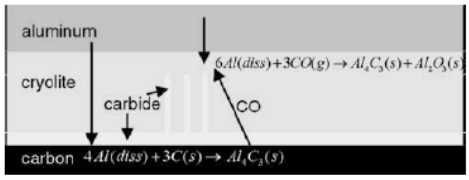

Figure 11: Proposed mechanism of aluminum carbide formation.

Conclusion

Al/C diffusion couple experiments with cryolite have shown that aluminum carbide is formed on the interface already at 1030 °C. Without presence of cryolite, at least 1100 °C is needed to form aluminum carbide. Compact aluminum carbide layer was observed towards carbon. Needles of aluminum carbide were found towards aluminum, the length depends on the local amount of cryolite. Small amount of cryolite has evaporated and was not found on Al/C interface after the experiment. Cryolite has probably dissolved the protective aluminum oxide layer and the wetting of aluminum on carbon was improved. The layer towards carbon is suggested to form by aluminum transported to the carbon surface by the diffusion through the cryolite layer. The needles are probably precipitated from the cryolite. Vapor-liquid-solid growth mechanism is suggested. Cryolite saturated with aluminum is fed with CO and aluminum carbide can be deposited on the top of the needles. Evaporation of saturated cryolite might also lead to aluminum carbide precipitation and the growth of the needles.

References

1. M. Sørlie and H.A. Øye, Cathodes in Aluminum Electrolysis, 3rd edition, Aluminum- Verlag, (2010).
2. A.T. Tabereaux, J.H. Brown, I.J. Eldridge and T.R. Alcorn, "Erosion of Cathode Blocks in 180 kA Prebake Cells", *Light. Metals* (1999) 187-198.
3. P. Patel, "On the Effect of Formulation and Porosity on Cathode Performance in Modern Aluminum Reduction Cells", PhD Thesis, The University of Auckland, July, 2009
4. W.L. Worell, "Carbothermic Reduction of Alumina. A Thermodynamic Analysis", *Can.Met.Quart.* 4 (1965), 87-95.
5. K. Landry, S. Kalogeropoulou, N. Eustathopoulos, "Wettability of Carbon by Aluminum in Aluminum Alloys" *Materials Science and Engineering* A254, (1998), 99-111.
6. B. Novak, K. Tschöpe, A.P. Ratvik and T. Grande, "Fundamentals of Aluminum Carbide Formation", *Light Metals* (2012), 1343-1348.
7. V. Laurent, D. Chatain, C. Chatillon and N. Estathopoulos, "Wettability of Monocrystalline Alumina by Aluminum between its Melting Point and 1273 K", *Acta Metall.* 36, (1988), 1797-1803.
8. R.C. Dorward, "Reaction between Aluminum and Graphite in the Presence of Cryolite", Met. Trans., 4 (1973), 386-388
9. R. Ødegard, Å. Sterten and J. Thonstad, On the Solubility of Aluminum Carbide in Cryolitic Melts - Influence on Cell performance, *Light Metals* (1987), 295-302.
10. A. Sterten, I Maeland, "Thermodynamic of Molten Mixtures of Na_3AlF_6-Al_2O_3 and NaF-AlF_3", *Acta Chem. Scand*, 39 (1985), 241-257.
11. K. Grjotheim, R. Næumann and H.A. Øye, "Formation of Aluminium Carbide in the Presence of Cryolite Melts", *Light Metals* (1977), 233-242.12. J. Rødseth, B. Rasch, O. Lund and J. Thonstad, "Solubility of Carbon in Aluminium and its Effect upon the Casting Process", *Light Metals* (2002), 883-888.
13. R.S. Wagner and W.C. Ellis, "Vapor-Liquid-Solid Mechanism of Single Crystal Growth", *Applied Physics Letters* 4 (1964), 89-90.
14. R. Ødegård, Å. Sterten and J. Thonstad, "On the Solubility of Aluminum in Cryolitic Melts", *Metallurgical Transactions* (1988), 449-457.